

Czech Technical University in Prague

Faculty of Electrical Engineering

Department of Electromagnetic Field

***RELIABILITY OF OPTICAL STRUCTURES
IN HARSH ENVIRONMENTS***

Doctoral Thesis

Jan Bohata

Prague, September 2017

Ph.D. Programme: Electrical Engineering and Information Technology (P2612)

Branch of study: Radioelectronics (2601V010)

Supervisor: Prof. Ing. Stanislav Zvánovec, Ph.D.

Supervisor-Specialist: Ing. Matěj Komanec, Ph.D.

Contents

1	Introduction	1
2	State-of-art.....	3
2.1	Advanced transmission formats and systems	3
2.1.1	Optical modulation formats.....	3
2.1.2	Optical infrastructures for wireless networks.....	4
2.2	Optical fibers in harsh environments.....	7
2.2.1	Tests of influences on attenuation/losses	7
2.2.2	Test of influences on chromatic dispersion.....	9
2.2.3	Tests of influence on PMD.....	12
2.2.4	Optical fiber aging.....	22
3	Objectives of the thesis	25
4	Achieved results	26
4.1	Results overview.....	26
4.2	Characterization of Dual-Polarization LTE Radio over a Free-Space Optical Turbulence Channel.....	28
4.3	Experimental Verification of Long-Term Evolution Radio Transmissions over Dual-Polarization Combined Fiber and Free-Space Optics Optical Infrastructures	35
4.4	Reliability of Aircraft Multimode Network.....	44
4.5	Testing of Optical Fiber Components for Harsh Environments.....	54
4.6	Outdoor Atmospheric Influence on Polarization Mode Dispersion in Optical Cables	57
4.7	Long-Term Polarization Mode Dispersion Evolution and Accelerated Aging in Old Optical Cables	62
4.8	Adaptation of Transmitting Signals over Joint Aged Optical Fiber and Free Space Optical Network under Harsh Environments	67
5	Conclusions	79
5.1	Contribution of the thesis	79
5.2	Future research opportunities	79
6	List of author's publications.....	80
7	References	84
8	Curriculum Vitae.....	89

Declaration of originality

I, the undersigned, hereby declare that this doctoral thesis is the result of my research in our research team and my contribution corresponds to that specified at the beginning of each research chapter. The thesis was written under the professional supervision of Prof. Stanislav Zvánovec, Dr. Matěj Komanec, using the literature and resources listed in the Bibliography and References.

In Prague, 15th September 2017,

.....

Ing. Jan Bohata

Acknowledgements

Special thanks to:

Prof. Stanislav Zvánovec who has supported and encouraged me during my studies and throughout the writing of this thesis while providing me with thought-provoking advice in conjunction with the technical support of my co-supervisor Dr. Matěj Komanec.

Finally, to my family, my girlfriend Klára and to the SK Slavia Praha football club which recently won the league title for the first time since I entered the CVUT post-graduate programme.

The research presented in this thesis was supported by:

The CTU grants no. SGS12/142/OHK3/2T/13, OHK3-037/14 and SGS14/190/OHK3/3T/13.

The Technology Agency of the Czech Republic, grant number TA03020439.

Abstract

Networks of decades-old optical fibers created for operating optical communications are still in use today and being applied to the harsh environments of avionics and military, marine, and space systems. Consequently, an analysis of optical component reliability and a description of the aging process is called to predict the behavior of these fibers in specific areas of utilization. In this thesis, harsh environments for optical components are investigated and a methodology for the long-term monitoring of optical fiber parameters for different service conditions is presented. Furthermore, several optical systems are tested over aged optical infrastructure.

Keywords: Optical fiber, harsh environment, aging, free-space optics, radio over fiber.

Abstrakt

Přestože optické vláknové infrastruktury byly instalovány již před několika desetiletími, jsou stále v provozu a na řadě míst navíc i extrémně zatěžovány. Extrémní zátěž úzce souvisí i s rozmachem optických komunikačních systémů v blízkých oblastech letectví, vojenství, kosmických aplikací apod. Vzhledem k těmto faktům je nezbytně nutná analýza spolehlivosti a stárnutí optických komponent, a to zejména za účelem předpovědi chování jednotlivých prvků ve zmíněných prostředích. V této práci je podrobena analýze rizikové prostředí pro optické komponenty a vytvořena metodika dlouhodobého monitorování parametrů optických vláken v různých provozních podmínkách. Dále jsou testovány vysokorychlostní optické a radiové přenosové systémy pro použití v zestárlých optických infrastrukturách.

Klíčová slova: Optické vlákno, rizikové prostředí, stárnutí, bezdrátové optické spoje, radiový přenos pře optická vlákna.

List of abbreviations

ALT	Accelerated Life Test
BBU	Baseband unit
BER	Bit error rate
CD	Chromatic dispersion
CRAN	Cloud radio access network
DGD	Differential group delay
DP	Dual polarization
DQPSK	Differential quadrature phase shift keying
DSF	Dispersion-shifted fiber
DTS	Distributed temperature sensing
DWDM	Dense wavelength division multiplexing
EDFA	Erbium doped fiber amplifier
EVM	Error vector magnitude
FSO	Free space optics
FUT	Fiber under test
GINTY	General interferometric technique
IL	Insertion loss
JME	Jones matrix eigenanalysis
LTE	Long term evolution
MFD	Mode field diameter
MMF	Multi-mode fiber
NRZ	Non-return-to-zero
OFDM	Orthogonal frequency division multiplexing
OOK	On-Off keying
OSNR	Optical signal-to-noise ratio
OTDR	Optical time domain reflectometer
PBC	Polarization beam combiner
PBS	Polarization beam splitter

PC	Polarization controller
PDL	Polarization dependent loss
PDM	Polarization division multiplexing
PMD	Polarization mode dispersion
POTDR	Polarization-sensitive optical domain reflectometer
PSP	Principal state of polarization
QAM	Quadrature amplitude modulation
QPSK	Quadrature phase-shift keying
RF	Radio frequency
RoF	Radio over fiber
RoFSO	Radio over FSO
RZ	Return-to-zero
SMF	Single mode fiber
SNR	Signal-to-noise ratio
SSMF	Standard single mode fiber
TINTY	Traditional interferometric technique
WDM	Wavelength division multiplexing

1 Introduction

Increasing demands on high data rates and quality of digital services in recent years have led to massive developments in the field of optical infrastructures. These demands go hand in hand with expanding radio wireless services such as mobile xG or worldwide interoperability for microwave access (WiMAX) networks [1], [2] [3]. It is clear that optical technologies play an irreplaceable role in such networks, especially backbone networks [4]. In addition, new modulation formats, affording extremely high transmission capacity [5], have been introduced to meet desired demands with various optical amplifiers (rare-earth doped fiber amplifiers, semiconductor amplifiers, Raman amplifiers) offering perfect tools for long-haul systems. Moreover, free space optics (FSO), which offer similar bandwidth as optical fiber, are being widely applied as a cost-effective alternative to optical fiber networks. Increases in capacity and distance need ever-improving optical component properties and higher system sensitivity [6, 7].

As some of the today's optical systems were installed 20 (or more) years ago, a huge number of old infrastructures have been in use as they cannot be easily replaced by new ones (from a costs perspective). Approximately 222 million kilometers of optical fibers were installed between 1998 and 2000 [8] and even older fibers and cables still coexist. Along with the variety of parameters of such structures, it is necessary to consider the conditions influencing optical transmission characteristics. Furthermore, fiber systems are not only found in backbone communication links, more and more photonics systems are used in harsh environments for avionics, as well as in the military, naval or automobile industries or combinations of them. Novel mobile 5th generation systems are also based on optical core infrastructures [9]. Due to advanced parameters suitable for data transfer, such as low signal attenuation, it is expected that optics will be installed in practically all fields where possible, and strict requirements on selected infrastructures may be enforced. Optical infrastructures also usually form an inseparable part of crucial communication routes including subway systems in urban areas. It all represents a package of different environmental conditions with specific limits, regulations and requirements on optical infrastructures.

New questions concerning reliability appear to determine those influences mentioned above. We encounter these problems with harsh environments formed by significant changes in temperature, humidity, vibrations, high transmitted optical power or turbulence. It seems that these factors, together with the massive expansion of optical systems, are having a severe impact on the quality of optical signal transmissions. Moreover, long-term exposure to these factors can permanently degrade optical fiber parameters, which leads to premature fiber aging. However, these problems can occur also in relatively safe areas since more sophisticated systems (dense wavelength division multiplexing (DWDM), polarization division multiplexing (PDM), etc.) or components (multi-core fibers, high-power amplifiers, etc.) are widely utilized in the older infrastructures which were not designed to carry today's systems.

The thesis first introduces harsh environment influences on fiber and wireless optical infrastructures. Chapter 2 discusses the current state of research in this area. In Part 2.1,

a brief introduction to optical and hybrid optical – radio frequency (RF) transmission formats is given. Afterwards, Part 2.2 describes environmental-induced optical attenuation increase, followed by influences on chromatic dispersion (CD), polarization mode dispersion (PMD) and, finally, a discussion of optical fiber aging. Chapter 3 then proposes the main objectives of the thesis and summarizes work accomplished related to the thesis. Chapter 4 presents achieved results based on published journal and conference papers of the author filling the timeline and objectives of the thesis. Moreover, the relationship of the papers with the thesis topic is described here. Finally, Chapter 5 contains the conclusion of the thesis and a final discussion.

2 State-of-art

Optical fibers have undergone significant development over the past decades, mainly in their transmission properties. Among the key features is low attenuation, which has led to the enormous replacement of existing metallic cables by optical fibers which have rapidly evolved in terms of low attenuation for a much wider range of wavelengths. However, attenuation, as well as the other key parameters of optical fiber like dispersion, can suffer significant impairment due to environmental influences. The aim of this thesis is to capture optical infrastructure behavior in harsh environments fully. At first, variable transmission formats are introduced to provide an overview of systems that can be deployed in old infrastructure, or, in infrastructure influenced by the harsh environment described. Subsequently, short-term and long long-term characterization of the crucial optical fiber parameters are described in the following chapters to form a methodology for the reliability of optical structures in harsh environments. The thesis is divided into the following chapters.

2.1 Advanced transmission formats and systems

According to growth in data rates, optical transmission systems are widely deployed in various areas including military applications, space platforms or avionics[10]. Nevertheless, the optical transmission system must be frequently adapted for cases of leveraged optical infrastructure which is placed in a hazardous area, or, for instance, whose transmission parameters are degraded through an aging process. In this section, a brief overview of transmission systems, used further in the thesis, is provided.

2.1.1 Optical modulation formats

Older optical infrastructures were initially designed to support on-off keying (OOK), non-return-to-zero (NRZ) signal formats with a maximum speed of 2.5 Gbps or 10 Gbps. However, subsequent higher bit rate systems (> 40 Gbps), mostly operate with higher optical power and minimum system requirements of 50 GHz channel spacing, optical signal-to-noise-ratio (OSNR) tolerance not exceeding 16 dB and maximum mean PMD tolerance of 30 ps with an outage probability of 10^{-5} [11, 12]. Therefore, with the coexistence of old and new optical fiber based telecommunication infrastructures, it is essential to ensure that optical fiber properties are fully characterized to ensure the required quality of services. One of the cost-effective and energy-efficient solutions for 100 Gbps systems is the deployment of a differential quadrature phase-shift keying (DQPSK) modulation format to enable DWDM with a spacing of 100 GHz [12], [13].

Tables 1 and 2 depict the comparison of 100 Gbps optical modulation formats from OOK to polarization multiplexed QPSK in terms of minimal bandwidth, spectral efficiency, symbol rate, OSNR, CD and differential group delay (DGD) tolerance.

Modulation format	OOK	OOK-VSB	DQPSK	RZ-DPSK-3ASK	PM-DQPSK	OP-FDM-RZ-DQPSK	PM-QPSK	PM-OFDM-QPSK
coh. / noncoh.	noncoh.	noncoh.	noncoh.	noncoh.	noncoh.	noncoh.	coh.	coh.
Bits/symbol	1	1	2	2.5	2x2	2x2	2x2	2x2x2
Symbol Rate (Gbd)	112	112	56	44	28	28	28	14
Constellation								
DWDM Grid (GHz)	200	100	100	50	50	100	50	50
Spectral Efficiency (bits/s/Hz)	0.5	1	1	2	2	1	2	2

Tab. 1. A comparison of 100 Gbps optical modulation techniques in terms of transmission properties. [12]

Modulation format	OOK	OOK-VSB	DQPSK	RZ-DPSK-3ASK	PM-DQPSK	OP-FDM-RZ-DQPSK	PM-QPSK	PM-OFDM-QPSK
coh. / noncoh.	noncoh.	noncoh.	noncoh.	noncoh.	noncoh.	noncoh.	coh.	coh.
DWDM Grid (GHz)	200	100	100	50	50	100	50	50
Estimated Reach (km)	< 500	< 500	1000	<500	600	1500	1500	2000
Tolerances	⊖	⊖	⊕	⊖	⊕	⊕	⊕	⊕
OSNR tolerance (dB) @ BER 4×10^{-3}	17.5	18.5	15.5	>20	15.5	15.5	< 15	< 15
CD tolerance (ps/nm) @ 2dB penalty	± 5	± 5	± 22	± 30	± 90	± 90	>>	>>
Max. DGD tolerance (ps) @ 2dB penalty	4	4	9	10	18	18	>>	>>
Compatibility with 10G and 40G	⊕	⊕	⊕	⊕	⊕	⊕	⊕	⊖
Filtering with ROADMs	⊖	⊖	⊕	⊕	⊕	⊕	⊕	⊖

Tab. 2. A comparison of 100 Gbps selected optical modulation techniques in terms of impairment tolerances. [12]

As can be seen, advanced modulation formats, in particular coherent systems, allow higher CD and DGD tolerance. On the other hand, the deployment of these systems brings significant additional costs. Note that coherence systems are adopted mostly for large backbone networks, whereas most other released systems are non-coherent. However, the transmission bit rates with standard installed single-mode fiber (SMF) can reach terabytes per second by using coherent systems. For example, a 16.2 Tbps transmission has been realized using dual-polarization (DP)-QPSK optical super-channels over 2,531 km of SMF [5]. The experimental results presented show that the maximal distance capacity obtained with this system is about 40.9 Pbps·km. Another high-bit-rate experiment was published in [14], where 22 optical DP-8QAM/QPSK super-channels were adopted to overcome a distance of 1,503 km in standard SMF (SSMF). The maximal achieved recorded bit rate was 21.7 Tbps proving feasible transport more than 20 Tbps on an installed SMF at long-haul distances was possible.

2.1.2 Optical infrastructures for wireless networks

The requirements for new-generation mobile networks are increasing with the growing volume of multimedia applications generated by mobile users. It is expected that the amount of internet protocol (IP) data in wireless networks will have exceeded a value

of 500 exabytes (EB) by 2020 compared to ~ 3 EB in 2010 [15]. To satisfy these demands for mobile data traffic, the 3rd Generation partnership project (3GPP) has launched long term evolution (LTE) to achieve data rates of 3 and 1.5 Gbps for the downlink and uplink, respectively, when using LTE-advanced (LTE-A) technology [16]. Moreover, mobile cellular networks are on the verge of launching fifth-generation networks (5G) [2]. In these networks, as well as LTE-A, it is possible to use cloud radio access network (C-RAN) architecture to improve both the energy consumption and costs [17]. In C-RAN architecture, the baseband units (BBU) are centralized into a cloud (or BBU pool) and the signal is distributed to the remote radio heads (RRH) in the evolved Node B (eNB) (in the case of LTE networks). This architecture makes the eNB more simple and robust, which is an ideal solution especially for small cells [18], [19] although it increases the demand for access and the optical fronthaul network [17].

A) Radio over fiber systems

Radio over fiber (RoF) technology combines the benefits of optical fiber and RF based signals in wireless applications (4G, 5G, Wimax, etc). RoF is capable of performing a function for transmissions between a BBU pool and base stations in the C-RAN architecture [20],[21]. The RoF application in C-RAN architecture, together with a RoF setup, is shown in Fig. 1 and 2.

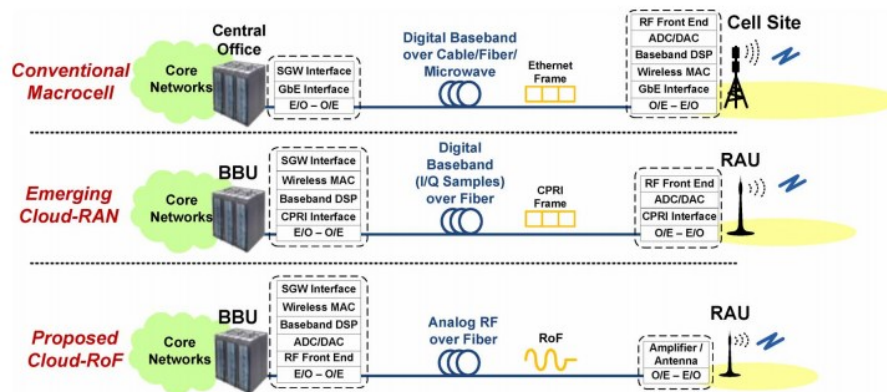


Fig. 1. Functions of central-office and cell-sites (or BBU and RAUs) for macrocell, conventional cloud-RAN, and the proposed cloud-RoF systems. [18]

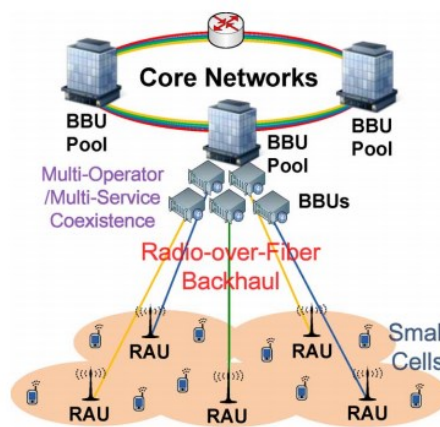


Fig. 2. Architecture of the proposed small-cell cloud-RoF access systems.[18]

The capacity of a general RoF link can be significantly increased by using polarization division multiplexing (PDM) techniques as proposed for transmitting ultra-wideband (UWB) signals [22] or for 3GPP multiple-input multiple-output (MIMO) LTE-A signals [23]. The analog RoF technology is, furthermore, capable of transmitting radio signals with carrier frequencies up to 100 GHz [24].

B) Radio-over-FSO systems

In most cases, providers use an existing fiber infrastructure, instead of replacing by making new fiber routes, due to lower costs. What is more, a wireless-based FSO can be adopted in places where optical fiber installation is not possible or economical, especially in dense urban areas. FSO technology, thus, offers optical fiber features (i.e., high data rates and longer transmission spans) and is a suitable option that can be deployed rapidly over transmission spans of up to a few kilometers [25], [26],[27]. Moreover, up-to-Tbps transmissions are possible when engaging FSO technology [28]. In such optical wireless scenarios, an alternative would be to transmit RF-based information over the FSO link in place of an OF, which was experimentally demonstrated in [29] where a 1-km-long radio-over-FSO (RoFSO) link was implemented at a wavelength of 1550 nm for the transmission of the digital television signal. Nevertheless, link availability and performance quality is mostly affected by harsh atmospheric weather conditions, such as atmospheric turbulence, fog, rain, etc. [26], [30]. Atmospheric scintillations are amongst the major adverse influences on FSO. Note that scintillation is characterized by Rytov variance as given by [31]:

$$\sigma_R^2 = 1.23k^7 C_n^2 L^{\frac{11}{6}}, \quad (1)$$

where k is the wave number, L is the length of the channel and C_n^2 is the refractive index structure parameter which depends on the strength of the turbulence and is defined as:

$$C_n^2 = \left(79 \times 10^{-6} \frac{P_a}{T^2}\right)^2 C_T^2, \quad (2)$$

where P_a is the atmospheric pressure in millibars. C_T^2 is the temperature structure constant, which is defined as:

$$C_T^2 = (T_1 - T_2)^2 / L_p^{2/3}, \quad (3)$$

where T_1 and T_2 are temperatures at two points separated by distance L_p . Knowing the thermal distribution along the FSO propagation path, it is possible to determine C_T^2 and C_n^2 . The impact of atmospheric turbulence on the propagating optical beam is given in detail in [26].

Fig. 3 shows the variation of received optical power and modulation error ratio (MER) with a dependence on experienced refractive index structure parameter C_n^2 . Results represent real data from a 1-km-long RoFSO link, mentioned above [29]. It can be observed that the higher the C_n^2 parameter, the lower the received power and corresponding higher MER and, thus, a worsened system performance.

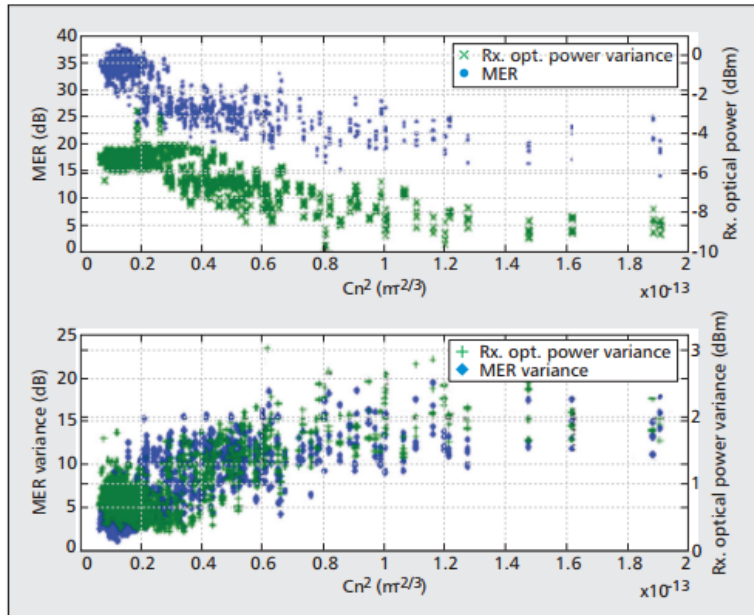


Fig. 3. Average, and a variation of, terrestrial broadcasting modulation error ratio with parameter C_n^2 . [29]

In [32], a DWDM system with RoFSO technology was used to transmit a range of various radio services over 1 km of an FSO link under turbulent conditions for both indoor and outdoor (short-range) applications with 99.9% link availability. A novel wireless network architecture using RoFSO for wireless local area networks (WLANs), together with an RF assignment mechanism based on RoFSO, was proposed and investigated in [33] offering efficient frequency utilization in terms of both the throughput and fairness index. The performance of OFDM-based RoFSO links was published in [34] and presented the bit error rate (BER) and the outage probability performance in a turbulence channel.

2.2 Optical fibers in harsh environments

In this section, harsh environments (mostly temperature changes) and their impact on key transmission parameters of the optical fiber networks are described.

2.2.1 Tests of influences on attenuation/losses

As mentioned above, the low attenuation of optical fibers has led to their massive inclusion in many applications. Unsurprisingly, attenuation is the best described phenomena in fibers with small dependence on temperature. Common industrial producers of silica fibers typically provide thermal dependence in datasheets, for example, Corning [35] provides data from environmental tests in temperatures typically ranging between -60 °C and $+85$ °C. Fig. 4 shows an example of a temperature cycling environmental test with controlled temperature changes between -10 °C and 85 °C. The specifications are provided in Tab. 3 and Tab. 4.

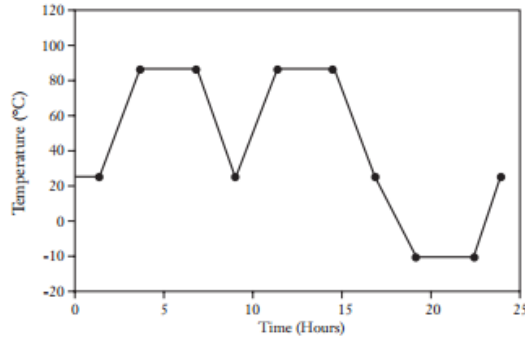


Fig. 4. Temperature cycling for environmental tests. [35]

Specifications indicate that induced attenuation during environmental tests of single-mode fiber SMF28 should be below 0.05 dB/km for wavelengths 1310 nm, 1550 nm and 1625 nm and below 0.2 dB/km for 850 nm.

Environmental test	Test Conditions	Induced attenuation @1310 nm, 1550 nm, 1625 nm [dB/km]
Temperature dependence	-60°C to +85°C	≤ 0.05
Temperature humidity cycling	-10°C to +85°C up to 98% RH	≤ 0.05
Water immersion	23°C ± 2°C	≤ 0.05
Heat aging	85°C ± 2°C	≤ 0.05
Damp heat	85°C at 85% RH	≤ 0.05

Tab.3 Environmental specifications for SMF. [35]

Environmental test	Test Conditions	Induced attenuation @850 nm & 1300 nm [dB/km]
Temperature dependence	-60°C to +85°C	≤ 0.10
Temperature humidity cycling	-10°C to +85°C up to 98% RH	≤ 0.10
Water immersion	23°C ± 2°C	≤ 0.20
Heat aging	85°C ± 2°C	≤ 0.20
Damp heat	85°C at 85% RH	≤ 0.20

Tab 4 Environmental specifications for SMF. [35]

In addition to official fiber optic manufacturers, induced attenuation in temperature-changing environments has been investigated by research groups. The investigation of extreme low-temperature conditions in different coated fibers for avionics applications has been presented in [36]. Different types of SMF with mode field diameters (MFDs) from 6.5 μm to 10.4 μm and numerical aperture (NA) from 0.12 to 0.2 were used with acrylate, silicone and carbon material coatings. Fibers, acclimated to an ambient temperature of 23 °C, were exposed to -196 °C in liquid nitrogen, then to hot steam with a temperature of +122 °C, pressure 220 kPa and humidity 100 %. Results indicate the greatest attenuation at wavelength 1550 nm does not exceed 1 dB/km. Since real optical distance in aircrafts is typically below

100 m and temperature cycling is not as great as in the experiment, maximum fiber attenuation of less than 0.1 dB can be expected. However, aircraft networks are formed by a number of connections which were not taken into consideration.

Another environmental test was carried out in [37] where the temperature dependent characterization for temperature sensing along geothermal wells in Iceland has been described. Distributed Temperature Sensing (DTS), using a backscattered Stokes signal, has been used to find thermal changes along fibers. The paper has shown the measurement of differently coated multimode fibers (MMFs) (50/125 μm). The test was performed on a 20-m-section between two 500-m fiber sections. The measurement was carried out in temperature cycles over a range of -90 $^{\circ}\text{C}$ to 385 $^{\circ}\text{C}$, and from -269 $^{\circ}\text{C}$ to +700 $^{\circ}\text{C}$ for polyimide coating and gold coating, respectively. The test was performed over a 180-hour cycle. The backscattered Stokes signal at wavelength 1064 nm was received to determine induced attenuation. While additional attenuation of the Stokes signal increased up to several dB/km in one heating and cooling cycle between 100 $^{\circ}\text{C}$ and 385 $^{\circ}\text{C}$, in the case of four cycles in a row the attenuation of the Stokes signal exceeded 50 dB/km within polyimide 145 μm coated fiber. However, the polyimide showed better performance in lower temperatures than metal coated fibers.

2.2.2 Test of influences on chromatic dispersion

Another important parameter of optical fibers which influences the quality of the transmitted signal is chromatic dispersion (CD). The temperature distribution along an ultra-long haul transmission link in USA giving an estimation to CD variation has been published in [38]. The authors collected data from the soil climate analysis network to evaluate seasonal temperature drifts. The situation of changes during warm and cold climatic profiles is depicted in Fig. 5 and Fig. 6 [38], respectively. In fact, long-haul optical links are typically buried at a depth of 0.6 m – 1.2 m and the distance typically extends a few thousand kilometers. The thermal data were taken for the depth of about 1 m. Expected peak-to-peak seasonal fluctuation of CD, based on thermal coefficient, was 375 ps/nm for non-zero dispersion-shifted fiber (NZ-DSF) and 570 ps/nm for large-core fiber in the 7500 km link. The maximum recorded fluctuation rate of CD was approximately 3 ps/nm/day over a two-month period for NZ-DSF and 4.8 ps/nm/day for large core fibers. The results provide better knowledge about potential CD drift in old fibers (the paper [38] was published in 2002) and show typical temperature conditions in a buried optical link, which can be applied to other buried optical links.

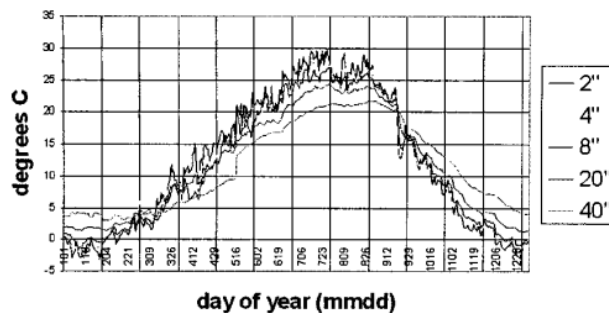


Fig.5. Typical cold-climate profile for various depths. [38]

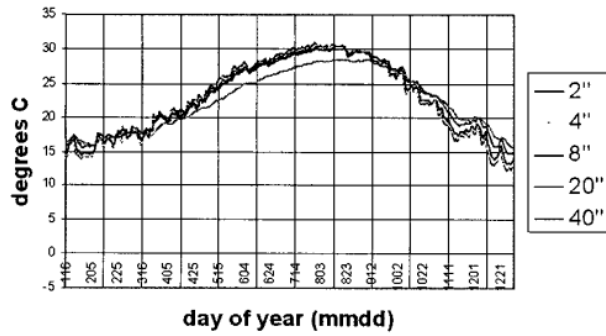


Fig. 6. Typical warm-climate profile for various depths. [38]

The evaluation of system outage probability due to temperature variation and distributed CD was published in [39]. The authors describe outage probability for optical systems using higher bit rate (>40 Gbps) in SMF and NZ-DSF optical fiber links placed in a temperature changing environment. It respects the fact that a long-haul link leads through different regions and experiences temperature variations up to $20\text{ }^{\circ}\text{C}$ and $70\text{ }^{\circ}\text{C}$ in buried and aerial sections, respectively. To ensure real conditions, fibers from several different manufactures were selected and the suitability of 40 Gbps RZ signal transmission was investigated with dependence on temperature variations. Fig. 7 illustrates the standard deviation of residual dispersion caused by temperature variation.

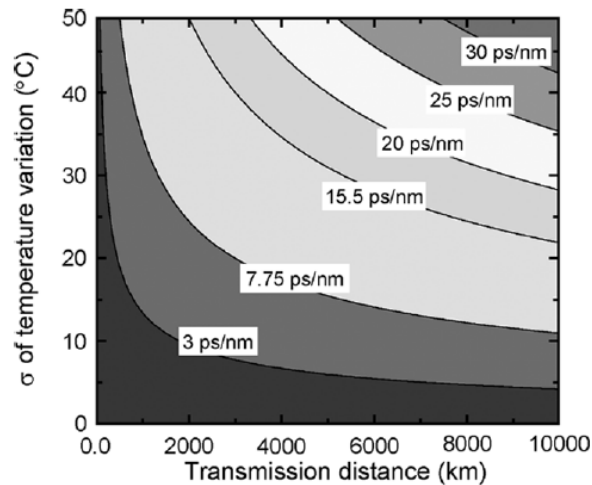


Fig. 7 Temperature variation limits for optical fiber link distances. [39]

It was determined that the outage occurs with a CD-induced penalty of 1 dB (7.75 ps/nm for 40 Gbps RZ) when outage probability does not exceed $5.5 \cdot 10^{-5}$ [39]. Results revealed that the maximum reachable distance for 40 Gbps RZ at wavelength of 1550 nm is limited from 27 km to 148 km, depending on fiber type and considering a dispersion penalty >1 dB.

The effect of temperature on the CD and CD slope of optical fiber was investigated in [40]. Calculations were based on the temperature dependence of silica refractive index which directly influences transmission characteristics. The temperature-dependent CD and CD slope at wavelength of 1550 nm are shown in Fig. 8.

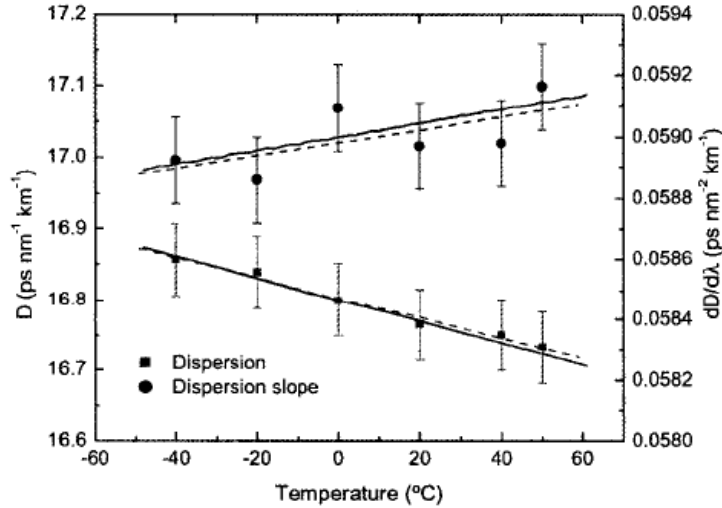


Fig. 8. Theoretical (solid) and experimental (dashed) values for chromatic dispersion and CD slope. [40]

The derived BER for a 40 Gbps signal in a temperature range between -40 °C and 60 °C is depicted in Fig. 9. It clearly demonstrates how CD, which is strongly connected to the material properties, relies on environmental changes and, in particular, on temperature.

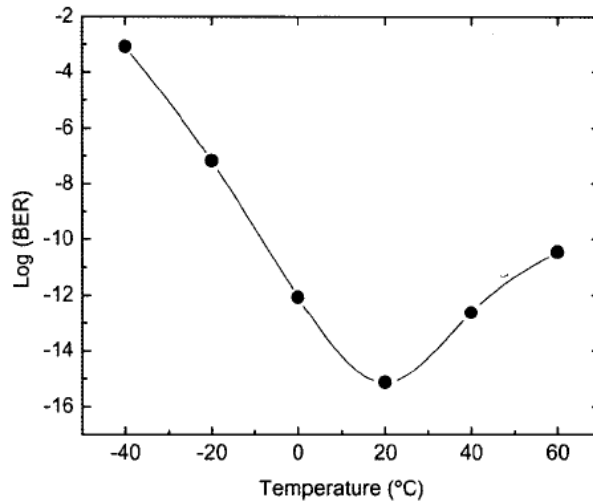


Fig. 9. Chromatic dispersion-induced BER versus thermal changes. [40]

The potential CD limits due to seasonal temperature variations for 40 Gbps and 160 Gbps transmissions at wavelength of 1550 nm for buried SSMF and NZ-DSF were investigated in [41]. Note that the temperature variations were ± 10 °C due to neglecting daily temperature fluctuations for depths greater than 0.6 meter. A high slope NZ-DSF can, however, operate up to 900 km when using a 40 Gbps bit rate, but the same fiber has a limitation of 100 km for 160 Gbps bit rate without any compensation. Results for a variety of distances are shown in Fig. 10.

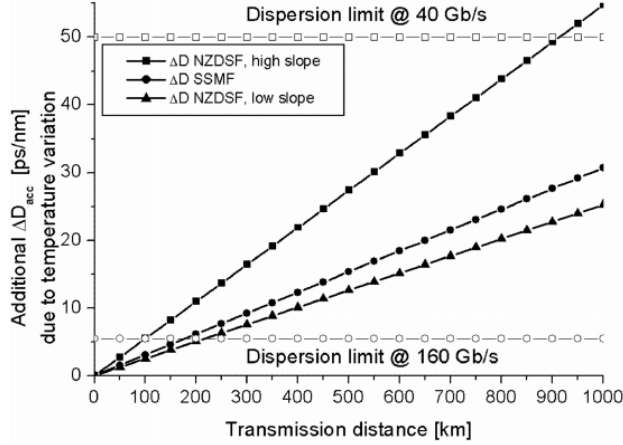


Fig. 10. Additional accumulated dispersion due to $\pm 10^\circ\text{C}$ temperature variations for SSMF, high slope NZDSF and low slope NZ-DSF. [41]

Other relevant works, investigating thermal dependent CD, can be found in [42-44].

2.2.3 Tests of influence on PMD

There are two orthogonally-polarized principal propagation modes in SMF. In an ideal cylindrically symmetrical optical fiber, these two modes are degenerated and they have identical propagation constant. However, in real optical fibers, cylindrical symmetry is not ideal. The two orthogonal modes then propagate with different group velocities due to the birefringence in the fiber. Therefore the polarization mode dispersion (PMD) evinces more sensitive and random behavior, compared to attenuation and CD, mentioned above. Hence, it is important to characterize the optical fiber link precisely, especially when the fiber is placed in a highly temperature variant or a harsh environment. The PMD comes from DGD, from which the mean value is referred to as the PMD [45]. The part concerning PMD is described in more detail to link the main results of the dissertation.

2.2.3.1 PMD measuring techniques

This section focuses on describing PMD measuring techniques which are often utilized in practice for real optical links monitoring and which have been adopted or mentioned in this thesis.

The interferometric methods have good accuracy and sensitivity. The principle of the interferometric methods is based on the measurement of the differential delay between the signals carried by two principal states of polarization (PSPs) using the low-coherent interferometer technique. The traditional interferometric technique (TINTY) [45] uses a Michelson interferometer with a polarization maintaining coupler featuring a 50/50 splitting ratio, a dividing incoming beam at a selected wavelength to two arms with fixed and movable mirrors. Reflected light from the arms are coherent when these two arms have almost the same length. By applying the proper length of the reference mirror, it is then possible to obtain the DGD value from the interference pattern which corresponds to the time when the light offends the given distance.

A General Interferometric technique (GINTY) has been derived from the traditional one in [46], [47]. Unlike the traditional method, the GINTY uses polarization scramblers and, thus, improves absolute uncertainty measurement results. In addition, another polarization splitter is employed to remove any contribution of the autocorrelation peak [48]. This method also boasts accurate measurement when an erbium doped fiber amplifier (EDFA) is included in the trace to make the method generally functional. The GINTY is, moreover, involved in IEC standard 60793 [49]. Fig. 11 shows an example of typical interferometer patterns for two types of fibers.

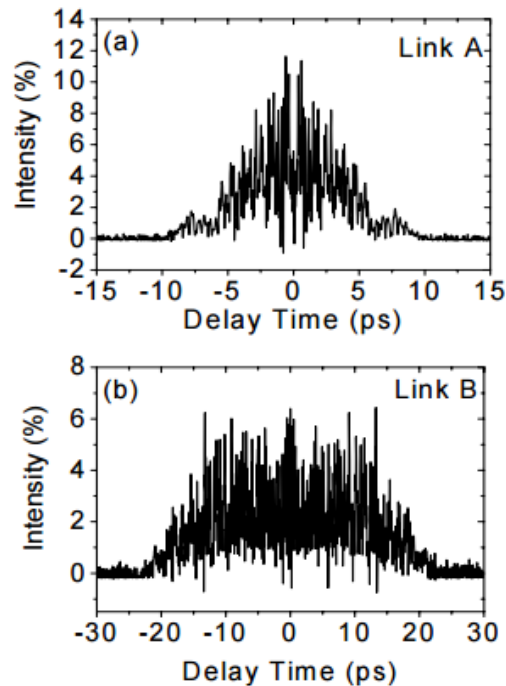


Fig. 11. Example of GINTY interferometer patterns for two links with weaker mode coupling (upper) and stronger mode coupling (lower). [46]

The Jones matrix eigenanalysis (JME) is a comprehensive measurement technique utilizing the placement of fiber-under-test (FUT) between the polarization-defined optical source and polarization detection. The input state of polarization (SOP) is systematically set by the polarizer and then analyzed by the polarimeter. The Jones matrix is generally used for describing polarized states of an optical wave or a passive optical component. The JME's advantage lies in the small number of transmitted wavelengths and easier polarization controlling and polarimeter setting. It is possible to carry out both frequency and time domain measurements [45].

A similar technique, called the Mueller matrix method (MMM), can be used to characterize the wavelength-dependent polarization rotation of an optical fiber. The MMM represents the polarization rotation characteristics of an optical device such as an optical fiber, which is determined by the relationship between a set of input polarization vectors and their corresponding output polarization vectors [45].

The EXFO company has introduced a unique transmission method called the "state-of-polarization scrambling analysis" (SSA) in 2011, which can even be used for measuring DWDM channels [50].

An effective tool for distributed polarization measurements is represented by the polarization-sensitive optical domain reflectometer method (POTDR) [51], [52]. There are two described types of POTDR measurement devices. The first is suitable for the measurement of localized birefringence as a function of distance employing only single wavelength analysis. Distributed PMD is then estimated indirectly from the distributed birefringence vector. It requires very short pulses to resolve a small beat or correlation length of the SOP. The second type allows measurements over a range of wavelengths ensured by a tunable laser. The plural-wavelength analysis enables us to measure cumulative PMD directly as a function of longitude distance z . This mechanism is done by the random-scrambling (RS) approach [52]. Unlike the first method, the second has been adopted more often in industry and brings more benefits for optical network monitoring.

While assuming propagation constants in two orthogonal principle axes β_x and β_y at frequency ω , these constants are different due to birefringence[45]:

$$\Delta\beta = (\beta_x - \beta_y) = \frac{\omega}{c} \Delta n_{eff}, \quad (4)$$

where Δn_{eff} refers to the differential effective refractive index for the two principal propagation modes. The relative group delay (known as DGD) between the orthogonal polarization modes for fiber length L is expressed by:

$$\Delta\tau_g = \frac{L\Delta n_{eff}}{c}. \quad (5)$$

The DGD round trip in position z , observed in PMD distributed measurement, is computed as follows [52]:

$$DGD_{RT}^2(z) = \frac{1}{\delta\omega^2} \alpha_{dT}^2 \Delta T_{ms}, \quad (6)$$

where $\delta\omega^2$ is relative wavelength spacing, α_{dT}^2 relative scrambling factor and ΔT_{ms} is mean-square value of number of wavelength differences. The random-scrambling POTDR scheme is shown in Fig. 12. [52]

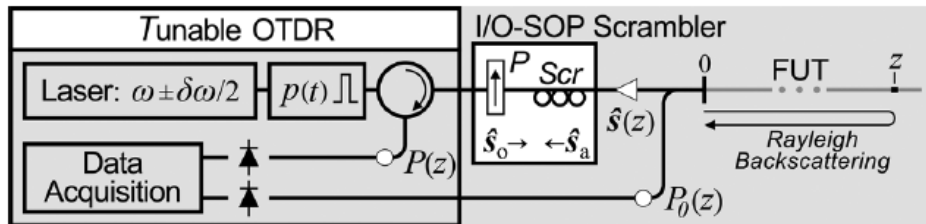


Fig. 12. RS POTDR principle; P- polarizer, S_{cr} - polarization scrambler, $\hat{s}_o(z)$ - launched SOP, $\hat{s}_a(z)$ - analyzer axis, $\hat{s}(z)$ - SOP backscattered at input from z . [52]

An accuracy verification was performed with PMD emulators and different fiber sections in a wavelength range between 1530 nm and 1570 nm in [52]. Total optical length was 18.9 km. Results from this measurement are depicted in Fig 13. The cumulative PMD can be seen from both sides (point A and F) of the link and the "double-side" measurement (A and F together).

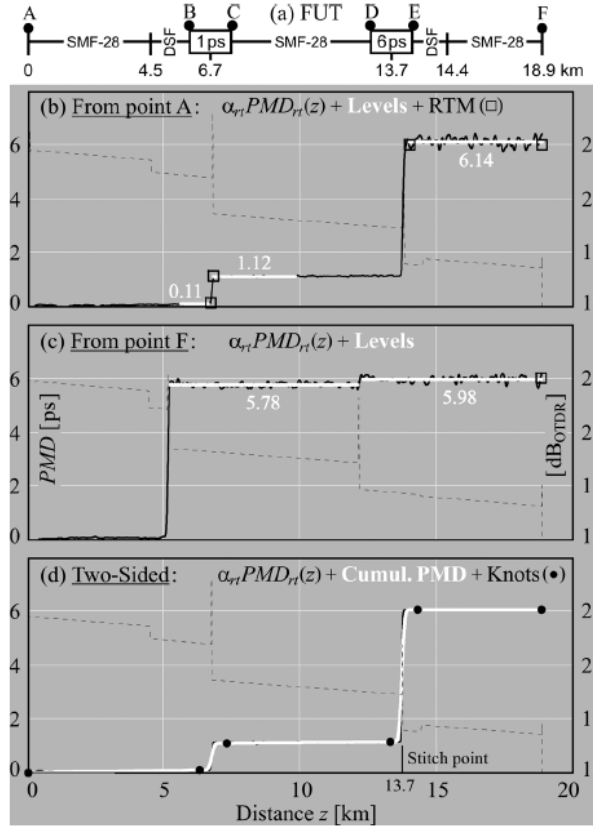


Fig.13 RS-POTDR results a) FUT b) one-side measurement (from A) c) second side measurement (from F) d) two-sided measurement. [52]

Cumulative PMD in [ps] is represented by the y axis, whereas distance in km is represented by the x axis. Note that there is an ordinary OTDR measurement along scrambling performed to detect splices, connectors, etc. Slightly different results in cumulative PMD originate from natural random behavior of the DGD and from the resolution of the equipment.

The P-OTDR method was tested with an EXFO FTB7400 device from Deutsche Telekom on buried fiber traces in [53]. The authors investigated the identification of high PMD sections and their replacement to fulfill demands for 40 Gbps backbone networks. Even the newly buried fibers contained parts with very high PMD, but they can be simply replaced instead of burying the whole route. The same authors then presented a field trial PMD measurement by POTDR in Germany [54].

The techno-economical aspect was taken into consideration in [55, 56] in cooperation with Deutsche Telekom. The papers investigated the process of replacing high PMD sections and concluding that the replacement of the short part of high-PMD fibers significantly reduces costs for the improvement of the fiber infrastructure

2.2.3.2 PMD monitoring campaigns

With increasing demands on optical fiber capacity, especially when considering their structural aging, a long-term PMD measurement with a precise fiber characterization seems to be necessary for reliable transmissions. Moreover, there are no proposed detailed recommendations for long-term PMD monitoring yet. The following results summarize significant published papers in this area.

The MMM was adopted for a two-day measurement of a 150-km-long optical route with a semiconductor optical amplifier (SOA) at a bandwidth of 100 nm, showing a slowly varying long-term structure of DGD spectra [57]. The author published a detailed characterization of installed long-haul buried optical cables by using the interferometric method and summarized experimental data in an empirical outage model [58]. The mean DGD results from February and August, taken from eight suburban buried fibers, are shown in Fig. 14. Although these were buried fibers, the daily fluctuations of the PMD are obvious.

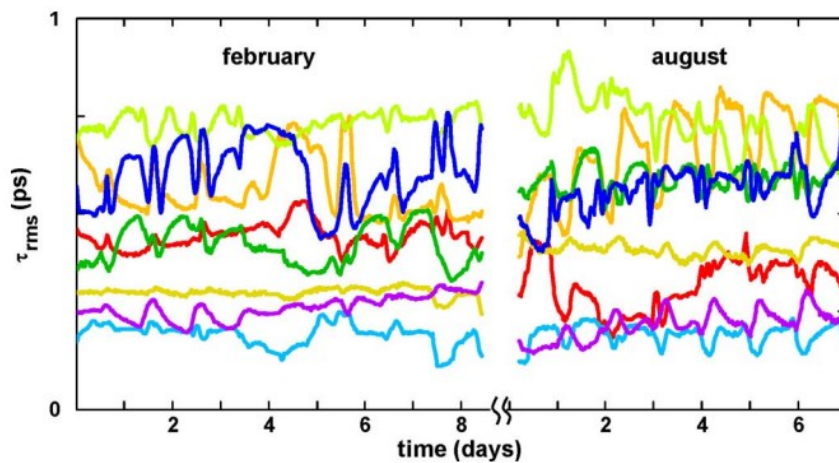


Fig. 14. Mean DGD measurement over 9 days in February and 7 days in August. [58]

Based on these results, the same authors published a new model of temporal dependence of PMD for long fiber links in [59]. Furthermore, the investigation of the accuracy of long-term PMD measurements was published and concluded that some fibers can be characterized during one week, but so called "live" fibers need months or years of characterization [60]. A 25-day PMD measurement with SMF G.652 [61] using the JME method within metropolitan area networks in Turin, Italy, was presented in [62] and demonstrated that mean DGD changes are inherently limited, due to the daily cycle with maximal variations of approx. 10%. The JME method was used to detail a DGD measurement over 35 days on two 127 km-long DSF fibers (zero dispersion at approx. 1548 nm) [63]. The authors then discussed the question of the isotropic distribution of the PMD vector. Data from the DGD measurement are shown in Fig. 15.

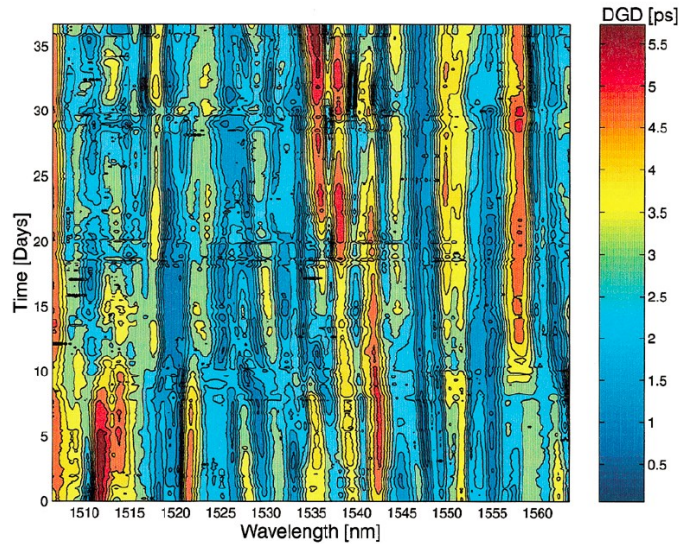


Fig. 15. DGD map for different wavelengths vs. time. [63]

The maximum difference of about 4 ps was observed in a single wavelength during only 15 days. Another interesting measured aspect is polarization drift, induced in both fibers under test (FUT), which is shown in Fig. 16. Polarization angle and mean DGD drift are shown correlating to temperature changes within the Jönköping area in Sweden. [63]

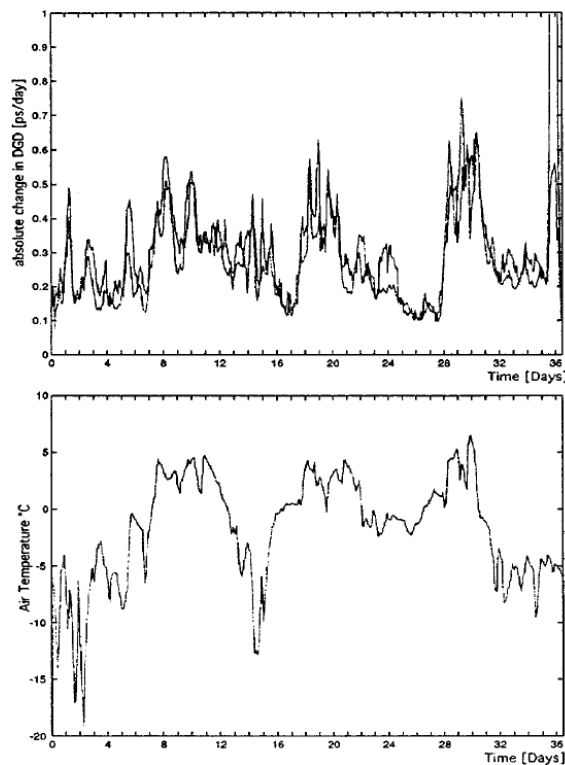


Fig. 16. The PSP change (upper) vs. time for two fibers (solid and dotted curves). The bottom figure plots air temperature in the Jönköping area over the measurement period. [63]

The conclusion in [63] leads to the fact that PMD drift cannot be predicted because it depends on installing performance and service conditions such as the amount of environmental perturbations and disturbances.

A 5-month long-term PMD continuous measurement was performed using the JME method at bandwidths between 1525 nm and 1620 nm with wavelength resolution of 0.05 nm [64]. Two routes, having a length of 79.5 km (#A) and 24.5 km (#B), respectively, were observed. Each measured route contained buried cables with four G.653 fibers, marked #1 to #4. Whereas route #B was completely buried, route #A involved an exposed section at a bridge. Although the exposed section was significantly shorter (several hundred meters) in relation to the overall length, strong daily variation in mean DGD was recorded. The daily variation can be easily seen in Fig. 17a) where the PMD fluctuations of fiber #1 and #2 within route #A are compared to thermal changes for a 10-day measurement. Moreover, Fig. 17b) depicts the autocorrelation function of fibers in route #A and #B showing strong peaks in fiber #1 in route #A (blue curve), which appear in a 24-hour interval when compared to route #B.

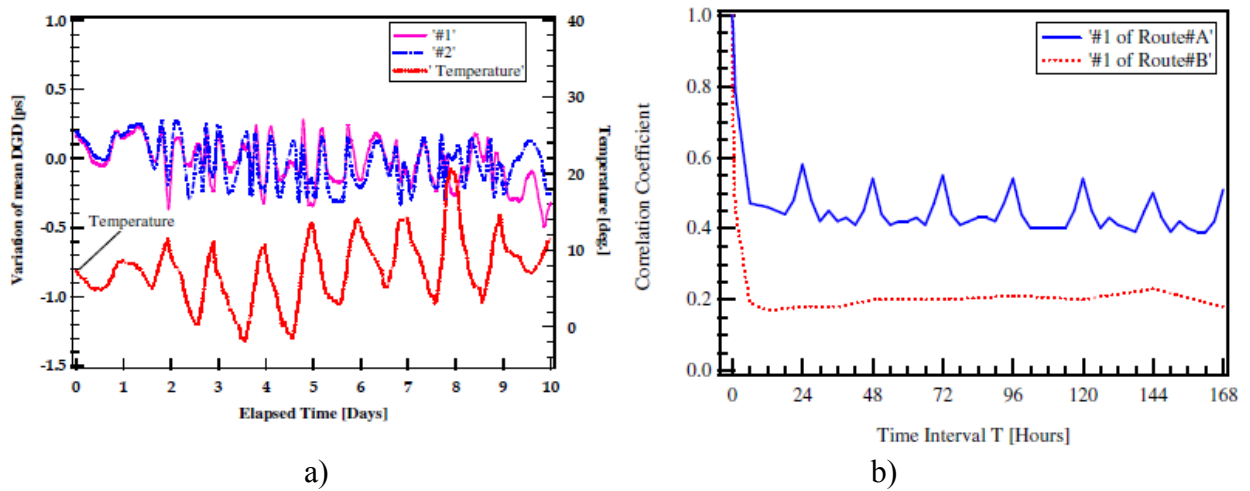


Fig. 17. a) PMD variation vs. temperature b) autocorrelation functions.[64]

The result after 150 days is depicted in Fig. 18.

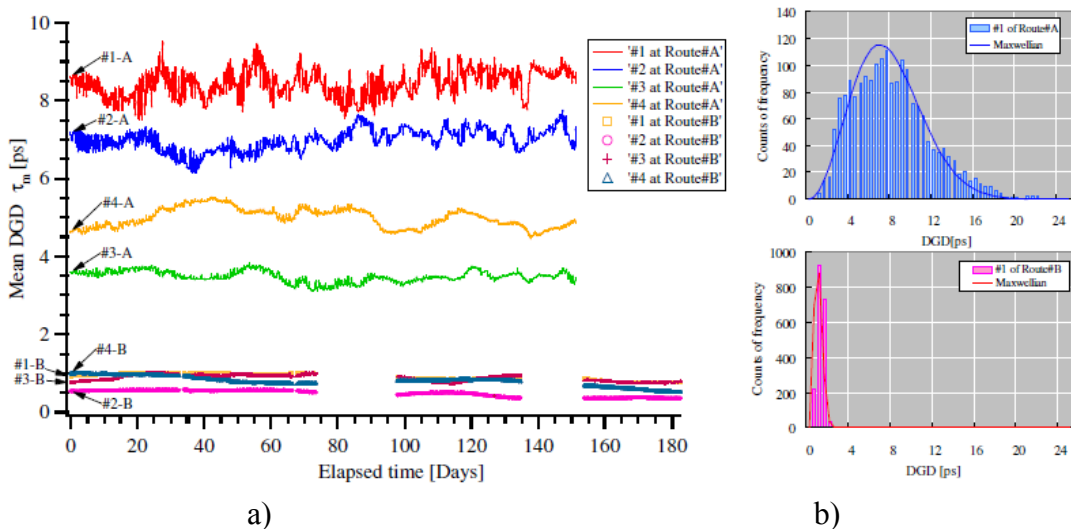


Fig. 18. a) time evolution of mean DGD b) histograms of two routes. [64]

It compares both #A and #B routes with tested fibers. It is obvious that the route with an exposed section evinces significantly higher variation in long-term measurement. The

biggest observed variation in fiber #1-A (red curve) was about 2 ps. However, the completely buried route #B shows minimal long-term variation in PMD. The performed measurement gives a better illustration of how temperature influences PMD changes.

The most detailed long-term PMD measurement to date was an 18-month field observation of SOP and corresponding PMD on three buried fiber links employing 40 Gbps transmissions [65]. Fig. 19 depicts results from long-term observation for 30-km- and 273-km- long fiber routes.

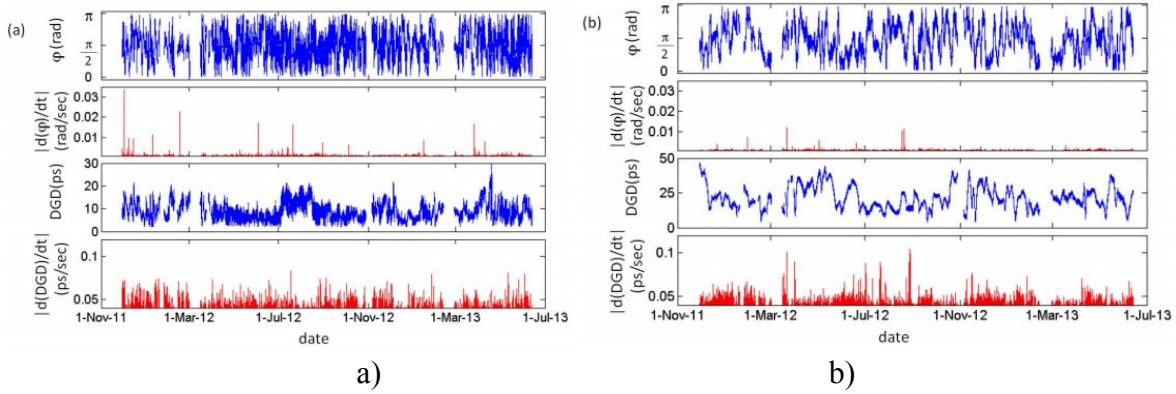


Fig. 19. Long-term SOP and DGD observation for a) short route and b) long route. [65]

It was revealed that SOP and PMD changes were in the order of days and the PMD was given by Maxwellian distribution. However, the longer fiber paths revealed the least activity and no correlation between variation in the SOP and the mean DGD was observed.

PMD thermal characterization was performed in [66] which led to a discussion concerning the accelerated aging process in silica fibers. The experiments were carried out with G.652 fibers using various buffers. The main focus was on optical ground wire (OPGW) cables which commonly operate along 110 kV, 220 kV and 400 kV power lines and have special requirements for the temperature range of -40 °C to 85 °C with occasional thermal shock up to +150 °C due to fault currents. The paper investigated the impact of the buffer material on PMD because high temperature variation can result in the changing of material properties of the buffer (for example shrinking).

Temperature [°C]	Time of measurement	PMD [ps]	Relative value of PMD [%]	Attenuation $\lambda=1550$ nm [dB]
+20	Before ALT No.1	0.076	100	3.69
+85	After 24 h exposure	0.086	114	3.74
+85	After 336 h exposure	0.076	100	3.72
+20	After ALT no.1	0.051	71	3.71
+20	Before ALT No.2	0.051	71	3.69
+85	After 24 h exposure	0.086	114	3.74
+85	After 336 h exposure	0.065	86	3.78
+20	After ALT no.2	0.065	86	3.76

Tab. 5 PMD aging results. [66]

Tab. 5 then shows the results during the accelerated life test (ALT) and PMD and attenuation thermal dependence for fibers inside the OPGW. The delay between the first and second ALTs was several months and during this time the cable was stored at room temperature with medium humidity (45% - 75 %).

We can see a maximal PMD increase of 14 % after 24-hour exposure to 85 °C. Attenuation resulted in a stable value at a wavelength of 1550 nm within the range of ± 0.02 dB. Another environmental test was done with G.652 fibers in primary coating and 0.99 mm cured tight buffer. High thermal shock is further shown in Fig. 20.

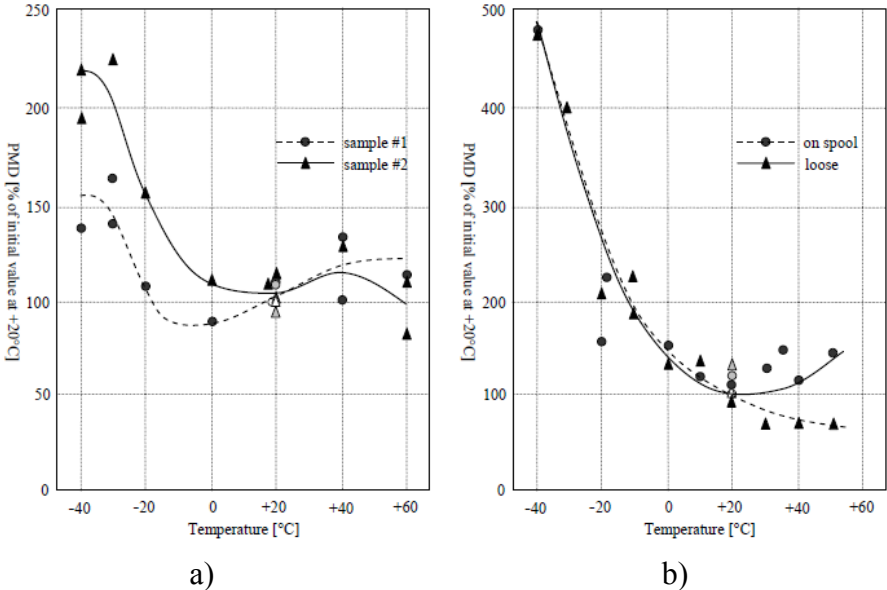


Fig. 20. a) PMD-temperature characteristics from two G.652 fiber samples in primary coating
 b) PMD-temperature characteristic from G.652 fiber in 0.9 mm buffer. [66]

We can observe PMD changes up to 490 % in the case of a 900 μ m tight buffer. Results revealed that PMD can also decrease during the thermal tests due to either frequent perturbation making coupling modes stronger or the fact that buffer pulls the primary coating away and reduces applied pressure. Generally, the primary coated fiber exhibited increased PMD at temperatures below -20 °C. The OPGW revealed better properties in terms of PMD increase during high temperature changes when compared to primary coated fibers. The same test was later carried out with NZ DSFs (ITU-T G.655 [67]) in [68]. The PMD coefficient vs. temperature for G.655 fibers is depicted in Fig. 21.

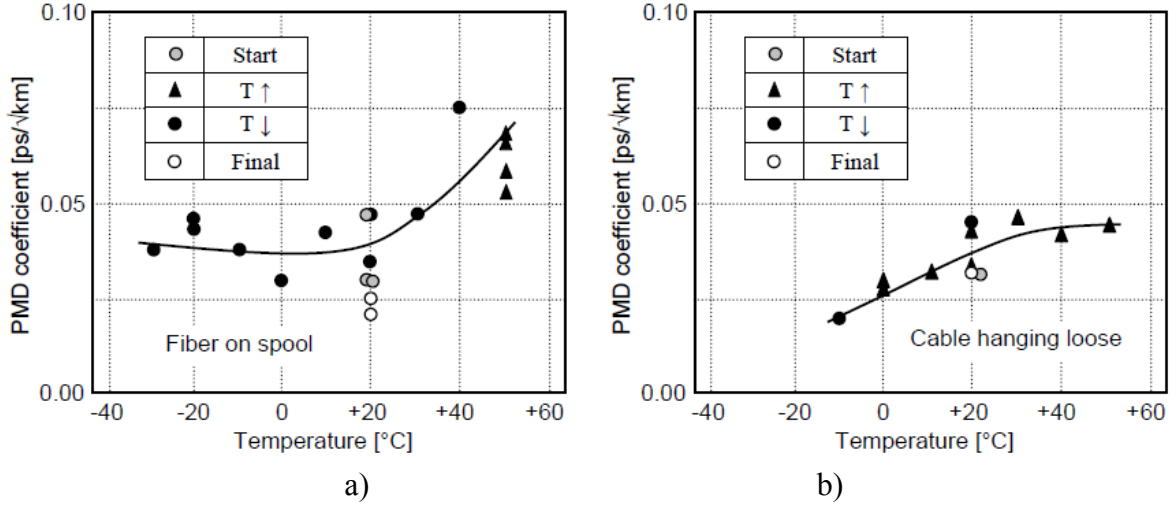


Fig. 21 a) PMD of G.655 fiber in 0.9 mm UV-cured tight buffer as function temperature
b) PMD of G.655 fiber in 2 mm indoor cable as function temperature. [68]

The authors then discussed the enormous PMD values, induced by mechanical forces and explained by a circular (twist) strain which has two effects [68]:

- Generates circular birefringence and a PMD component (k_{PMDS}) proportional to twist rate [68]:

$$k_{PMDS} = 0.065 \sqrt{\frac{h}{1000}} \gamma, \quad (7)$$

where h is mode coupling length expressed in [m] and γ fiber twist rate measured [rev/m].

- Reduces beat length (L_B) and PMD induced by a lateral strain of fixed rotation:

$$PMDRF = \frac{1}{\sqrt{1 + g^2 \left[\left(\frac{L_B}{\lambda_s} \right)^2 + \left(1 - \frac{g}{2} \right) \left(\frac{L_B}{\lambda_s} \right)^4 \right]}}, \quad (8)$$

where $PMDRF$ is PMD reduction factor due to twist, L_B is fiber "natural" beat length, g is elasto-optic coefficient of silica, λ_s is fiber twist pitch in [m]; $\gamma = 1/\lambda_s$. The dependence of $PMDRF$ on λ_s is shown in Fig. 22. The authors concluded that the presence of the circular strain in the core of single mode fiber greatly improves stability of PMD when the fiber is subjected to bending and mechanical pressure, e.g., generated by a tight buffer applied during the manufacturing of the cable.

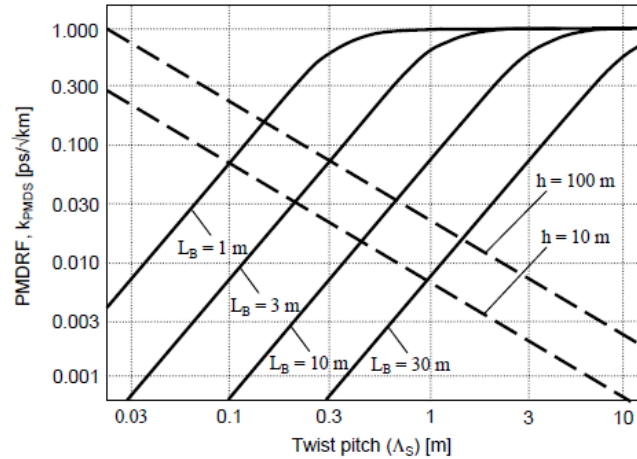


Fig. 22. PMD reduction factor (PMDRF) in twisted SMF (solid lines) and the PMD component resulting from twist (dotted lines). [68]

The same authors published a paper integrating previously mentioned results while focusing on PMD temperature and the aging of optical fibers [69]. It was presented that PMD rises quickly when temperature drops below approximately 0°C and stated that OPWG cables show negligible attenuation change and good PMD stability even in accelerated aging tests.

Several papers have been published on the suitability of high PMD fibers for higher bit rate transmissions and application in high speed WDM systems [70], [71], [72], [73] and [74].

2.2.4 Optical fiber aging

Material properties changes go hand in hand, as discussed previously, with the aging of photonic structures [75]. The changes can be evoked by high optical power which subsequently leads to the potential damaging of the structures [76]. Moreover, optical component aging represents a very specific area with various fields of interest. Mostly the discussion leads to the silica fibers aging process, but it is not necessarily related only to optical fibers - the aging investigation includes passive components as well as optical component shielding materials.

The aging process in all dielectric self-supporting optical fiber cables along high voltage lines was investigated in [77] according to the fact that these cables had been installed since 1979 and true aging had occurred. The authors found a threshold of about 7 kV and 2 mA for the combination of an applied voltage and leakage current, respectively. Note that this work was focused only on material properties and did not investigate any optical characteristics. Another aging test of the whole optical system was published in [78] when performing several tests to determine optical component behavior under damp-heat aging. The components, including a laser source with pigtails and passive optical components, underwent a 600-hour aging test with a temperature range of 80 °C to 140 °C. The rapid increase of insertion loss (IL) of passive components was detected after 168 hours of the aging process. Moreover, it was determined that optical detected power, after 50 hours of recovering, can be restored to ~94 % of the original value. The author summarized that output power and IL, during the test and optical parameter recovery after baking, were attributed to moisture diffusion that resulted in the degradation of physical properties of the

cured epoxy used for the subassembly of the devices. The analysis of optical fibers aging in aggressive reagents was presented in [79]. Silica SMFs were employed in a test with acrylate polymer coating which was chosen to provide outer protection against stressed conditions. Selected fibers were soaked in a tetramethoxysilane solution (TMSO) and dimethyl-sulfoxide (DMSO) reagent for various time. Selected pictures of the soaked fibers are depicted in Fig. 23.

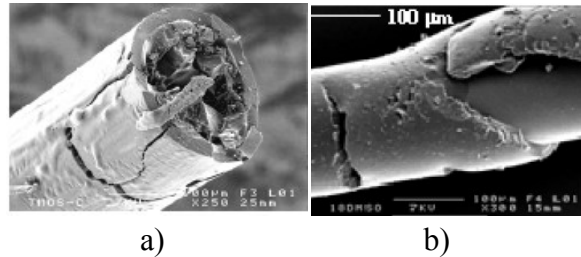


Fig. 23. Photos of fibers aged a) 40 minutes in TMSO b) 18 hours in DMSO. [79]

The impact of a maritime environment on optical fibers aging is described in [80] for 20-cm long SMFs having 250 μm acrylate coating. They were tested in NaCl aqueous solutions with various concentrations for 100 days at a room temperature of 23 $^{\circ}\text{C}$. The process showed that the solution penetrated the fiber coating after some time, depending on the concentrations, and through this process decreased physical resistance. The fracture stress values were fitted to a Boltzmann function - see Fig. 24.

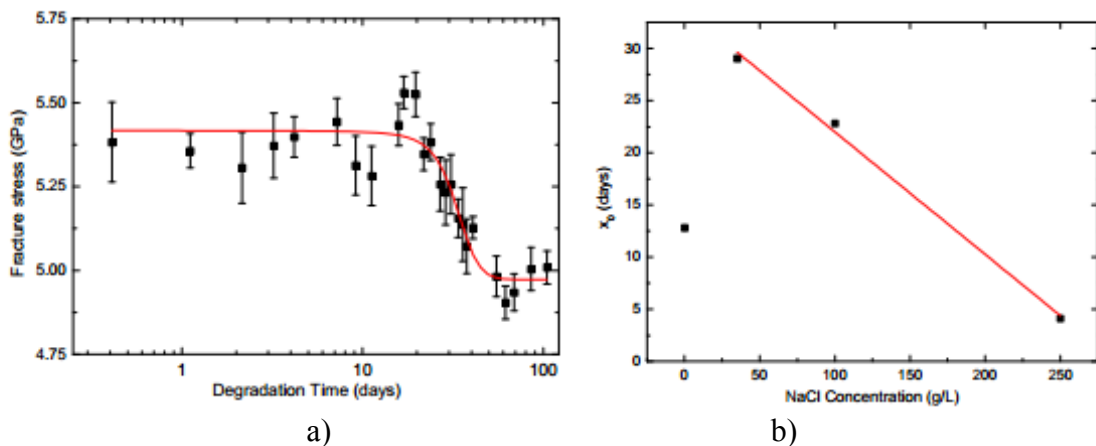


Fig. 24. a) fracture stress as a function of exposure time for 35 $\text{g}\cdot\text{L}^{-1}$ NaCl solution b) fracture transition time as a function of NaCl concentration. [80]

The results imply that for a typical coastal scenario (NaCl concentration of 35 $\text{g}\cdot\text{L}^{-1}$) the decay period is about 29 days. The authors also revealed that the degradation of the fiber due to the diffusion through the acrylate coating also occurs when the fiber is placed in pure water.

The impact of optical fiber aging in a transatlantic transmission system was shown in [81]. The 96 x 10 Gbps DWDM system with 28 nm bandwidth and 50 GHz spacing was utilized over three years. Over 6,550 km cable routes were installed in 2001 and repaired in 2004 on the bottom of the sea from New Jersey, USA to Highbridge, UK. The routes

consisted of DSF with zero dispersion at a wavelength of 1550 nm. The aging process resulted in a negative spectral tilt of the system gain shape as shown in Fig.25. The highest decrease in the gain spectrum was about 2 dB which led to the total degradation performance resulting in diminished OSNR and Q-factor of about 0.3 dB and 0.4 dB, respectively. Fig. 26 depicts the OSNR and Q factor changes due to cable aging.

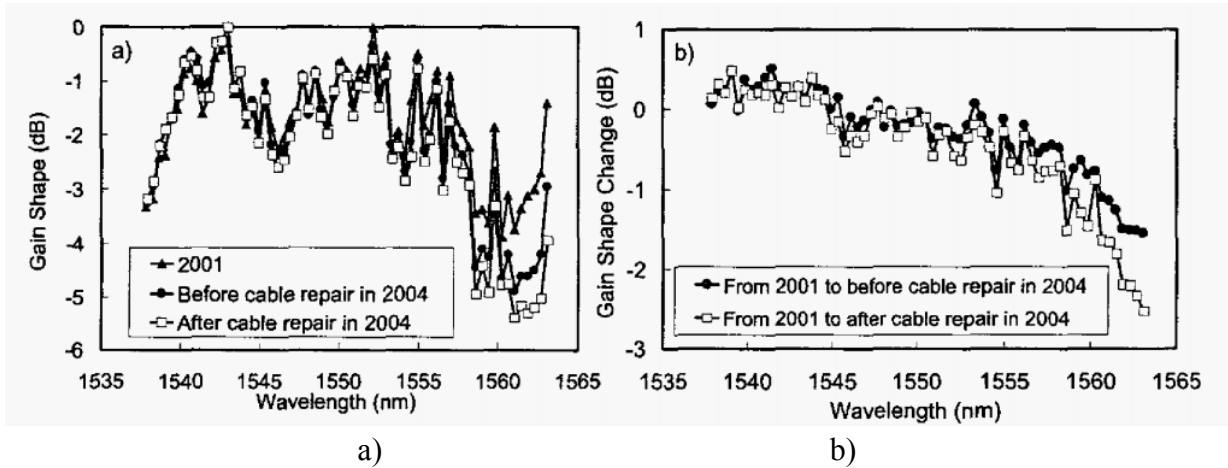


Fig. 25. a) system gain spectrum in 2001, 2004 before and 2004 after repairs b) gain spectrum changes. [81]

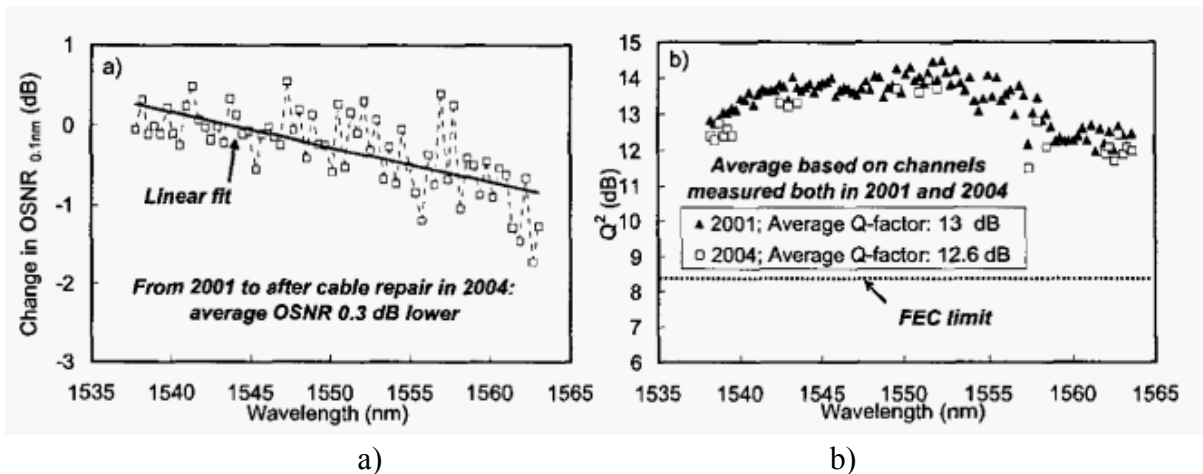


Fig. 26 a) OSNR channel changes from 2001 to the time of repairs in 2004 b) Q-factor versus channel wavelength following the transmission of 96 channels. [81]

The suitability of high speed transmission in long-haul optical links employing an aged fiber structure was presented in [82]. Polarization multiplexed 16-QAM 400G channels with 50 GHz spacing were employed within a 1,504-km long optical link. The authors highlighted the possibility of the systems mentioned deploying in existing long-haul networks by reducing signal degradation during signal propagation and increasing forward error correction (FEC) coding gain. Note that a high coding FEC and all-distributed Raman amplification system played a key role in the experiment.

3 Objectives of the thesis

The previous chapters have revealed that optical infrastructures under harsh environments have not been properly characterized yet. Therefore, this thesis has the following main goals:

- To determine aging processes in old installed optical fibers.
- To study services under harsh conditions to identify potential outages.
- To form a new methodology for the long-term aging process measurements and evaluation.
- To determine the main impact of the aged optical fiber infrastructure under harsh environments on the total fiber-FSO system performance.

In order to achieve these goals, the following milestones have been set:

- A special testbed for optical cables long-term monitoring in a harsh area was established.
- Over three years of continuous measuring of the key optical network parameters has been assembled and a novel statistical model for such optical networks and components with an impact on transmission parameters has been derived.
- Along with long-term measurements, laboratory short-term tests were performed (e.g., to mimic specific harsh environments for aircraft photonic networks).
- A new approach for combined RoF and RoFSO systems to increase link transmission capacity was introduced. Regarding the FSO subpart, turbulence-induced fades had to be determined.
- PMD suppression in dual-polarization (DP) transmission systems has been measured within the special testbed.

4 Achieved results

4.1 Results overview

Results, forming the core of this thesis, have been published in significant scientific journals and international conference proceedings. The main results, forming the following chapters, are in particular five journal papers [J1 – J5] completed by two conference papers [C1][C2]. The full list of the author's publications and citations, including other relevant publications, is then given in Chapter 6.

Chapter 4.2 contains results from the analyses of DP LTE signal transmission over a FSO turbulence channel [J1] which provides the first such evaluation of a DP RoFSO in a turbulent channel. It is determined that the DP signal in RoFSO links significantly increases capacity and does not cause any polarization errors, even under a stronger turbulence regime, which had not been investigated before.

Chapter 4.3 provides extended analyses of DP LTE signal transmission over a combined fiber and FSO channel [J2]. The proposed scenario offers an effective utilization towards C-RAN architecture for mobile networks along with optical fiber infrastructure adopted to FSO links to overcome areas where burying optical cables is difficult or costly. Furthermore, the detailed noise conditions of such a system are investigated. The impact of atmospheric turbulence is also discussed to propose the best system performance. The paper introduces the main results and approaches, whereas consecutive tests with this system can then be found in other published papers (see list of author's publications).

Chapter 4.4 presents evaluations of short-term vibrational and temperature changes in optical fiber infrastructures [J3]. Special examples of harsh environments are then provided for an extreme case of a short MMF link within an aircraft, including several connections which emphasize the evaluation of IL changes and mode field distribution. These two issues are crucial to fulfill requirements on high data rates. Therefore, the paper provides a remarkable relationship between harsh environments and detailed optical mode conditions highlighting the reliability of the optical system.

Chapter 4.5 then extends analyses from Chapter 4.4 courtesy of additional extreme temperature tests for MMF connections for an aircraft photonic network simulating enormous temperature variations along a plane [C1]. The measurements, which are always crucial for the characterization of network reliability and consequent safety, have revealed strong IL dependence on temperature, even for the case of shorter links (less than 20 meters).

Chapter 4.6 describes partial results from the setting of a long-term PMD measurement methodology highlighting the influences of temperature fluctuations in selected measuring intervals [C2]. The results represent the first part of the measurement campaign and, in particular, the optical fibers utilized are characterized in detail.

Chapter 4.7, which reveals the first complete long-term results from the unique measuring testbed [J4], follows. An attenuation increase of 0.15 dB/year has been determined in a 36-km long fiber route which was loaded by high optical power of 27 dBm at 1550 nm. To the best of the authors' knowledge, the longest PMD and attenuation monitoring, so far, is

presented in the paper and provides novel derived statistics. Moreover, three commonly utilized PMD measuring methods were experimentally validated in the testbed. From this experimental setup, strong seasonal fluctuation of PMD in exposed cables, which correspond to bimodal probability distribution, has been derived. The results provide a very helpful methodology for network designers.

Chapter 4.8 then gives the final summary of the achieved results from the testbed providing derived statistics of long-term measurements [J5]. In addition, a method for the estimation of long-term mean PMD variation is provided. The leveraged aged optical infrastructure/testbed (including splitters, couplers, etc.) was further tested with two major types of optical transmission systems. One was the OOK 10 Gbps optical ethernet format and as the second, the previously proposed DP RoF and RoFSO system was utilized. Along with experiments, the infrastructure was, subsequently, analytically investigated in terms of higher modulation formats with bit rates of 100 Gbps and 200 Gbps. Last but not least, the PMD reduction by applying the DP RoF and RoFSO scheme was presented. The article thus forms a comprehensive study on old optical infrastructure behavior, located in harsh environments.

4.2 Characterization of Dual-Polarization LTE Radio over a Free-Space Optical Turbulence Channel

This chapter is a version of published manuscript:

- [J1] J. Bohata, S. Zvanovec, M. M. Abadi and Z. Ghassemlooy, "Characterization of dual-polarization LTE radio over a free-space optical turbulence channel," *Applied Optics*, vol. 54(23), 2015, pp. 7082-7087.

Points pertaining to my PhD thesis:

To build a complex joint fiber and FSO network as part of fronthaul optical network for mobile systems of novel generations, increased capacity with multiplexing access is desired. For such a scheme, at the onset, FSO, involving a DP multiplexed link for the first time, had to be investigated, especially in terms of the crucial fading effect - atmospheric turbulence. It was proved that the DP signal in RoFSO links significantly increases capacity and does not cause any polarization induced error vector magnitude (EVM) increase even under stronger turbulence regime, which had not been investigated before.

Characterization of dual-polarization LTE radio over a free-space optical turbulence channel

J. BOHATA,^{1,*} S. ZVANOVEC,¹ T. KORINEK,¹ M. MANSOUR ABADI,² AND Z. GHASSEMLOOY²

¹Department of Electromagnetic Fields, CTU in Prague, Faculty of Electrical Engineering, Technicka 2, Prague, Czech Republic

²Optical Communications Research Group, NCRLA, Faculty of Engineering and Environment, Northumbria University, Newcastle upon Tyne, NE1 8ST, UK

*Corresponding author: bohata2@fel.cvut.cz

Received 12 June 2015; revised 20 July 2015; accepted 20 July 2015; posted 21 July 2015 (Doc. ID 242873); published 6 August 2015

A dual polarization (DP) radio over a free-space optical (FSO) communication link using a long-term evolution (LTE) radio signal is proposed and analyzed under different turbulence channel conditions. Radio signal transmission over the DP FSO channel is experimentally verified by means of error vector magnitude (EVM) statistics. We demonstrate that such a system, employing a 64 quadrature amplitude modulation at the frequency bands of 800 MHz and 2.6 GHz, evinces reliability with <8% of EVM in a turbulent channel. Based on the results, we show that transmitting the LTE signal over the FSO channel is a potential solution for last-mile access or backbone networks, when using multiple-input multiple-output based DP signals. © 2015 Optical Society of America

OCIS codes: (060.2605) Free-space optical communication; (060.5625) Radio frequency photonics; (010.1330) Atmospheric turbulence; (060.2310) Fiber optics.

<http://dx.doi.org/10.1364/AO.54.007082>

1. INTRODUCTION

The fourth generation of digital cellular systems, currently being adopted for mobile networks, will provide users with rapid data transfer capabilities and improved mobility requirements. In addition, the long-term evolution (LTE) advanced technology is being deployed to meet the demands for significantly higher data rates [1,2]. In developing network infrastructures, a number of backbone sections are realized via the radio-over-fiber (RoF) technologies. In such networks, optical fiber (OF) based systems play an inseparable role, offering high transmission capacity, low attenuation, and reduced cost. The RoF technology allows radio frequency (RF) signals to be centralized and distributed via OF to the remote access units (RAU). To increase the link capacity and implement the advanced network features (i.e., dynamic resources allocations, etc.), the wavelength division multiplexing (WDM) technique has been adopted [3]. Such an approach utilizes advanced classical radio wireless schemes, including direct transmission through the antenna arrays, wide-frequency scales ranging up to millimeter waves and terahertz systems, photonics and optical signal processing, etc. [4].

In [5], the RoF technique, together with the complete transmission system, was demonstrated for frequencies up to 120 GHz. In [6], it was shown that transmission of LTE signals over the OF backhaul can generally improve power and cost effectiveness of the radio network. RoF techniques are also used in distributed antenna systems (DAS) with centralized joint

signal processing functionality, and their utilization in micro-to femto-cell deployment, in particular, was reported in [7]. A comparison of directly and externally modulated RoF schemes, together with OF nonlinear compensation, was described in [8]. The authors in [9] investigated the suitability of three types of RoF links (directly modulated laser, Mach-Zehnder modulator (MZM) and reflective semiconductor optical amplifier) focusing on the link parameters (i.e., gain, noise and maximum input power). The authors used orthogonal frequency division multiplexing (OFDM) together with employing higher-order modulations at a frequency of 1 GHz for the cellular systems. In [10], an experimental investigation using RAUs and a microwave amplifier for RoF LTE and WLAN systems was reported.

One possible optical scheme that improves the efficiency of optical communications is based on polarization division multiplexing (PDM). This offers the increased transmission capacity, as different modulated signals are transmitted over the orthogonal states of polarization (SOP) of the same light beam [11]. In PDM, the two orthogonal SOPs can be detected using two identical photodetectors to obtain the modulated signals independently, provided orthogonality is maintained throughout the link. The SOP can be temporarily degraded during light propagation in optical networks, particularly when exposed to changes in the ambient temperature [12]. The experimental distribution of polarization multiplexed 3GPP MIMO LTE signals using MZM is reported in [13]. For the RoF link

employing quadrature phase shift keying (QPSK) mapping, the evolved universal terrestrial radio access (E-UTRA) frequency bands of 2.6 GHz and 800 MHz were used for the transmission span up to 100 km. In [14], a PDM RoF system for passive networks using OFDM-based ultra-wideband (UWB) signals was reported. In this scheme, the main investigated parameter was the polarization cross talk between the polarization multiplexed channels (with the highest achieved polarization discrimination of ~ 30 dB [14]). The experimental results showed that 4 dB of an additional polarization cross-talk-induced interference could be translated to 2.4 dB of the EVM penalty in OFDM UWB signals [14].

The urban areas are characterized by a high concentration of buildings and, thus, are more complex and costly to be connected using the combination of RAUs and the RoF technology. In such environments, the deployment of wireless technologies (RF and optical) to interconnect RAUs may be the most effective solution. Furthermore, the network throughput can be improved by adopting the FSO technology, which offers a high data-rate capability and much reduced RF interference. The radio over an FSO (RoFSO) system, operating at 1550 nm wavelength for transmitting integrated services broadcasting terrestrial signals over 1 km of free-space channel (FSC) with assessment of the link reliability under different environmental conditions was investigated in [15]. One of the main constraints in FSO systems is the atmospheric turbulence, which leads to amplitude fluctuations and phase distortion of the propagating optical beam [16–18]. In optical transmissions, the polarization states of the propagating optical beam are the most stable properties. The influence of atmospheric scattering on polarization qubits for Earth to satellite-based quantum communications based on the vector Monte Carlo simulation has been reported in [19]. Results showed that polarization qubits are well preserved in the uplink and downlink. In [20], it was shown that the polarization states can be maintained over a long propagation link. In [21], it was demonstrated that, under turbulence regimes, FSO links employing multilevel polarization shift keying combined with the diversity techniques offered improved error performance.

The performance of OFDM-based RoFSO links, in terms of the bit error rate (BER) and the outage probability in a turbulence channel, was studied in [22]. The suitability of the RF signal transmission over an FSO link was analyzed in [23], whereas [24] outlined the analytical investigation of RF wide-band code division multiple access signal transmission over a turbulent FSO link. The authors also introduced a dense WDM-based RoFSO system, which is capable of transmitting multiple RF signals for ubiquitous wireless services [25].

As outlined above, there is the need to combine state-of-the-art technologies with commonly used mobile radio services and carry out system utilization analyses using OF as well as the optical wireless technologies for the last-mile and last-meter access networks or as part of the backbone network infrastructure. In this work, we propose a DP-LTE-based RoFSO communication system and verify its performance experimentally in terms of the EVM under turbulence regimes. An extensive measurement campaign is conducted, and results show that the proposed system offers a higher transmission capacity by transmitting two independent signals using the same RF and wavelength. This paper is organized as follows: Section 2 outlines the experimental setup for LTE over fiber and FSO and the supporting theoretical background to turbulence. In Section 3, results of several tests especially focused on turbulence aspects are presented and discussed. Concluding remarks are given in Section 4.

2. MEASUREMENT SETUP

The block diagram of the experimental setup for the proposed DP-RoFSO system is depicted in Fig. 1. The system is composed of two orthogonally polarized optical signals, both combined and optically amplified prior to being transmitted through the turbulence channel and detected independently at the receiver (Rx). The transmitter (Tx) side features a common single wavelength (1550 nm) distributed feedback (DFB) laser source, which is used to ensure the same spectral profile for polarization multiplexing. Note that using two light sources would lead to spurious intermodulation products and a

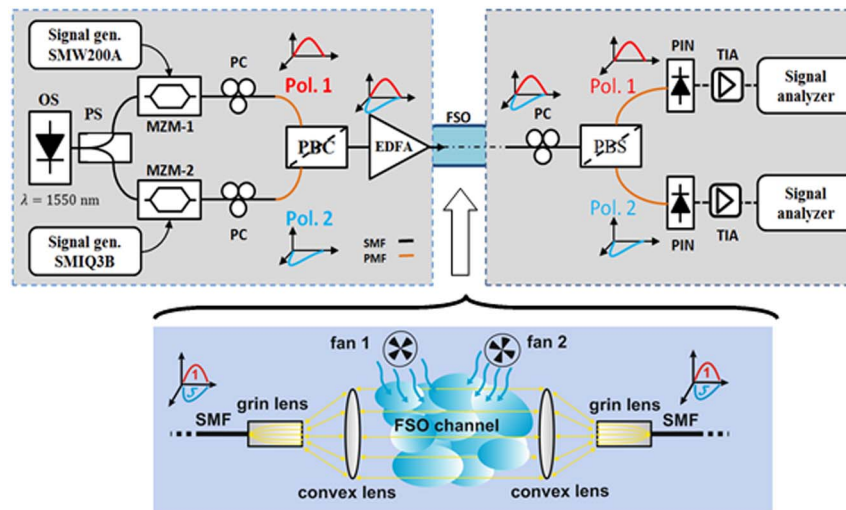


Fig. 1. Block diagram of the DP-RoFSO system using two polarizations.

mismatch in the output spectrum. The output of the DFB laser is split into two using a power splitter (PS), and then the separated outputs are transmitted via a single-mode fiber (SMF) to two external MZMs. MZM1 is modulated by the LTE EUTRA test signals (signal LTE generator R&S SMW 200A) with frequency division duplex (FDD), whereas MZM2 is modulated by the 64-QAM (quadrature amplitude modulation) RF signal (R&S SMIQ 03B signal generator). The same carrier frequencies and bandwidth were chosen for both signal generators to represent different RF services in each channel (both were tested at frequencies of 800 and 2.6 GHz). The modulated signals at the outputs of MZMs were adjusted using polarization controllers (PC) to achieve the desired orthogonal SOP prior to being combined by a polarization beam combiner (PBC). The outputs of PCs are labeled as polarization states 1 and 2 (POL1 and POL2). The output of the PBC is then amplified using an erbium-doped fiber amplifier (EDFA) to compensate for the loss experienced by the optical beam propagating along the FSC. The amplified optical signal is launched into FSC by means of a gradient-index (GRIN) lens with an aperture of 1.8 mm and a plano-convex lens with a diameter of 25.4 mm. At the Rx, the same plano-convex lens with a GRIN lens is employed to launch the optical beam back into the SMF. A PC is utilized to adjust the polarization conditions and followed by a polarization beam splitter (PBS), which separates POL1 and POL2. POL1 and POL2 are then detected by PIN photodiodes followed by transimpedance amplifiers (TIA) (New Focus 1544-B-50). The outputs of TIAs are captured and analyzed using a real-time spectrum analyzer (R&S FSVR). The main system parameters are summarized in Table 1.

The SOP can be defined by using Stokes parameters and represented in the Poincaré sphere. Prior to FSO turbulence measurements, we experimentally validated the polarization orthogonality using the Thorlabs PAX5720 polarimeter. Measured orthogonal polarization of both channels in the Poincaré sphere is shown in Fig. 2. The polarization diversity in both channels was controlled by setting the two different carrier frequencies at each signal generator output and then switching between the Rx output branches and observing the power difference between the two signals. The smallest difference between the two carriers, in the available orthogonally polarized states, was over 36 dB. Therefore, in such a scenario

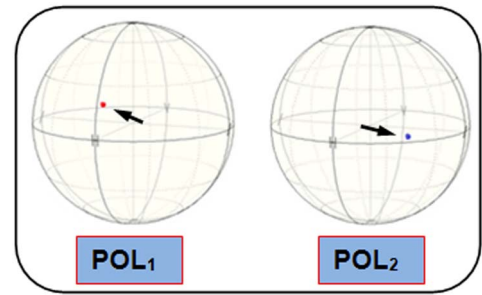


Fig. 2. Measured orthogonal polarization representation in Poincaré sphere observed at two signal branches.

with RF signals having the same frequency, the interference can be greatly reduced.

The most common parameter used to qualify the effect of turbulence is the scintillation index σ_I^2 which is defined as the normalized irradiance variance of the optical beam intensity I , as given by [26]

$$\sigma_I^2 = \frac{E[I^2] - E[I]^2}{E[I]^2}, \quad (1)$$

where $E[\cdot]$ denotes the expected value of optical intensity. In a weak turbulence regime, the behavior of channel fading is modeled by log-normal distribution [27] and σ_I^2 and variance of irradiance σ_x^2 related as [28]

$$\sigma_I^2 = \exp(4\sigma_x^2) - 1 \cong 4\sigma_x^2. \quad (2)$$

Knowing the thermal distribution along the FSO path, it is possible to determine the temperature structure constant C_T^2 , which depends on the temperature difference between two selected adjacent thermal sensors ($T_1 - T_2$) distant by L_p as [28]

$$C_T^2 = (T_1 - T_2)^2 / L_p^{2/3}. \quad (3)$$

The refractive index structure parameter C_n^2 is given as [27]

$$C_n^2 = \left(79 \times 10^{-6} \frac{P}{T^2}\right)^2 C_T^2, \quad (4)$$

where P is the atmospheric pressure in millibar, and T is the average temperature in Kelvin. The variance of log-intensity signal fluctuation defined by Rytov variance σ_R^2 is given by [26]

$$\sigma_R^2 = 1.23 k^2 C_n^2 L^3, \quad (5)$$

where $k = 2\pi/\lambda$ is the wavenumber, and λ is the transmission wavelength.

There are a number of methods for generating turbulence, including near-index matching, liquid-filled chambers, spatial light modulators, ion-exchange phase screens, surface etching, and hot air chambers [29]. For testing the proposed scheme, we have adopted the latter and used an artificial turbulence generator with known, realistic, and repeatable characteristics and low cost. Two fans were used to blow hot air into the channel perpendicular to the propagating optical beam. To measure the temperature profile and determine the temperature gradient along the channel, we placed 10 thermal sensors at an interval of 18 cm (see Fig. 3). Convex lenses, which were used for launching and coupling light at the Tx and Rx ends, are also shown in Figs. 3(a) and 3(b), respectively.

Table 1. Setup Parameters

Parameter	Value
Carrier frequencies	800 MHz and 2.6 GHz
System bandwidth	10 MHz
RF output power	-5 dBm
Modulation scheme	16- and 64-QAM
LTE test model	TS 36.104 FDD
DFB laser output power	8 dBm
Wavelength	1550 nm
FSO channel length	1.9 m
FSO channel loss	15 dB
PIN responsivity	0.9 A/W
TIA bandwidth	12 GHz

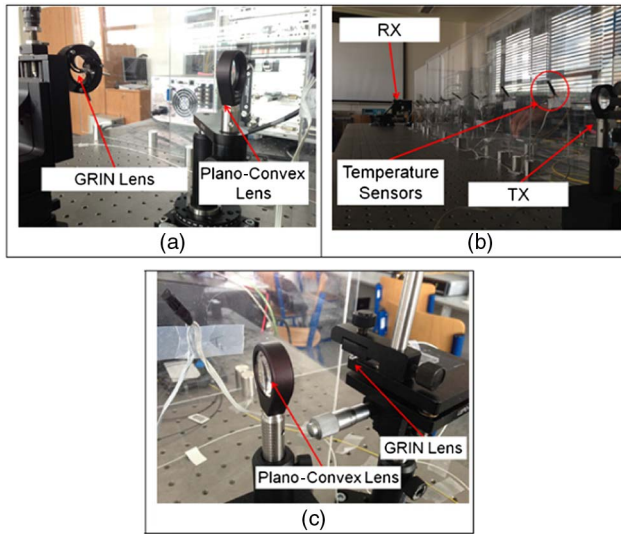


Fig. 3. FSO (a) Optics used at the Tx. (b) Channel with temperature sensors. (c) Optics used at the Rx.

3. RESULTS AND DISCUSSION

The experimental investigation was focused on testing the LTE signal, including advanced modulation formats for various turbulence regimes on the edge of reliability in one channel, while the second RF channel was operating at the same frequency but at a different polarization state. We used the 800 MHz and 2.6 GHz frequency bands for LTE technology in the Czech Republic with a bandwidth of 10 MHz.

To determine the channel properties, we selected two LTE EUTRA models from the 3GPP Group [30], known as the E-UTRA Test Model 2 (E-TM2) and E-UTRA Test Model 3.2 (E-TM3.2). The E-TM2 is typically adopted to determine the dynamic range of a system employing OFDM with a minimum transmit power and uses the 64-QAM modulation scheme with a tolerance limit of reliability 8% for EVM. The E-TM3.2 model is used to investigate the quality of the transmitted signal, particularly using 16-QAM modulation with 12.5% of the EVM tolerance limit. Figures 4 and 5 depict the measured EVM against the refractive index structure parameter at an RF carrier of 800 MHz for 16- and 64-QAM and for E-TM2 and E-TM3.2 test models, respectively. The dashed red lines show the average EVM limits of 12.5% and 8% for 16- and 64-QAM, respectively; the dark blue line

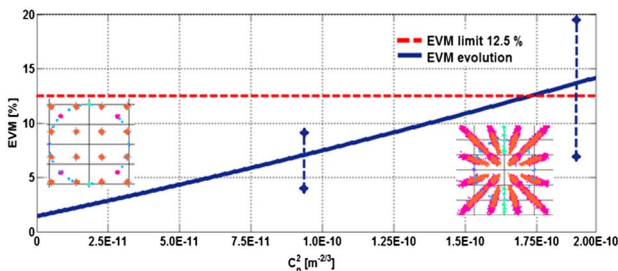


Fig. 4. EVM dependence on C_n^2 for 16-QAM at 800 MHz (E-TM3.2).

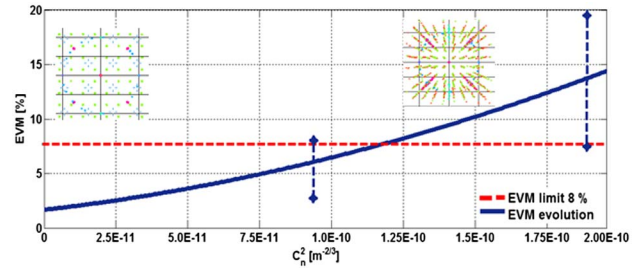


Fig. 5. EVM dependence on C_n^2 for 64-QAM at 800 MHz (E-TM2).

represents the evolution trend of EVM, which deteriorates with the strength of the turbulence regime. The inset figures show the captured constellation diagrams for the channel without turbulence and under the influence of very strong turbulence. Note that the testing procedure was used in parallel as well as other pilot subchannel signals having different modulations (other points drawn at the background of insets). However, the EVM results were obtained for 16- and 64-QAM only. Under laboratory conditions and using a short FSC span, values of C_n^2 induce cumulated small-scale scintillation and Rytov variance. In this work, for $L = 1.9$ m and $\lambda = 1550$ nm and using Eq. (4), the range of values for C_n^2 from $2.5E - 11$ to $2.0E - 10$ (see Figs. 4–7 and 9) are interpreted to σ_R^2 in the range of 0.0051–0.0408 and are, thus, clearly classified as the weak regime. This is in line with the work reported on scaling of the weak and strong turbulence dependency on the propagation span in [28].

Figures 6 and 7 show the measured EVM against the refractive index structure parameter for the RF carrier frequency at

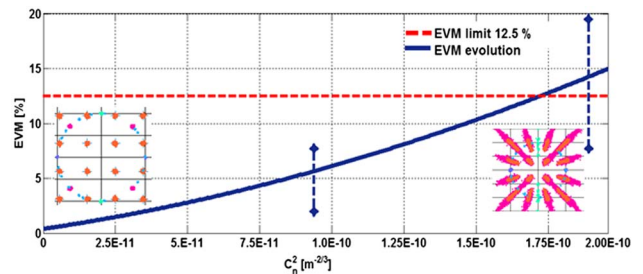


Fig. 6. EVM dependence on C_n^2 for 16-QAM at 2.6 GHz (E-TM3.2).

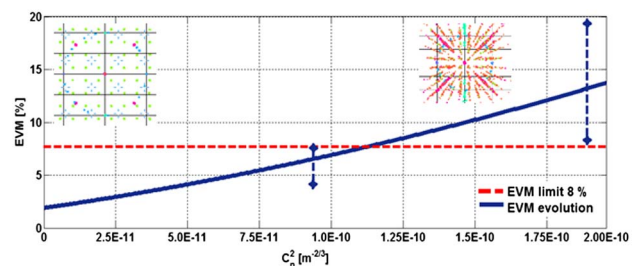


Fig. 7. EVM dependence on C_n^2 for 64-QAM at 2.6 GHz (E-TM2).

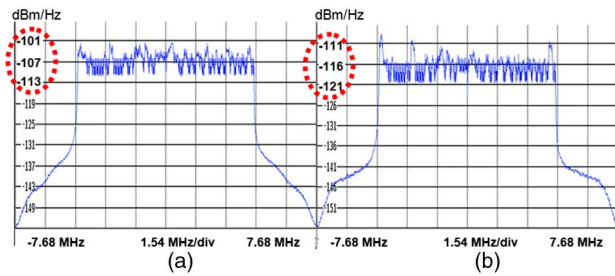


Fig. 8. LTE 10 MHz spectra for (a) a clear chamber and (b) with strong turbulence.

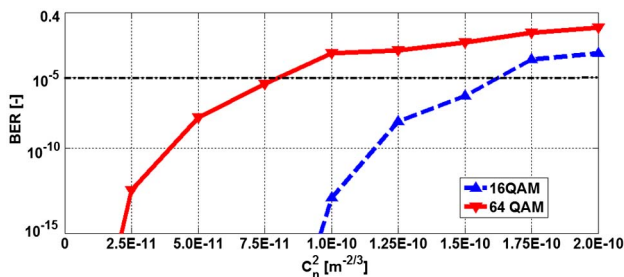


Fig. 9. BER versus C_n^2 for 64 and 16 QAM at 2.6 GHz.

2.6 GHz for E-TM2 and E-TM3.2 test models, respectively. The EVM parameter in the LTE signal demonstrates the link's stability for the case of a clear chamber without the influence of the second orthogonally polarized signal. We tested the system with and without the POL2 signal and observed no change in EVM for POL1. For both test models in a clear chamber without turbulence, the magnitude of EVM was determined to reach 2% or better. At higher turbulence levels (range of $C_n^2 \sim 10E - 10 \text{ m}^{-2/3}$) we observed strong fluctuations along the entire frequency bandwidth and the corresponding averaged EVM, as shown in Figs. 5–8 (blue dashed lines), which also led to the loss of synchronization.

The measured frequency spectra of the LTE signals are depicted in Fig. 8 for the channel with and without turbulence. With high turbulence, the spectrum in the RF domain displays increased fluctuation and a mean level drops by ~ 10 dB.

The evolution of EVM is associated with the BER performance under increased turbulence regimes as captured in Fig. 9, which shows the predicted BER (determined from interpolated EVM data) as a function of C_n^2 for 16- and 64-QAM at a frequency of 2.6 GHz. For the lower range of C_n^2 , the system displays lower BER performance; however, at higher values of C_n^2 , the BER increases rapidly, thus exceeding the error limit of $10E - 5$ at C_n^2 of approximately $7.5E - 11 \text{ m}^{-2/3}$ and $1.6E - 10 \text{ m}^{-2/3}$ for 64- and 16-QAM, respectively. Therefore, higher turbulence levels lead to the loss of link synchronization and, consequently, cause the outage of the RoFSO system. Finally, we tested the system at 800 MHz and 2.6 GHz under turbulence regimes and did not observe any significant differences between them.

4. CONCLUSION

This paper proposed and experimentally evaluated a dual polarized RoFSO LTE system. The averaged EVM parameter was monitored, thus displaying higher stability ($<2\%$) in the order of tenths of percentage points during the steady-state condition without the need for polarization maintaining fibers. Thus, the proposed system becomes more universal but at a cost of increased sensitivity to polarization of the propagating optical beam. We showed that, under the turbulence regime with a refractive index structure parameter of $\sim 1.0E - 10 \text{ m}^{-2/3}$, the proposed system tolerated higher levels of signal fluctuation and achieved the required EVM limit of 8% for the 64-QAM modulation scheme. The combination of polarization multiplexed RF signals, together with WDM in a wireless optical medium, promises to be an attractive solution for future wireless network convergence. The next logical step for extending the current work would be to experimentally assess the RFoFSO link performance under the medium to strong turbulence regimes by means of adopting adaptive optics schemes, which is rather effective in combating the phase distortions, in order to validate the analytically predicted results reported in [18].

Funding. European Cooperation in Science and Technology Action IC 1101 OPTICWISE; SGS14/190/OHK3/3T/13.

Acknowledgment. The authors would like to thank Rohde & Schwarz–Praha, s.r.o. for the technical support.

REFERENCES

- S.-C. Shin and Y.-P. Lee, "Testing of early applied LTE-Advanced technologies on current LTE service to overcome real network problem and to increase data capacity," in *15th International Conference on Advanced Communication Technology (ICACT)*, PyeongChang, 2013, pp. 275–281.
- S. Kanchi, S. Sandilya, D. Bhosale, A. Pitkar, and M. Gondhalekar, "Overview of LTE-A technology," in *Global High Tech Congress on Electronics (GHTCE)* (IEEE, 2013), pp. 195–200.
- T. Kanesan, N. Wai Pang, Z. Ghassemlooy, and L. Chao, "Experimental full duplex simultaneous transmission of LTE over a DWDM directly modulated RoF system," *J. Opt. Commun. Netw.* **6**, 8–17 (2014).
- C. H. Lee, *Microwave Photonics* (CRC Press, 2006).
- A. Hirata, M. Harada, and T. Nagatsuma, "120-GHz wireless link using photonic techniques for generation, modulation, and emission of millimeter-wave signals," *J. Lightwave Technol.* **21**, 2145–2153 (2003).
- S. Aleksic, M. Deruyck, and W. Joseph, "Energy efficiency of optically backhauled LTE: a case study," in *Electromagnetics in International Conference on Advanced Applications (ICEAA)*, Torino, 2013, pp. 390–393.
- N. J. Gomes, P. P. Monteiro, and A. Gameiro, *Next Generation Wireless Communications Using Radio Over Fiber* (Wiley, 2012).
- T. Kanesan, W. P. Ng, Z. Ghassemlooy, and C. Lu, "Investigation of optical modulators in optimized nonlinear compensated LTE RoF system," *J. Lightwave Technol.* **32**, 1944–1950 (2014).
- D. Wake, A. Nkansah, N. J. Gomes, G. de Valicourt, R. Brenot, M. Violas, L. Zhansheng, F. Ferreira, and S. Pato, "A Comparison of radio over fiber link types for the support of wideband radio channels," *J. Lightwave Technol.* **28**, 2416–2422 (2010).

10. A. Urzedowska, K. Godziszewski, and Y. Yashchyshyn, "Radio-over-fiber link for WLAN and LTE systems," in *19th International Conference on Microwave Radar and Wireless Communications (MIKON)*, Warsaw, 2012, pp. 674–677.
11. M. I. Hayee, M. C. Cardakli, A. B. Sahin, and A. E. Willner, "Doubling of bandwidth utilization using two orthogonal polarizations and power unbalancing in a polarization-division-multiplexing scheme," *Photon. Technol. Lett.* **13**, 881–883 (2001).
12. L. J. Cimini, I. M. I. Habbab, R. K. John, and A. A. M. Saleh, "Preservation of polarisation orthogonality through a linear optical system," *Electron. Lett.* **23**, 1365–1366 (1987).
13. M. Morant, J. Prat, and R. Llorente, "Radio-over-fiber optical polarization-multiplexed networks for 3GPP wireless carrier-aggregated MIMO provision," *J. Lightwave Technol.* **32**, 3721–3727 (2014).
14. M. Morant, J. Pérez, and R. Llorente, "Polarization division multiplexing of OFDM radio-over-fiber signals in passive optical networks," *Adv. Opt. Technol.* **2014**, 269524 (2014).
15. C. B. Naila, K. Wakamori, M. Matsumoto, A. Bekkali, and K. Tsukamoto, "Transmission analysis of digital TV signals over a Radio-on-FSO channel," *Commun. Mag.* **50**(8), 137–144 (2012).
16. X. Zhao, Y. Yao, Y. Sun, and C. Liu, "Circle polarization shift keying with direct detection for free-space optical communication," *J. Opt. Commun. Netw.* **1**, 307–312 (2009).
17. A. Raj, J. Selvi, and S. Durairaj, "Comparison of different models for ground-level atmospheric turbulence strength (Cn2) prediction with a new model according to local weather data for FSO applications," *Appl. Opt.* **54**, 802–815 (2015).
18. M. Li and M. Cvijetic, "Coherent free space optics communications over the maritime atmosphere with use of adaptive optics for beam wavefront correction," *Appl. Opt.* **54**, 1453–1462 (2015).
19. M. Li, M. Cvijetic, Y. Takashima, and Z. Yu, "Vector Monte Carlo simulations on atmospheric scattering of polarization qubits," *J. Opt. Soc. Am.* **30**, 448–454 (2013).
20. M. M. Karbassian and H. Ghafouri-Shiraz, "Transceiver architecture for incoherent optical CDMA networks based on polarization modulation," *J. Lightwave Technol.* **26**, 3820–3828 (2008).
21. T. Xuan, Z. Ghassemlooy, S. Rajbhandari, W. O. Popoola, and G. L. Chung, "Coherent heterodyne multilevel polarization shift keying with spatial diversity in a free-space optical turbulence channel," *J. Lightwave Technol.* **30**, 2689–2695 (2012).
22. A. Bekkali, C. Ben Naila, K. Kazaura, K. Wakamori, and M. Matsumoto, "Transmission analysis of OFDM-based wireless services over turbulent radio-on-FSO links modeled by gamma-gamma distribution," *Photon. J.* **2**, 510–520 (2010).
23. D. Pham Tien, A. M. Shah, and K. Kazaura, "Investigation of suitability of RF signal transmission over FSO links," in *International Symposium on High Capacity Optical Networks and Enabling Technologies (HONET)*, Dubai, 2007, pp. 1–6.
24. D. Pham Tien, A. M. Shah, and K. Kazaura, "A study on transmission of RF signals over a turbulent free space optical link," in *International Topical Meeting on Microwave Photonics* (jointly held with the 2008 Asia-Pacific Microwave Photonics Conference (MWP/APMP), Gold Coast, Australia, 2008, pp. 173–176.
25. D. Pham Tien, A. Shah, and K. Kazaura, "An innovative technology for ubiquitous communication using Radio on FSO links," in *International Conference on Advanced Technologies for Communications (ATC)*, Hanoi, 2008, pp. 124–127.
26. R. L. Fante, "Electromagnetic beam propagation in turbulent media," *Proc. IEEE* **63**, 1669–1692 (1975).
27. S. M. Navidpour, M. Uysal, and M. Kavehrad, "BER performance of free-space optical transmission with spatial diversity," *Wireless Commun.* **6**, 2813–2819 (2007).
28. L. C. Andrews and R. L. Phillips, *Laser Beam Propagation Through Random Media* (SPIE, 2005).
29. R. Rampy, D. Gavel, D. Dillon, and S. Thomas, "Production of phase screens for simulation of atmospheric turbulence," *Appl. Opt.* **51**, 8769–8778 (2012).
30. "The 3rd generation partnership project," Available: <http://www.3gpp.org/>.

4.3 Experimental Verification of Long-Term Evolution Radio Transmissions over Dual-Polarization Combined Fiber and Free-Space Optics Optical Infrastructures

This chapter is a version of the published manuscript:

- [J2] J. Bohata, S. Zvanovec, P. Pesek, T. Korinek, M. M. Abadi and Z. Ghassemlooy, “Experimental verification of long-term evolution radio transmissions over dual-polarization combined fiber and free-space optics optical infrastructures,” *Applied Optics*, vol. 55(8), 2016, pp. 2109-2116.

Points pertaining to my PhD thesis:

As soon as the DP RoFSO system has been tested in various turbulence regimes, the extension to the entire combined RoF and RoFSO system was analyzed and experimentally tested in terms of signal-to-noise-ratio (SNR) performance and the most suitable channel deployment. Consequently, the specific limitations were derived in order to determine highly reliable system transmissions. Other detailed short-term tests with RoF and RoFSO were then published in international conferences, see [C3], [C6], [C7].

Experimental verification of long-term evolution radio transmissions over dual-polarization combined fiber and free-space optics optical infrastructures

J. BOHATA,^{1,*} S. ZVANOVEC,¹ P. PESEK,¹ T. KORINEK,¹ M. MANSOUR ABADI,² AND Z. GHASSEMLOOY²

¹CTU in Prague, Department of Electromagnetic Fields, Technicka 2, Prague, Czech Republic

²Optical Communications Research Group, NCRLab, Northumbria University, Newcastle upon Tyne NE1 8ST, UK

*Corresponding author: bohata2@fel.cvut.cz

Received 30 November 2015; revised 28 January 2016; accepted 29 January 2016; posted 1 February 2016 (Doc. ID 254703); published 10 March 2016

This paper describes the experimental verification of the utilization of long-term evolution radio over fiber (RoF) and radio over free space optics (RoFSO) systems using dual-polarization signals for cloud radio access network applications determining the specific utilization limits. A number of free space optics configurations are proposed and investigated under different atmospheric turbulence regimes in order to recommend the best setup configuration. We show that the performance of the proposed link, based on the combination of RoF and RoFSO for 64 QAM at 2.6 GHz, is more affected by the turbulence based on the measured difference error vector magnitude value of 5.5%. It is further demonstrated the proposed systems can offer higher noise immunity under particular scenarios with the signal-to-noise ratio reliability limit of 5 dB in the radio frequency domain for RoF and 19.3 dB in the optical domain for a combination of RoF and RoFSO links. © 2016 Optical Society of America

OCIS codes: (060.2605) Free-space optical communication; (060.5625) Radio frequency photonics; (010.1330) Atmospheric turbulence; (060.2310) Fiber optics.

<http://dx.doi.org/10.1364/AO.55.002109>

1. INTRODUCTION

The deployment of small cells and the use of higher radio frequency (RF) bands (e.g., millimeter-wave) are two possible options to fulfill the demand for higher data rates in next-generation wireless access networks. The third-generation partnership project (3GPP) of long-term evolution (LTE) with low latency, also known as the fourth-generation technology, supporting high data rates of up to 300 and 75 Mbps for the downlinks and uplinks, respectively, has been proposed and developed [1,2]. LTE intended for urban areas and operating at a carrier frequency of 2.6 GHz imposes higher loss in wireless transmission, which limits the cell radius due to the degradation of the signal-to-noise ratio (SNR) [3]. In small-cell-based systems, optical fibers are considered as an ideal backhaul medium to provide sufficient bandwidth as well as a future-proof capacity upgrade. More recently, cloud-based radio access networks (C-RAN) technology has been proposed as a cost-effective and power-efficient option for deploying small cells to meet the capacity demand of future wireless access networks. C-RAN decouples the digital baseband processing unit (BBU) from the largely analog remote antenna unit (RAU) and

moves it to the BBU pool or BBU hotel, thus allowing for the centralized operation of BBUs and a scalable deployment of RAUs as small cells [4]. In such schemes, optical fiber (OF) communications technology plays a significant role when developing network infrastructures, particularly for connections between adjacent cells, RAUs, and a central unit pool. OF technology covers approximately 35% of the connections between base stations (BSs), while the remaining 55% are based on RF wireless technology [5]. This will rise to over 60% of fiber-connected base stations making fourth and upper generations of mobile communications, resulting in optical infrastructures becoming the most suitable medium for transportation of radio signals from/to RAUs. The functions of RAUs can be further simplified by transmitting analog RF signals over OF backhaul networks. Unlike the conventional digital baseband transmission schemes supporting only one service at a time, the radio-over-fiber (RoF) transmission network [6] enables the coexistence of multiple services and multiple operators in shared resources, thereby offering increased link capacity, advanced networking (i.e., dynamic resources and allocations), and features such as wavelength division multiplexing (WDM)

[7] without the need for frequency up- or down-conversion. Transmission of the LTE signals over OFs was presented in [8] and highlighted improvements of the OF backhaul in terms of power and cost effectiveness. A field trial demonstration of high-capacity optical super-channel transmission, based on optical orthogonal frequency division multiplexing with hybrid dual-polarization (DP) quadrature amplitude modulation (QAM)/phase-shift-keying modulations, was reported in [9], providing up to 21.7 Tb/s transmission capacity over long-haul optical links. Polarization division multiplexing (PDM) of two distinctive orthogonal frequency division multiplexing (OFDM) signals, based on ultrawide band standards over the RoF system in passive optical networks, was experimentally demonstrated recently in [10] and effectively doubled the capacity of the system. In [11], an experimental investigation of the RoF system over 100 km of fiber was demonstrated using PDM and the RF frequency bands of 2.6 GHz and 800 MHz, with the highest polarization discrimination of ~ 30 dB.

However, the application of RoF depends on the availability of installed OFs between various network facilities to connect BBU and RAU within the C-RAN architecture, and therefore it is possible to considerably extend multiple services over one fiber by using several frequency channels or the WDM technique as showed in [12]. Installation of OF cables can be challenging and costly, especially in urban areas with dense building structures. Once OF cables are installed, rewiring then becomes a difficult and time-consuming task when the distribution of wireless users (WU) and the number of WUs are changed. Therefore, a limited amount of installed OFs highlights the usefulness of free space optics (FSO) [13] technology as it offers the same features as OFs, but with considerably reduced deployment cost and significantly higher capacity [14] compared to conventional RF wireless approaches.

The concept of radio over FSO (RoFSO) has been experimentally introduced by combining a full optical FSO system (employing a 1 km FSO turbulent link at a wavelength of 1550 nm) with a digital TV RF signal without any signal conversion in [15,16]. In [17], a Dense WDM system with RoFSO technology was used to transmit a range of various radio services over 1 km of FSO link under turbulence conditions offering a similar bandwidth to OF for both indoor and outdoor (short-range) applications with 99.9% of link availability. Therefore, it is desirable to extend the existing RoF concepts to RoFSO so as to cover the entire optical transmission technology within future C-RAN. In such scenarios, it is essential to determine system statistics under various channel configurations (i.e., OF, FSO, or a hybrid OF-FSO). A typical scenario employing combined RoF and RoFSO systems is shown in Fig. 1. Among the number of challenges encountered in FSO systems, the atmospheric-induced fading effects (both amplitude and phase) of the received optical signal are the most important [18]. RoFSO can transmit all types of RF signals without interference, and therefore increasing the number of independent channels and expanding the capacity in the optical domain becomes highly desirable. WDM based on an optical power allocation scheme, with consideration of the optical modulation index under a total optical transmission power limitation for an adaptive RoFSO link design, was proposed



Fig. 1. Example of RoF and RoFSO scenario adopting C-RAN architecture.

in [19]. A novel wireless network architecture using RoFSO for WLANs, together with an RF assignment mechanism based on RoFSO, was proposed and investigated in [20] and offered efficient frequency utilization in terms of both the throughput and fairness index. A coherent multilevel polarization shift keying transceiver using spatial diversity detection in the FSO channel was theoretically investigated in [21] for different turbulence regimes. The authors reported a predicted power penalty of ~ 25 dB at a symbol error probability of $10E-8$ for the strong turbulence regime (Rytov variance σ_R^2 of 3.5). The first concept of the dual-polarization-multiplexing RoFSO system proposed for the LTE radio signal was investigated in [22].

In this paper, an optical dual-polarization LTE RoF and RoFSO system for C-RAN networks using the PDM scheme is proposed. Novel experimental results in terms of the measured and simulated error vector magnitude (EVM) statistics are presented and evaluated. We consider four typical channel configurations using combinations of RoF and RoFSO. The performance of the RoFSO system is highly influenced by environmental factors, and thus we focus on the FSO channel under the turbulence regime. Based on the investigation of the channel dynamic range and noise immunity tests, we have extended the measurement results to include EVM characteristics and have derived specific limits of utilizations of RoF and RoFSO systems. We show that the performance of the proposed link based on the combination of RoF and RoFSO for 64 QAM at 2.6 GHz is more affected by the turbulence based on the measured difference EVM value of 5.5%. We further show that the proposed systems can offer higher noise immunity under particular scenarios with the SNR limit of 5 dB in the RF domain for RoF and 19.3 dB in the optical domain for the combination of RoF and RoFSO links.

The rest of the paper is structured as follows: Section 2 introduces the properties of the proposed system with different configurations and atmospheric turbulence. Results from the measurements and simulations are discussed in Section 3, and the conclusions are presented in Section 4.

2. EXPERIMENTAL SETUP

A. Main Setup Description

The experimental setup consists of transmitter (Tx), channel, and receiver (Rx) parts as shown in Fig. 2. On the Tx side, both branches are modulated by two independent RF signals prior to

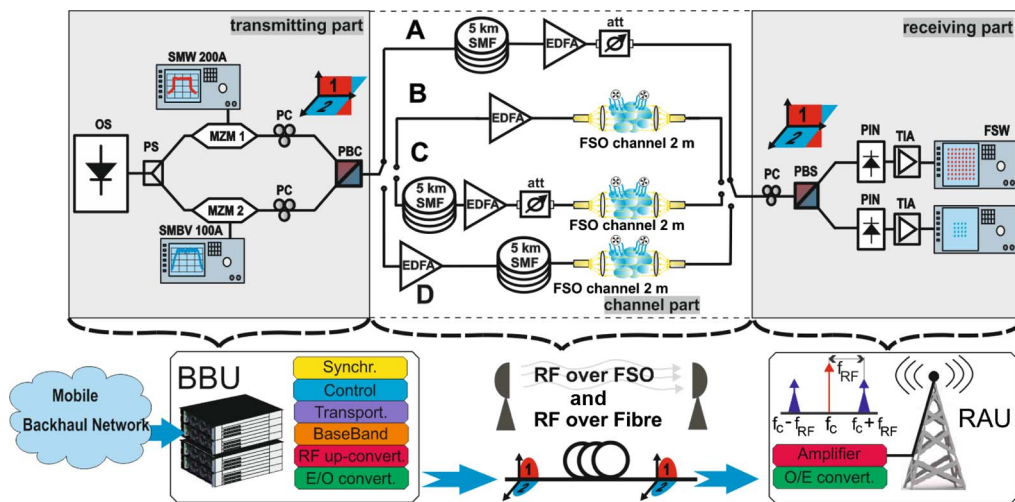


Fig. 2. Schematic diagram of DP-LTE over optical communications for C-RAN architecture (upper part shows laboratory setup; the corresponding network structure is illustrated below).

the application of a polarization-multiplexing technique for transmitting over the optical channel (OF and FSO).

A distributed feedback (DFB) laser diode (ID-Photonics TL CoBrite Dx4) at a wavelength of 1550 nm was used as the optical source (OS). The output of the OS, passing through a power splitter (Opneti PBS 15-L-1-1-FA), is externally modulated with two digital RF signals (vector signal generators R&S SMBV 100 A and SMW 200 A) of the same carrier frequency and equal bandwidth using Mach-Zehnder modulators (MZMs) (Thorlabs LN81S). For a detailed description of the influence of MZMs on RoF, please refer to [23]. The two orthogonal polarization states of the modulated light beams were controlled using two polarization controllers (PCs) and combined via the polarization beam combiner prior to being launched into standard SMFs. As shown, erbium-doped fiber amplifiers (EDFAs) (Keopsys KPS-BT2-C-10-LN-SA) were used to compensate for the channel loss. Four types of the RoF/RoFSO-based channel configurations were investigated:

- (i) Setup A: 5 km of SMF and EDFA
- (ii) Setup B: EDFA and the FSO channel
- (iii) Setup C: 5 km of SMF, EDFA, and the FSO channel
- (iv) Setup D: EDFA, 5 km of SMF (representing the typical transmission span for RoF links), and the FSO channel.

Since the focus in this work was only on the RoF and RoFSO parts of the RAN system, we did not consider retransmission or signal recovery between the OF and FSO parts, which is typically done by the remote RoF units. At the Rx, a PC was used to adjust the polarization states of the incoming optical signal before being fed into a polarization beam splitter (PBS) according to [10] and [11]. PDM optical signals can be potentially demultiplexed by coherent detection and digital signal processing. Polarization dependence of coherent detection can then be managed by means of optical dynamic polarization control or a polarization diversity Rx [24,25]. In a conventional polarization diversity Rx, two sets of Rxs are used to independently detect signal components in the two orthogonal polarization states and the original signal

is recovered after combining two components, which is rather inefficient in terms of hardware. However, when two PDM channels are simultaneously transmitted at orthogonal polarization states, a polarization diversity Rx in principle can receive both channels—for example, by using optical dynamic polarization control at the Rx. An all-optic scheme for PDM systems using a dynamic PC has been proposed in [26]. It has been suggested that PDM optical signals can potentially be demultiplexed by combining coherent detection and polarization/phase diversity [27].

The Rx is composed of a pair of encapsulated balanced PIN photodiodes (PDs) and a transimpedance amplifier (TIA, Newport 1544-B50). The output of the TIA was captured for further processing using a signal analyzer (R&S FSV). We used LTE-evolved universal terrestrial radio access (E-UTRA) test models with 16 and 64 QAM in polarization state 1 (noted as Pol 1). An independent digital mobile radio service with 16 QAM, having the same parameters (frequency, bandwidth, and power) as the signal in Pol 1, was launched to polarization state 2 (Pol 2).

The polarization orthogonality was continuously verified by monitoring the parameters at the Tx for one polarization state (i.e., Pol 1) while the signal in the second polarization state (i.e., Pol 2) was switched off and on with no influence observed on either the original power magnitude, SNR, optical signal to noise ratio (OSNR), or the corresponding EVMs. In the experimental setup, we used two commonly adopted LTE frequency bands of 800 MHz and 2.6 GHz with the bandwidth set to 10 MHz. We also set the peak envelope power below the limit of 15 dBm to avoid harmonic distortions at the recovered RF spectrum. All key adopted system parameters are listed in Table 1. For the FSO links, graded-index lenses (Thorlabs 50-1550A-APC) with an aperture of 1.8 mm and convex lenses with a diameter of 25.4 mm (SMPF_115-APC) were used to launch and couple light from/into the SMF. FSO links were subjected to atmospheric turbulence in order to assess the performance of the proposed system.

Table 1. Setup Parameters

Parameter	Value
Carrier frequencies	800 MHz and 2.6 GHz
System bandwidth	10 MHz
OFDM subcarriers	667
OFDM symbols/subframe	7
RF output power	-5 dBm
Modulation scheme	16 and 64 QAM
LTE test models	E-TM2 and E-TM3.2
DFB	
-laser output power	8 dBm
-wavelength	1550 nm
FSO channel length	2 m
FSO channel loss	15 dB
Fiber 5 km loss	1.7 dB
EDFA	
-noise figure	<5 dB
-return loss	> -40 dB
PIN responsivity	0.75 A/W
TIA bandwidth	10–12 GHz

B. Noise Conditions

In this section, we outline the noise sources associated with the link, in particular the shot noise, thermal noise, and relative intensity noise (RIN).

The power of the shot and thermal noise sources can be expressed as the fundamental noise [28],

$$N_{\text{fund}} = (g_{\text{rf}} + 1)k_B T f + \frac{1}{2}qI_{\text{DC}}fR_{\text{out}} \quad (1)$$

where g_{rf} is the RF gain, k_B is Boltzmann's constant, T is the temperature, q is the electronic charge constant, I_{DC} is the average PD DC current, and R_{out} is the matching load resistance.

Additionally, there is the excess photon noise due to fluctuations of the intensity of the light source as a result of the beating of various spectral components having random phases. For a purely spontaneous source, it is given as [29]

$$\Delta i_{\text{ex}}^2 = \left(\frac{(1 + \alpha^2)I^2 \Delta f}{\Delta \nu_{\text{eff}}} \right), \quad (2)$$

where α is the degree of polarization and $\Delta \nu_{\text{eff}}$ is the effective bandwidth. Though all three noise sources can be used to estimate the RIN, it should be noted that Δi_{ex}^2 should only be used for optical sources with a purely spontaneous emission profile.

The RIN, associated with the optical devices, represents the total amount of photon noise per unit bandwidth and is defined as

$$\text{RIN}_{\text{total}} = \frac{P_f^2}{P^2} = \frac{\Delta i_{\text{th}}^2 + \Delta i_{\text{sh}}^2}{I^2 \Delta f} = \frac{4N_{\text{total}}}{I_{\text{dc}}^2 R_{\text{out}}}, \quad (3)$$

where P_f^2 is the autocorrelated value of the optical power fluctuation at frequency f , which can be measured using an electrical spectrum analyzer to represent the total output noise power spectral density N_{total} delivered to R_{out} . P is continuous wave optical power, which contributes to I_{DC} .

Note that the shot noise is divided into two branches (matching circuit and load). With the links employing optical

amplifications, there are additional noise contributions. The primary noise source in optical amplifiers (e.g., EDFA) adopted in optical communications is amplified spontaneous emission (ASE), with a spectrum almost the same as the gain spectrum of the amplifier. When detected, these spontaneously generated photons result in signal-spontaneous (sig-sp) and spontaneous-spontaneous (sp-sp) beat noise currents. The sp-sp beat noise power density is inversely proportional to the OSNR², whereas the sig-sp beat noise power density is inversely proportional to the OSNR. The sp-sp beat noise also depends on the baseband frequency, with the noise density decreasing with increase of the baseband frequency. In principle, the sp-sp beat noise intensity spectrum could be as wide as the optical amplifier bandwidth in the absence of optical filtering. From a practical point of view, the excess noise regime is highly important, where the noise level is higher than the level of shot noise due to the influence of sig-sp beat noise, etc. Therefore, here we only consider the sig-sp beat noise, which is given as [28]

$$\text{RIN}_{\text{sig-sp}} = \frac{4n_{\text{sp}}h\nu}{g_{\text{opt}}P_{\text{sig}}}, \quad (4)$$

where n_{sp} is the spontaneous emission factor, h is Planck's constant, ν is optical frequency, g_{opt} represents the optical power gain of the EDFA, F_{opt} is the noise factor of the EDFA, and P_{sig} stands for average optical signal power input to the EDFA. Assuming that $g_{\text{opt}} \gg 1$, Eq. (4) can be expressed as

$$\text{RIN}_{\text{sig-sp}} \approx \frac{2F_{\text{opt}}h\nu}{P_{\text{sig}}}. \quad (5)$$

F_{opt} is related to the shot noise and the detection scheme. For an ideal detector, $F_{\text{opt}} = 2n_{\text{sp}}$. The degradation of SNR in RoF and RoFSO links is represented by the RF noise factor F_{rf} with respect to thermally limited input and is defined in terms of the RoF link output noise power N_{out} as [28]

$$F_{\text{rf}} \equiv \frac{N_{\text{out}}}{g_{\text{rf}}k_B T}. \quad (6)$$

Typically, F_{rf} is enumerated under $T = 290$ K. We can rewrite the definition of the noise factor by using Eq. (3) and the RF gain as

$$F_{\text{rf}} \equiv \frac{V_{\pi}^2 \text{RIN}_{\text{total}}}{\pi^2 R_{\text{in}} k_B T}, \quad (7)$$

where R_{in} is the input resistance of the MZM and V_{π} is a convenient parameter to specify the efficiency of an electro-optic intensity modulator, which is defined as the voltage required to change the optical power transfer function from the minimum to the maximum.

In the experimental test setup, the SNR was set in the RF domain directly via the signal generator by including an additional noise source while the OSNR was controlled by adding a variable optical attenuator placed directly behind the EDFA in setups A and C to avoid the amplifier's gain-induced OSNR fluctuations as depicted in Fig. 2. In setup C, we positioned the optical attenuator in front of the optical link to maintain the desired OSNR level over the FSO channel. OSNR was measured using an optical spectrum analyzer. Here, we have adopted the intensity modulation with direct detection (IM/DD) scheme and used single-drive MZMs which were biased

at their maximal transmission point. At the input of the MZM, the field waveform (in time t) can be expressed as [28]

$$E_{IN}(t) = \kappa \sqrt{2P_{laser}} e^{j\omega_0 t}, \quad (8)$$

where P_{laser} is average laser power at angular frequency ω_0 and κ is a constant relating field and average power. The input voltage to the MZM is defined by

$$V_{IN}(t) = V_{dc} + V_{RF} \sin(\omega_0 t), \quad (9)$$

where V_{dc} stands for bias voltage and the expression $V_{RF} \sin(\omega_0 t)$ defines the modulating RF signal V_{RF} . Among other factors, IM/DD introduces additive noise to the hybrid radio and photonic system.

C. FSO Turbulence Effects

There are a number of methods for generating turbulence within an indoor controlled environment, including near-index matching, liquid-filled chambers, spatial light modulators, ion-exchange phase screens, surface etching, and hot air chambers [30]. For assessing the performance of the proposed scheme, we have adopted the latter and used an artificial turbulence generator with known, realistic, and repeatable characteristics. Two fans were used to blow hot air into the channel perpendicular to the propagating optical beam. To measure the temperature profile and determine the temperature gradient along the channel, we placed 20 thermal sensors at an interval of 10 cm along the FSO channel. We used Rytov variance and the refractive index structure parameter to characterize strength of the turbulence according to [22]. The variance of the log-intensity signal fluctuation defined by Rytov variance σ_R^2 is given by [31]

$$\sigma_R^2 = 1.23 k^7 C_n^2 L^{14/3}, \quad (10)$$

where $k = 2\pi/\lambda$ is the wavenumber and λ is the transmission wavelength.

C_n^2 is the refractive index structure parameter (the main measure of the turbulence scale), which is given as [18]

$$C_n^2 = \left(79 \times 10^{-6} \frac{P_a}{T^2}\right)^2 C_T^2, \quad (11)$$

where P_a is the atmospheric pressure in millibars. C_T^2 is the temperature structure constant, which is defined as [18]

$$C_T^2 = (T_1 - T_2)^2 / L_p^{2/3}. \quad (12)$$

T_1 and T_2 are temperatures at two points separated by distance L_p . Knowing the thermal distribution along the FSO propagation path, it is possible to determine C_T^2 and then C_n^2 .

3. EXPERIMENTAL AND SIMULATION RESULTS

The experimental section is divided into three parts. In part A, the transmission properties of four selected scenarios (setups A–D; see Fig. 2) were tested under the steady-state condition with no turbulence. Part B describes the detailed investigation of the dynamic range and noise conditions of the RoF system compared to the hybrid RoF and RoFSO (setups A and C) systems. Finally, part C outlines the comparison of the links including the FSO channel under turbulence regimes (setups B–D).

A. System Properties

We have tested the suitability of proposed scenarios A–D using the polarization multiplexed technique for RF signals. Two standardized E-UTRA test models were selected for the investigation of the channel quality: Test models 2 and 3.2 [32]. Both test models are specified for testing E-UTRA systems with an emphasis on either the dynamic range or the quality of the transmitted signal using 64 and 16 QAM, respectively.

Scenarios A and B evinced EVM around 1%, while scenarios C and D evinced EVM between 2% and 3%. It can be observed that scenarios A and B offer roughly two or three times better EVM performance when compared to the hybrid RoF and RoFSO systems (C and D). Nevertheless, all scenarios show EVM values dramatically below the maximal 3GPP LTE EVM threshold of 8% recommended for high-data-rate systems [33]. Note that for setup A, with 5 km of SMF, the output power of EDFA had to be decreased in order to ensure that the PIN PD was not saturated or damaged. The gain of the EDFA was preserved throughout the experimental work in order to maintain similar conditions. Last but not least, we simulated the conditions of a real system by employing an EDFA in order to further increase the transmission span.

B. Noise Parameters

Next, we carried out several tests focusing on the quality of the E-UTRA signals transmitted over the optical channels for a range of OSNR and SNR values. These tests were focused on the hazard noise effects described in Section 2B, which can significantly reduce both OSNR and SNR, thus degrading the performance of RoF and RoFSO systems. At first, we carried out simulations for the EVMs for the proposed system featuring SMF and FSO sections (setups A and C). Subsequent measurements using a frequency of 2.6 GHz and 64 QAM were also carried out to validate the simulated results. The constellation diagrams of the 64 QAM and the evolution of the EVM parameter were evaluated both experimentally and by means of simulation, which was then correlated. Figures 3 and 4 depict the predicted and measured EVM as a function of the OSNR for setups A and C, respectively. For setup A, there is a mismatch between the measured and predicted EVMs, with the maximum difference of <2% at an OSNR of 28 dB. This is, in all probability, caused by the slightly different properties of simulated and real behavior of EDFAs, which

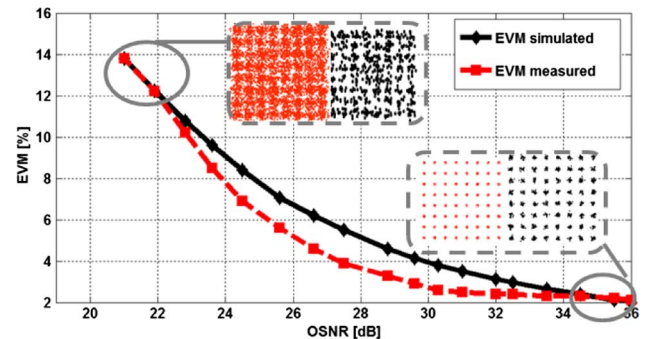


Fig. 3. Simulated and measured EVM as a function of OSNR for 64 QAM at a frequency of 2.6 GHz for 5 km of SMF (setup A). Inset shows the constellation diagrams.

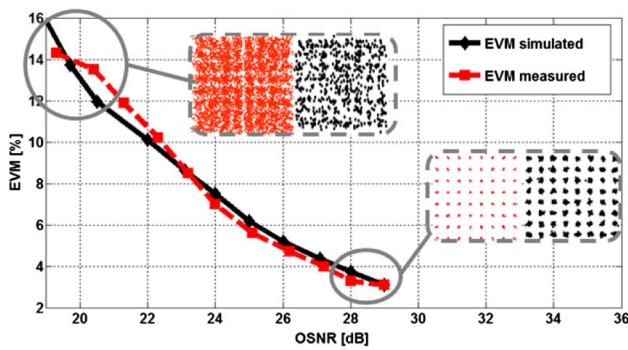


Fig. 4. Simulated and measured EVM as a function of OSNR for 64 QAM at a frequency of 2.6 GHz for 5 km of SMF + FSO channel (setup C). Inset shows the constellation diagrams.

are due to the ASE being the main noise source in the optical domain. For setup C, there is a good match between the measured and predicted plots. The measured (red) and simulated (black) constellation diagrams are also shown in Figs. 3 and 4. These plots show that the RoF with 5 km of fiber can operate over a wide range of OSNR (i.e., from 36 to 21 dB) whereas, for the hybrid RoF and RoFSO links, the OSNR range is only 10 dB (from 29 to 19.3 dB). In the case of the FSO channel, this can be attributed to the power budget being significantly lower and the noise floor belonging to a particular scenario. The experimental and simulated EVM curves for setup C show the same trend for OSNR values of 29 and 21 dB as in setup A, with the only difference being the initial EVM values. In addition, as just described, the EDFA power had to be reduced while using setup A, which resulted in a minimal OSNR value of ~ 21 dB. It can be observed that the proposed systems even operate over the recommended 8% EVM limit when using 64 QAM, but at the cost of higher error probability.

Next we investigated the EVM as a function of the SNR, which was measured on the Rx side, for setup C for 64 QAM at a frequency of 2.6 GHz with no turbulence, as shown in Fig. 5. The insets illustrate the corresponding constellation diagrams. The plots demonstrate a good agreement between the measured and simulated results. The SNR dynamic range shows a decrease of ~ 5 dB compared

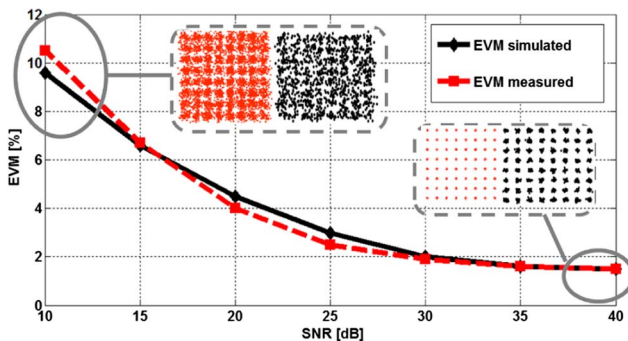


Fig. 5. Simulated and measured EVM as a function of SNR for 64 QAM at a frequency of 2.6 GHz for 5 km of SMF (setup C). Insets show the constellation diagrams.

to setup A (while employing only 5 km of SMF). Both scenarios meet dynamic range requirements for home, local, and wide-area BSs specified by [32].

C. Turbulence

Finally, we compared the performance of both RoFSO (setup B) and the hybrid RoF and RoFSO (setups C and D) systems under the influence of atmospheric turbulence. The average values of ΔEVM for these particular scenarios were captured for a range of the refractive index structure parameter C_n^2 . Since the initial magnitude of EVM was different for particular scenarios, all EVM values were aligned by showing the ΔEVM . We have adopted the frequency of 2.6 GHz for further detailed investigations since the performance of the systems for 800 MHz and 2.6 GHz are almost the same. We compare all optical-based systems including the FSO part (setups B, C, and D from Fig. 2) at 2.6 GHz for 64 QAM for different turbulence regimes in terms of changes in EVM, as illustrated in Fig. 6.

The higher C_n^2 is, the larger the fluctuation of the power magnitude and its corresponding EVM values, which can exceed the reliability limits of the RAN system. The proposed LTE test model for 64 QAM fulfills the reliability and the high data-rate limit of EVM (i.e., $<8\%$). Results indicate that a RoFSO scenario evinces the best properties comparable to the hybrid RoF and RoFSO setups C and D, where tolerable limits were exceeded approximately beyond the threshold C_n^2 of $\sim 7.0\text{E} - 11 \text{ m}^{-2/3}$, in particular because of high fluctuations observed in EVM. In other words, the use of the RoF technology, together with RoFSO under the turbulence condition, resulted in slightly reduced performance compared with the RoFSO link in terms of increased mean value of ΔEVM by 2.5% and 5.5% in setups C and D, respectively, at C_n^2 of $\sim 1\text{E} - 10 \text{ m}^{-2/3}$. This cannot be attributed only to added SMF (with an average EVM of 1%), and therefore the overall EVM system has to be determined. The hybrid setups (C and D) offer a reliable, high data rate transmission for the C_n^2 value up to $\sim 7\text{E} - 11 \text{ m}^{-2/3}$, which corresponds to C_n^2 of $5.37\text{E} - 14 \text{ m}^{-2/3}$ in the case of a 100 m long FSO link extrapolated through the Rytov variance expression in Eq. (11). The predicted values largely fall into the moderate turbulence regime, thus representing typical maximal turbulence strength according to [18] and [34], where a 1 km long FSO link under a real turbulence condition was investigated. By placing the EDFA between the RoF and RoFSO systems so as to compensate

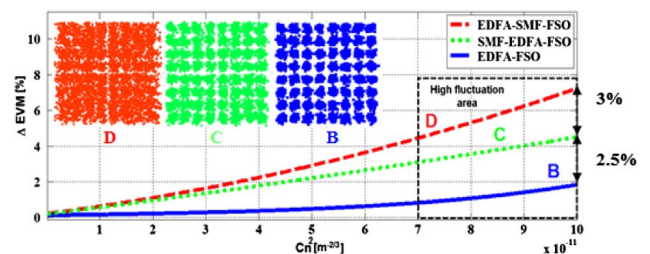


Fig. 6. ΔEVM as a function of the refractive index structure parameter C_n^2 for setups B, C, and D for 64 QAM at 2.6 GHz and OSNR corresponding to maximal values for each particular scenario.

for the loss in the RoF link and boost the incoming signal prior to the RoFSO link, the EVM is improved by $\sim 3\%$, as shown within the high fluctuation region in Fig. 6. Note that the optical output power (OS and EDFA) levels were kept at a relatively low level to avoid the more significant role of nonlinear effects in OF.

4. CONCLUSION

Having proposed an optical dual-polarization LTE RoF and RoFSO system for C-RAN networks and having evaluated its performance in terms of the measured and simulated EVM statistics, we showed the configuration of radio systems for 64 QAM at 2.6 GHz, incorporating FSO under the turbulence regimes, which lead to EVM values below 8% for C_n^2 of up to $5.37E - 14 \text{ m}^{-2/3}$ when considering a 100 m long FSO link. We also showed that the performance of the proposed link based on the combination of RoF and RoFSO was more affected by the turbulence, with the measured ΔEVM value increased to 5.5%. However, the EVM was reduced by $\sim 3\%$ when placing an EDFA between the RoF and RoFSO links. The proposed systems can offer higher noise immunity under particular scenarios, with SNR reliability limits of 5 dB in the RF domain for RoF and 19.3 dB in the optical domain for RoFSO links. There were no significant changes in the polarization of the radio PDM system while propagating through the fiber and FSO channels, thus illustrating proposed system attributes to a higher transmission capacity. The employment of the dual-polarization solutions, as part of the C-RAN infrastructures, creates a dense network between the RF base-end parts and central cloud pools, thus making the infrastructure simpler and more robust. Moreover, the proposed technique can be adopted for other radio services such as WiFi or Wimax, thus leading to improved network convergence.

Funding. European Cooperation in Science and Technology (COST) (IC 1101); SGS (SGS14/190/OHK3/3T/13).

Acknowledgment. Authors would like to thank Rohde and Schwarz–Praha, S.R.O., for their technical support.

REFERENCES

1. S. Seung-Chul and L. Young-Poong, "Testing of early applied LTE-advanced technologies on current LTE service to overcome real network problem and to increase data capacity," in *Proceedings of 15th Annual Conference on Advanced Communication Technology* (IEEE, 2013), pp. 275–281.
2. S. Kanchi, S. Sandilya, D. Bhosale, A. Pitkar, and M. Gondhalekar, "Overview of LTE-A technology," in *Proceedings of IEEE Global High Tech Congress on Electronics* (IEEE, 2013), pp. 195–200.
3. T. Wirth, V. Venkatkumar, T. Haustein, and E. Schulz, "LTE-advanced relaying for outdoor range extension," in *Proceedings of IEEE 70th Vehicular Technology Conference Fall* (IEEE, 2009), pp. 1–4.
4. A. Checko, H. L. Christiansen, Y. Yan, L. Scolari, G. Kardaras, M. S. Bertger, and L. Dittman, "Cloud RAN for mobile networks—a technology overview," *Commun. Surveys Tuts.* **17**, 405–426 (2015).
5. J. Segel, "Lightradio portfolio: white paper 3," Technical Report p.17 (Alcatel-Lucent Bell Labs, 2011).
6. S. Ting, J. Zheng, J. Wang, M. Zhu, Z. Dong, M. Xu, M. Zhang, X. Chen, and G. K. Chang, "Multiservice wireless transport over RoF link with colorless BS using PolM-to-IM convertor," *IEEE Photon. Technol. Lett.* **27**, 403–406 (2015).
7. H. Al-Raweshidy and S. Komaki, *Radio Over Fiber Technologies for Mobile Communications Networks* (Artech, 2002).
8. S. Aleksic, M. Deruyck, and W. Joseph, "Energy efficiency of optically backhauled LTE: a case study," in *Proceedings of Electromagnetics in Advanced Applications* (IEEE, 2013), pp. 390–393.
9. H. Y. Huang, M. F. Huang, E. Ip, E. Mateo, P. N. Ji, D. Qian, A. Tanaka, Y. Shao, T. Wang, Y. Aono, T. Tajima, T. J. Xia, and G. A. Wellbrock, "High-capacity fiber field trial using terabit/s all-optical OFDM superchannels with DP-QPSK and DP-8QAM/DP-QPSK modulation," *J. Lightwave Technol.* **31**, 546–553 (2013).
10. M. Morant, J. Perez, and R. Llorente, "Polarization division multiplexing of OFDM radio-over-fiber signals in passive optical networks," *Adv. Opt. Technol.* **2014**, 269524 (2014).
11. M. Morant, J. Prat, and R. Llorente, "Radio-over-fiber optical polarization-multiplexed networks for 3GPP wireless carrier-aggregated MIMO provision," *J. Lightwave Technol.* **32**, 3721–3727 (2014).
12. C. Liu, L. Zhang, M. Zhu, J. Wang, L. Cheng, and G. K. Chang, "A novel multi-service small-cell cloud radio access network for mobile backhaul and computing based on radio-over-fiber technologies," *J. Lightwave Technol.* **31**, 2869–2875 (2013).
13. Z. Ghassemlooy, W. Popoola, and S. Rajbhandari, *Optical Wireless Communications: System and Channel Modelling with MATLAB®* (Taylor & Francis, 2012).
14. G. Parca, A. Shahpari, V. Carrozzo, G. M. Belleffi, and A. L. J. Teixeira, "Optical wireless transmission at 1.6-Tbit/s (16 × 100 Gbit/s) for next-generation convergent urban infrastructures," *Opt. Eng.* **52**, 116102 (2013).
15. C. Ben Naila, K. Wakamori, M. Matsumoto, and K. Tsukamoto, "Transmission analysis of digital TV signals over a radio-on-FSO channel," in *Proceedings of ITU Kaleidoscope: the Fully Networked Human?—Innovations for Future Networks and Services* (ITU, 2011), pp. 1–7.
16. C. B. Naila, K. Wakamori, and M. Matsumoto, "Transmission analysis of digital TV signals over a radio-on-FSO channel," *IEEE Commun. Mag.* **50**(8), 137–144 (2012).
17. D. Pham Tien, A. M. Shah, K. Kazaura, and K. Wakamori, "A study on transmission of RF signals over a turbulent free space optical link," in *Proceedings of International Topical Meeting on Microwave Photonics, Jointly Held with the Asia-Pacific Microwave Photonics Conference* (IEEE, 2008), pp. 173–176.
18. L. C. Andrews and R. L. Phillips, *Laser Beam Propagation through Random Media* (SPIE, 2005).
19. K. Kyung-Hwan, T. Higashino, K. Tsukamoto, and S. Komaki, "WDM optical power allocation method for adaptive radio on free space optics system design," in *Proceedings of International Topical Meeting on Microwave Photonics & Microwave Photonics Conference* (IEEE, 2011), pp. 361–364.
20. P. Yue, X. Yi, and Z. Li, "Research on radio frequency assignment mechanism of the distributed antenna system based on radio over free space optics technology," in *Proceedings of IEEE Services Computing Conference* (IEEE, 2010), pp. 526–530.
21. X. Tang, Z. Ghassemlooy, S. Rajbhandari, W. O. Popoola, and C. G. Lee, "Coherent heterodyne multilevel polarization shift keying with spatial diversity in a free-space optical turbulence channel," *J. Lightwave Technol.* **30**, 2689–2695 (2012).
22. J. Bohata, S. Zvanovec, T. Korinek, M. A. Abadi, and Z. Ghassemlooy, "Characterization of dual-polarization LTE radio over a free-space optical turbulence channel," *Appl. Opt.* **54**, 7082–7087 (2015).
23. T. Kanesan, W. Pang Ng, Z. Ghassemlooy, and C. Lu, "Investigation of optical modulators in optimized nonlinear compensated LTE RoF system," *J. Lightwave Technol.* **32**, 1944–1950 (2014).
24. B. Glance, "Polarization independent coherent optical receiver," *J. Lightwave Technol.* **5**, 274–276 (1987).
25. Y. Han and G. Li, "Coherent optical communication using polarization multiple-input-multiple-output," *Opt. Express* **13**, 7527–7534 (2005).

26. X. Steve Yao, L.-S. Yan, B. Zhang, A. E. Willner, and J. Jiang, "All-optic scheme for automatic polarization division demultiplexing," *Opt. Express* **15**, 7407–7414 (2007).
27. M. G. Taylor, "Coherent detection method using DSP for demodulation of signal and subsequent equalization of propagation impairments," *IEEE Photon. Technol. Lett.* **16**, 674–676 (2004).
28. C. H. Lee, *Microwave Photonics*, 2nd ed. (Taylor & Francis, 2013).
29. Y. Wang, I. Tomov, J. S. Nelson, Z. Chen, H. Lim, and F. Wise, "Low-noise broadband light generation from optical fibers for use in high-resolution optical coherence tomography," *J. Opt. Soc. Am. A* **22**, 1492–1499 (2005).
30. R. Rampy, D. Gavel, D. Dillon, and S. Thomas, "Production of phase screens for simulation of atmospheric turbulence," *Appl. Opt.* **51**, 8769–8778 (2012).
31. R. L. Fante, "Electromagnetic beam propagation in turbulent media," *Proc. IEEE* **63**, 1669–1692 (1975).
32. "The 3rd generation partnership project," <http://www.3gpp.org/>.
33. B. Bangerter, S. Talwar, R. Arefi, and K. Stewart, "Networks and devices for the 5G era," *IEEE Commun. Mag.* **52**(2), 90–96 (2014).
34. C. B. Naila, A. Bekkali, K. Wakamori, and M. Matsumoto, "Performance analysis of CDMA-based wireless services transmission over a turbulent RF-on-FSO channel," *J. Opt. Commun. Netw.* **3**, 475–486 (2011).

4.4 Reliability of Aircraft Multimode Network

This chapter is a version of the published manuscript:

- [J3] J. Bohata, S. Zvanovec, M. Pisarik and P. Peterka, "Reliability of aircraft multimode network," *Optical engineering*, vol. 53(9), 2014.

Points pertaining to my PhD thesis:

In this paper we focused on the extreme short-term harsh condition tests of parts of the optical infrastructures. To illustrate their impact, specific conditions in aircrafts, which represent one of the most challenging areas for modern fiber networks, were analyzed. A special vibrational test was proposed and carried out to determine the influence of vibrations, occurring in optical aircraft network infrastructure, on MM connections in terms of IL and modal distribution. It was revealed that the vibrations, in conjunction with lower manufacturing tolerance of MM components, resulted in up to a 20 % reduced bandwidth. Furthermore, detailed temperature tests were performed for an avionic photonics network. Considering several connections in a short MMF network, each connector can be placed in a different temperature area resulting in additional IL. For the whole network, up to 1 dB of IL was recorded which subsequently lead to transmission performance degradation. The presented results were discussed from a reliability and safety point of view and provide limits for MMF network design. Moreover, the impact of the harsh environment described on transmission quality was demonstrated.

Optical Engineering

OpticalEngineering.SPIEDigitalLibrary.org

Reliability of aircraft multimode optical networks

Jan Bohata
Michael Písařík
Stanislav Zvánovec
Pavel Peterka

Reliability of aircraft multimode optical networks

Jan Bohata,^{a,*} Michael Písařík,^{a,b} Stanislav Zvánovec,^a and Pavel Peterka^c

^aCzech Technical University in Prague, Department of Electromagnetic Field, 2 Technická, 16627 Prague, Czech Republic

^bSQS Vlaknova Optika a.s., Komenskeho 304, 509 01 Nova Paka, Czech Republic

^cAcademy of Sciences of the Czech Republic, Institute of Photonics and Electronics, v.v.i., Chaberská 57, 182 51 Prague, Czech Republic

Abstract. Results from tests and analyses of multimode optical fibers for an avionic optical network under a variety of stress conditions are presented. Experiments revealed vibrational and temperature changes of distinct multimode fibers. Results lead to the discussion of influenced insertion losses and especially reduced bandwidth corresponding to modal distribution changes. It was determined that these crucial parameters could affect system reliability when an airplane network intersects thermal and vibrational variable environments. © 2014 Society of Photo-Optical Instrumentation Engineers (SPIE) [DOI: 10.1117/1.OE.53.9.096102]

Keywords: optical fiber; optical connectors; multimode; photonic network; avionics; harsh environment.

Paper 140831 received May 22, 2014; revised manuscript received Aug. 1, 2014; accepted for publication Aug. 1, 2014; published online Sep. 3, 2014.

1 Introduction

New developments in the construction of aircrafts result in a multitude of demands on digital and analog networks placed inside airplanes. Needs such as infrastructure weight recalculated during fuel consumption, power consumption, available bandwidth, electromagnetic resistance, and the ability to implement the next generation of sensors cannot be satisfied by currently utilized copper links, therefore, a massive development of optical systems for civil aircraft is foreseen.¹

Due to flight safety requirements,² the avionic industry is a conservative area that harbors a wariness for new technologies; therefore, there must be convincing reasons to change well-tested, reliable technologies.³ One of the most important reasons to modify technologies results from newly revealed composite materials being used, such as in the gigantic A380 shell.⁴ The absence of a common ground brings serious problems with electromagnetic interference since the cost of additional shielding for cables rapidly increases the fixed mass of aircrafts.⁵ The weight difference between optical and copper cables, assuming all necessary shielding and coating within the A380, was investigated in Refs. 5 and 6 and revealed a decrease of ~3000 kg when optical infrastructure is implemented. Another notable reason to switch to fiber optics is the increased bandwidth for advanced nodes such as hi-resolution cameras. Lowering power consumption for transmission, which was investigated by the DAPHNE consortium where simulations revealed savings of up to 10 kW of power on analog antenna systems alone,⁵ is another promising area. Optical fiber structures offer other benefits, including their ability to monitor fiber Bragg grating (FBG) stress and temperature⁷ (already implemented in military aircraft and civil rotorcraft), gas and humidity, and the photonic network itself,⁸ not to mention the wide bandwidth suitable for transmission of modulated analog signals for antennas [radio frequency over glass (RFoG)] based on Raman or Brillouin scattering. Several such aspects dealing with optical infrastructures were

investigated within the DAPHNE consortium, a project of the European Union Framework Program 7 (EU FP7).^{5,6}

Civil aircrafts are introducing a complex network system with many slave nodes and one centralized mainframe node with backup. There are several common aspects in the fiber of the x broadband network and optical backbone systems within aircraft that could prove to be interesting for future implementation within avionics. All aircraft systems/infrastructures were closely investigated within the EU FP7 DAPHNE consortium where different network types were identified. The most promising designs investigated were (1) passive star with single-mode optical fibers (PON), (2) active star with multimode optical fibers, and (3) daisy chain with single-mode and multimode optical fibers.⁵ Star topologies for single-mode fiber networks and their potential and robustness in terms of scalability limits at different crossing traffic loads were analyzed in Ref. 9, revealing the trade-offs between latency, system complexity, and scalability.

Despite the potentials mentioned above, fiber optics deployment on civil aircrafts still has not overcome all the challenges yet and proper discussions, especially on the selection of fibers and their behaviors under in-flight conditions, have yet to be held. That said, single-mode fiber 8/125 μm is used in military aircrafts, like rotorcrafts,¹⁰ and developed FBG stress and temperature sensors are used in some critical parts of the aircraft.⁸ The advantage of a single-mode fiber is demonstrated by the stability of power couplers, filters, and multiplex elements for dense wavelength division multiplexing; therefore, single-mode fibers are implemented for communication links and infrastructures. Nevertheless, multimode fibers were historically preselected due to a larger diameter, which should be less difficult for connections and more resistant to vibrations and temperature changes. Although they have already been integrated in A340 and A380 aircrafts for hi-definition digital cameras to assist landing (landing camera),¹ their utilization within aircrafts is still being debated.

*Address all correspondence to: Jan Bohata, E-mail: bohatja2@fel.cvut.cz

A photonic network falls under the auspice of ground operations and has to fulfill most requests over the long term as specific, rigid aircraft conditions require a closer reconsideration of every aspect of fiber optics and their particular influences. It has to be emphasized that temperature changes during ground operations are more than 1000 times slower than during in-flight conditions. Multimode fibers were stable in combination with a light-emitting diode light source, but most systems (high data rate systems and RFOG) use laser sources such as vertical cavity surface emitting laser. Some network components are, or will be, installed in unpressurized zones with high temperature differences. Unpressurized zones should be considered as a harsh environment because temperatures close to the engine range from 80 up to 120°C can be found in some places, but can drop to $\sim -60^\circ\text{C}$ (Ref. 11) only a few meters away, which could result in a change of the stress and basic parameters, including reflection loss and insertion loss.⁵

This paper closely investigates the influences of temperature cycling and vibrations on multimode fibers and some basic optic components, such as the connectors used in aircrafts, and their impact on the optical network. The impact of launch conditions in combination with failures on fiber splice was also closely investigated. The paper is organized as follows. Section 2 introduces simulation results for misaligned multimode fibers in terms of modal distribution. Section 3 presents the experiment laboratory setup to investigate thermal and vibrational influences during in-flight and results from these measurements are discussed. Key findings for the entire aircraft network are introduced and discussed in Sec. 4, with concluding remarks given in Sec. 5.

2 Simulation Results

To determine transmission characteristics, changes in field distribution for propagating modes were analyzed for typical cases of aerial influences, especially vibrational changes. Fiber misalignment brings an additional extrinsic loss to connections. To assess them, our studies focus on transverse offset considering loss due to a displacement δ (μm) while assuming uniformly distributed power in the first fiber. Insertion loss (IL) can be expressed by¹²

$$L = 10 \log \left\{ \frac{1}{\pi} \left[2 \cos^{-1} \frac{\delta}{2a} - \frac{\delta}{a} \sqrt{1 - \left(\frac{\delta}{2a} \right)^2} \right] \right\}, \quad (1)$$

where $2a$ introduces the diameter of the core.

Another definition for IL, computed with mode field diameter (MFD), originates from misalignment of the field distribution. Figure 1 shows how shifting cores with various MFD according to Ref. 13 could depend on IL.

It is obvious that the narrower the mode field, the smaller the IL. However, it is necessary to consider the tendency of producing a narrower laser beam loaded to a fiber core with just a few modes guided to achieve better bandwidth.

Simulations were carried out featuring a shifting of the forehead by 50/125 multimode \times (MM) fibers with a parabolic refractive index and distribution of the mode field being observed at a wavelength of 1310 nm. Three modes, LP₀₁, LP₁₁, and LP₀₂, were chosen to illustrate the influence of shifting fibers. Two multimode fibers are connected (spliced) with different shifting to simulate vibrating conditions. The

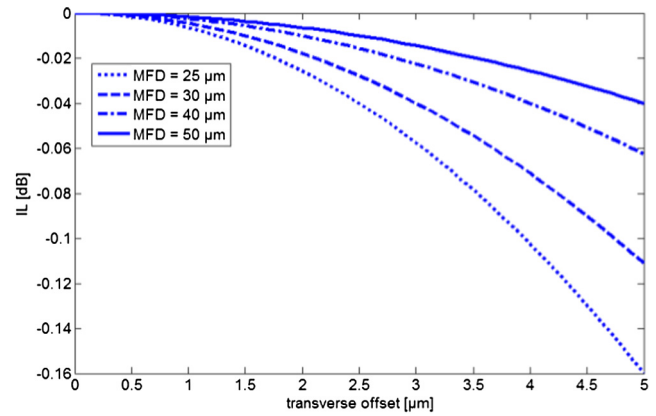


Fig. 1 Insertion loss (IL) dependent on transverse offset with different mode field diameter.

positional range was changed from 0 to 3.5 μm . Chosen results are shown in Fig. 2 corresponding to the LP₀₁, LP₁₁, and LP₀₂ modes with the position of the vibration-affected connector denoted. Multimode fibers were fed from below.

The influence was investigated on two spliced MM fibers, typical of an airplane camera infrastructure, and how the modes become distorted behind the connection (in figures placed 200 μm from bottom) is clearly illustrated.

Under recommendation ITU-T G.651.1,¹⁴ related to the MM fiber characteristics of a 50/125 μm multimode graded-index optical fiber cable for the optical access network, the tolerance of the core size can be up to $\pm 3 \mu\text{m}$. We have also performed simulations for connecting two MM fibers from different manufacturers with distance limits of core diameter tolerance containing modes LP₀₁ and LP₁₁. Multimode 52/125 μm fiber joined to 48/125 μm is described. The impact on mode structure was tested again with shifting cores from 0 to 3.5 μm . In this case, mode distribution has become more distorted and covers a larger area in the core. An evanescent wave also radiates more power. The recommendation allows for $\sim 1 \mu\text{m}$ higher tolerance of core than was actually used. Distribution of power in a three-dimensional view for two selected modes with a 3.5 μm radial shifting of cores is also shown in Fig. 3. Results represent shifted eccentricity cores (52 to 48 μm) for basic modes.

Dependence of vibrational shifting was also modeled by simulation software with the simulation scheme in Fig. 4 referring to the vibrational measurement setup. It contains a continuous wave laser of 1310 nm with an output power of 0 dBm, three spatial connectors with variable connections, and an optical power meter placed at the end of the setup. The connectors are joined by graded-index MM 50/125 fibers with the movement of the fibers being realized within two principal axes. The forehead shift was set from 0 to 4 μm in the x axis, from 0 to 4 μm in the y axis in the second connector, and combinations up to 2.2 μm in both x and y axis in the third connector to achieve different shifting directions. The difference in IL per connection was up to 0.034 dB for the maximum shift with reference power -0.632 dBm. Three connectors were joined by two 1-m-long MM fibers and connected by 20-m-long MM fibers to the source and detector. With dependence on the number of modes, shifting, rotation, and performance of the connectors, these impacts could lead to an additional attenuation of up to 0.1 dB for the case of three connectors.

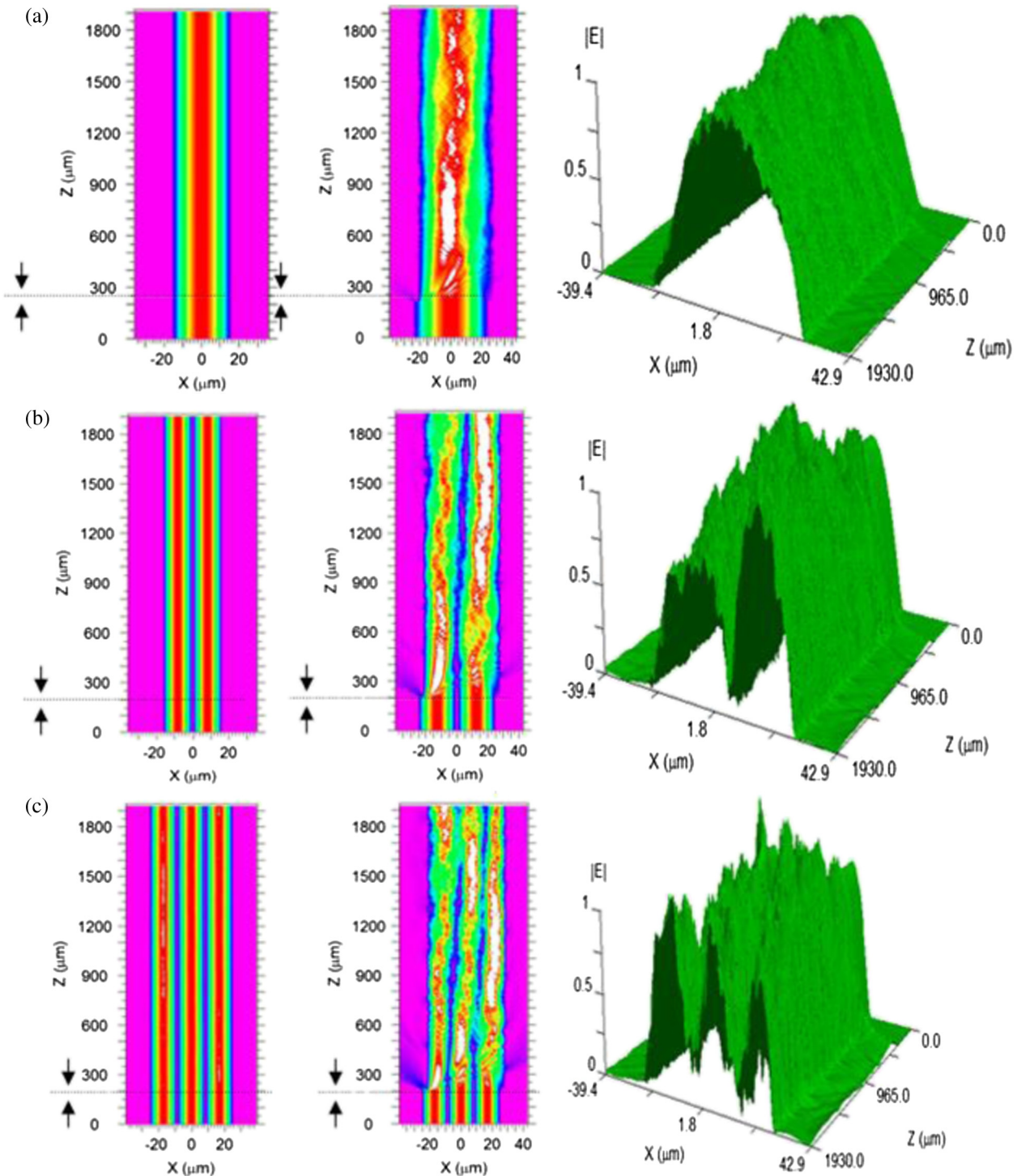


Fig. 2 Dependence of modes LP_{01} , LP_{11} , and LP_{02} (from top to bottom) on shifting fibers with three-dimensional illustration of distributed power: (a) LP_{01} , (b) LP_{11} , and (c) LP_{02} .

3 Experimental Setup and Results

We carried out several measurement tests for 50/125 MM fiber and their connections for avionic applications. Contrary to the first generation of multimode fibers (OM1/OM2), novel MM fibers OM3 and OM4 (known as laser-optimized fibers) are utilized for their enhanced bandwidth. The fibers are designed for a laser-based high bit-rate transmission,

working in a few-modes' regime. Modern OM3/OM4 fibers differ from the first generation by an almost ideal graded refractive index, which rapidly reduces the differential mode delay (DMD) and increases the bandwidth.¹⁵ We investigated the resistance of connected MM graded-index fibers OM3 and OM4 against temperature changes and vibration set to identical in-flight conditions.

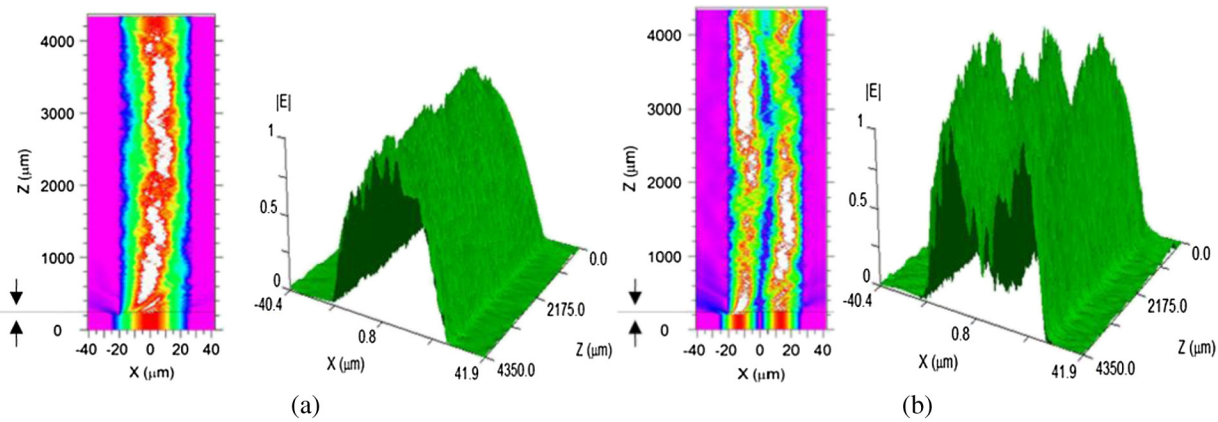


Fig. 3 Dependence of modes LP_{01} on shifting fibers with core eccentricity $48/52 \mu\text{m}$: (a) LP_{01} and (b) LP_{11} .

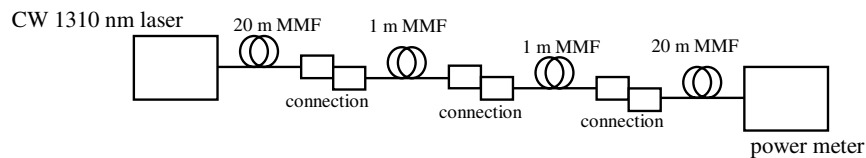


Fig. 4 Simulation setup of fiber shifting.

3.1 Thermal Tests

First, a measurement setup having various temperature sections was realized as shown in Fig. 5. Two MM fibers types OM3 and OM4 are connected by four FC/PC connectors. Two types of optical sources were used: a polychromatic halogen lamp (Ocean Optics H2000, Dunedin, Florida) and a distributed feedback laser (DFB) 1310-nm laser, respectively. Fluctuations of IL were observed at a wavelength of 1310 nm with changing temperature conditions. The optical link, having a total length of 6 m, passed through an open space section (22°C), temperature chamber 1 (temperatures up to 85°C), another open space section (22°C), cycling temperature chamber 2 (temperature set from -60 to 20°C), and via the last open section without a connector splice.

The first case contained a polychromatic source with a constant temperature of 22°C away from the chamber, a constant temperature of 85°C in chamber 1, and a continuously changing temperature in chamber 2. The temperature decreased from 22 to -60°C and back to 22°C in 10-min steps within a 6-h duration. It simulated different thermal conditions along an airplane and their changeability from take-off until landing. Results of the measurements are depicted in Fig. 6(a). It is obvious that parameter Δ IL (green curve) follows temperature changes. The highest deviation of IL was ~ 0.13 dB and it is evident that the lower the temperature, the higher the IL. Detection of the

received power at 1550 nm clearly duplicates the received power at 1310 nm. We presented a more detailed process to capture a more precise correlation between the temperature change and IL change than in previous results.

The second measurement was performed with a DFB 1310 nm source. The temperature was changed only in chamber 1, which was heated to 85°C and then cooled down. All remaining parts of the setup had the same temperature of 22°C . We observed the highest change in IL of ~ 0.024 dB after fluctuating the temperature as seen in Fig. 6(b), where the difference between thermal conditions of 85 and 22°C is easily discernible. During both thermal changes (chamber 1 and chamber 2), the total Δ IL fluctuated around a range of 0.025 dB.

3.2 Vibrational Tests

The impact of vibrations of optical connections on insertion loss was investigated next. The whole optical setup, consisting of optical connectors, was placed on a special vibration membrane with a flexible pad as shown in Fig. 7. The rest of the deployment was loosely gripped. The acoustic tester platform allowed the undertaking of vibrational tests within a frequency range from 10 Hz up to 2 kHz. The total length of the fiber setup was 6 m with OM3 and OM4 fibers connected by three FC/PC connectors. Connectors with OM3 and OM4 fibers, manufactured on the limits of recommendations from the standards for MM fibers, such as ISO/IEC

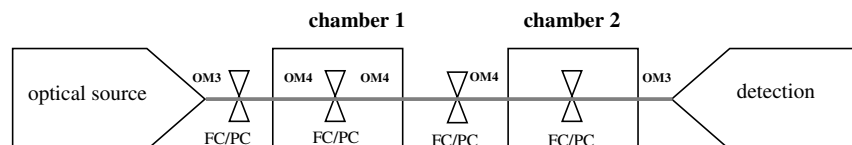


Fig. 5 Schematic of temperature measurement.

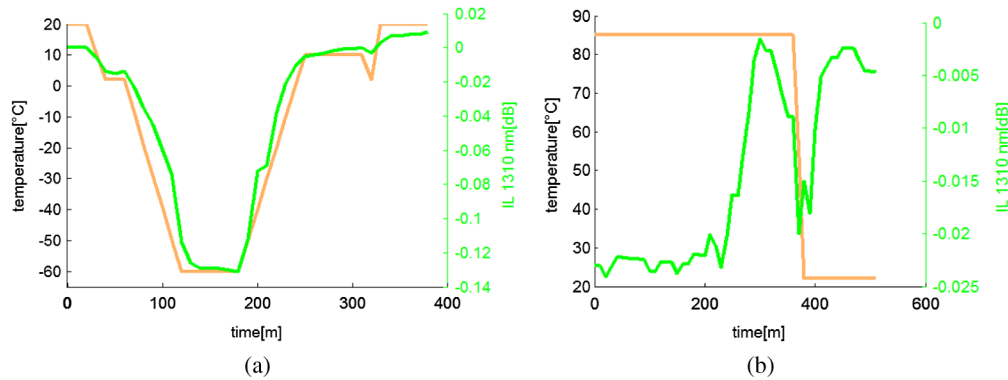


Fig. 6 (a) IL by chamber 2 temperature cycling with polychromatic source. (b) IL by chamber 1 temperature cycling with distributed feedback laser (DFB) laser source.

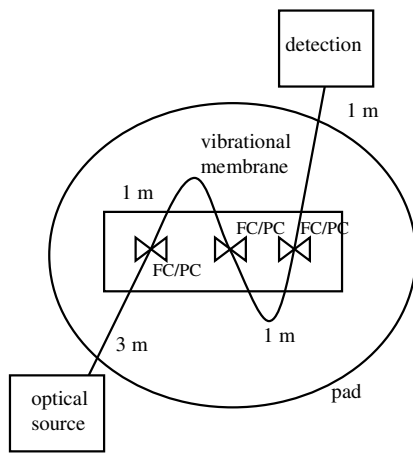


Fig. 7 Schematic of vibrational measurement.

11801, IEC 60793-2-10, TIA/EIA, and ITUG 651.1, were used to simulate the worst-case scenarios that can occur. Recommendations allow, for example, maximum span distances for 40G/100G systems of 100 m in OM3 and 150 m in OM4, respectively.¹⁵

To achieve realistic properties of the optical link, the same two sources were used as in the previous measurement. The vibration frequency was changed from 5 Hz to 2 kHz and the Δ IL of the whole link was observed. Three cases were used to determine the influence due to MM fibers. Only a standard OM3 was involved in the first measuring case. The second case contained a combination of OM3-OM4-OM4-OM3 and

the third case was, unlike the first case, realized by using only OM4 fibers. The fibers had a 900 μ m tubing instead of a 20-cm section next to the optical source and only had a 250 μ m coating.

All connectors and fibers gripped on the membrane were drifted as given by the acceleration in a particular frequency which causes an overload even over 20 G. The measured dependence of the acceleration on frequency is shown in Fig. 8(a). It is very possible to find an almost linear growth up to 200 Hz. The characteristic of the acceleration was related to the measured results described below. The first test was performed with only OM3 fibers with a polychromatic H2000 source. Δ IL increased up to 0.003 dB in the first test and up to 0.006 dB in the second case. The progress of the first test is shown in Fig. 8(b), with the blue curve representing the increase in frequency from 5 Hz to 2 kHz and the green line covering the decrease in frequency from 2 kHz to 5 Hz.

The second test contained a combination of OM3 and OM4 fibers. Two 1-m-long OM4 fibers were placed on the membrane and connected to the OM3 fibers. See two results for polychromatic and monochromatic sources in Figs. 9(a) and 9(b), respectively. We measured four series of tests with the highest Δ IL equal to 0.042 dB at a frequency of 1 kHz with a polychromatic source and 0.007 dB with a monochromatic source. All shapes contain a decrease of IL around a frequency of 200 Hz; then the IL increased rapidly and became more stable, according to the accelerative process.

Only OM4 fibers were measured during the third test as seen in the results in Fig. 10. The IL evidently changes and

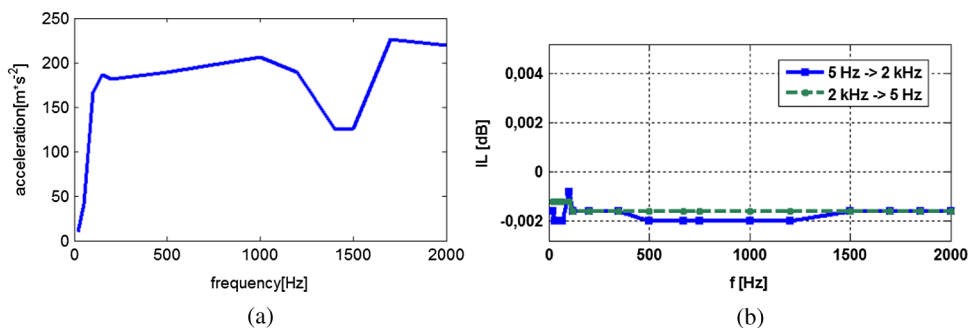


Fig. 8 (a) Dependence of acceleration influencing the connectors. (b) OM3 connection test with halogen lamp.

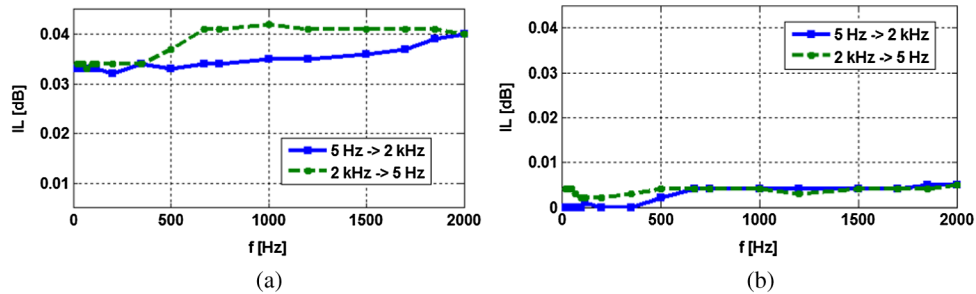


Fig. 9 OM3-OM4 connection test with (a) halogen lamp and (b) DFB 1310 laser.

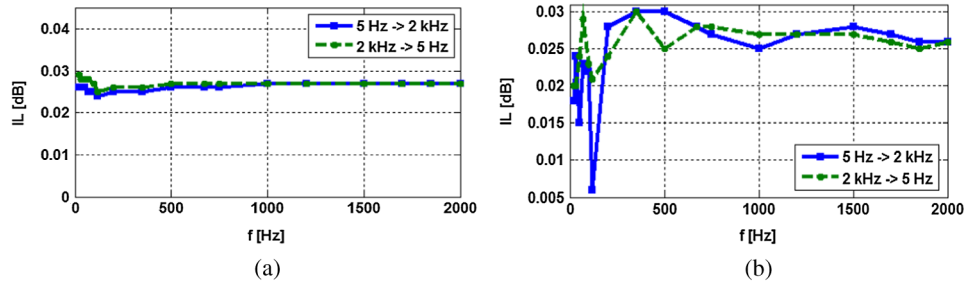


Fig. 10 OM4 connection test with (a) halogen lamp and (b) DFB 1310 laser.

decreases around 200 Hz and then increases behind this point within all performed series. Δ IL reached a maximum of 0.038 and 0.03 dB for the polychromatic and monochromatic sources, respectively.

The progress of Δ IL for all tests has oscillations around a frequency of 200 Hz where the smallest attenuation can also be found, and the shape of Δ IL becomes more linear and constant behind this point. The measured stability of the setup was ± 0.001 dB, which implies the results were correct. Three connectors were tested with a total length of 6 m for the setup. An entire aircraft optical network would have ~ 10 connectors⁵ and a length of optical link in the hundreds of meters causing attenuation of at least three times that in the performed tests, possibly worsening the optical signal-to-noise ratio. If we considered both thermal and vibrational changes, Δ IL would be ~ 1 dB for the worst case scenario with a dependence on wavelength, source, fiber recommendations, etc.

4 Whole Network Analyses

According to the temperature and vibrational measurements, the influence of the spliced IL was further exploited and demonstrated via simulations of the whole airplane network. There are many requirements for sensor systems, including landing cameras, which are already placed on Airbus aircrafts. An optical multimode link is led through various sections, including connectors, as proper maintaining reconfiguration tools for supervising. The connectors bring a potential additive loss to the network and can be less resistant to harsh conditions. The entire network is built on the concept of point-to-point links led from a central unit at the head of the airplane to particular landing cameras as shown in Fig. 11. The longest distance, led from the central unit to the tail camera, measures ~ 250 m long with stressed occurrences seriously limiting possible transfer bandwidth (e.g.,

OM3 fibers allow 10 G systems for 300 m and 40 G systems for only 100 m).¹⁵

The impact of a harsh environment, such as thermal and vibrational changes, was observed when increasing the bit error rate (BER), decreasing the Q-factor and deformed eye diagram. Several cases were considered with continuously increasing IL due to a harsh environment from 0 to 1 dB for all connections in the link. The link was analyzed for 10 Gbps nonreturn to zero (NRZ) with results illustrated in Fig. 12.

Increasing BER was registered from $1.19 \cdot 10^{-6}$ to $8.59 \cdot 10^{-5}$ for 10 Gbps NRZ and increasing Q-factor with a difference of 0.96. Raising the optical power brought an improved error rate, but at the expense of higher demands on the transmission systems.

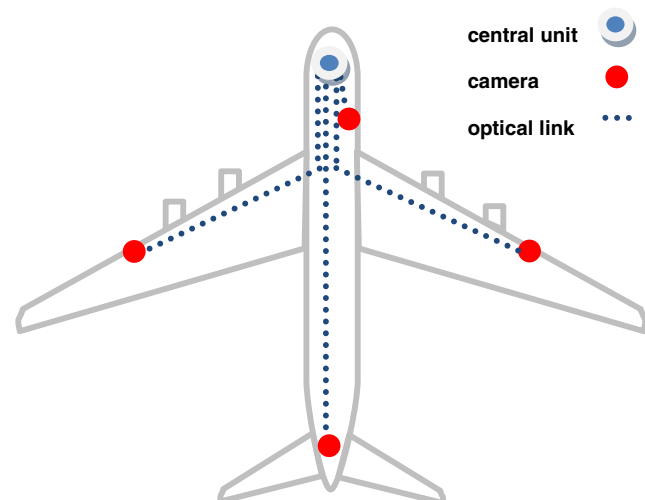


Fig. 11 Airplane MM camera network.

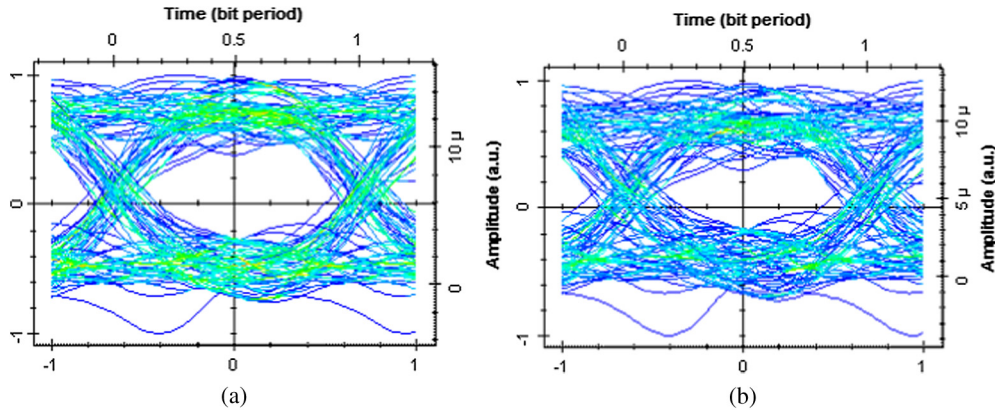


Fig. 12 Eye diagrams for 10 Gbps nonreturn to zero: (a) IL = 0 dB and (b) IL = 1 dB.

The most limiting factor reducing the bandwidth of multimode fibers is modal dispersion.¹⁶ Dispersion could be highly suppressed by the proper performance of the refractive index, but due to the radial shifting of the fiber end faces, a different modal distribution can result in bandwidth reduction. We carried out a simulation on an OM3 measured, refractive, and profiled fiber to investigate the statistics of DMD, the number of guided modes, and changes in the bandwidth.

Simulation of DMD was performed with radial shifting of the transmitted beam coupling with a beam featuring a 5 μm profile and a step of movement of 1 μm. A test was performed at a wavelength of 850 nm to investigate convenient conditions for transmission. Pulse broadening and bandwidth reduction was observed at each point of the shift. The simulation scheme corresponds to the vibrational scenario described in Sec. 2.

Significant changes in transmission characteristics were observed in the case of maximal shifts. This can be clearly shown via pulse broadening in Fig. 13, which starts with beams guided closer to the cladding. In other words, the figure shows how the DMD affects the duration of the launched pulse in respect to radial position. Figure 14 depicts a comparison of the bandwidth in MHz·km for the used fiber section with a drop for radial offsets > 10 μm during vibrational influence.

Both figures demonstrate how the DMD influences modal bandwidth (directly or indirectly). In a steady state, the pulse

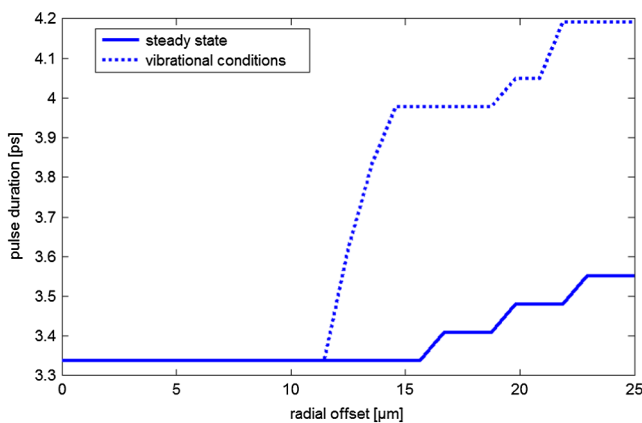


Fig. 13 Pulse broadening due to radial shifting.

broadening starts approximately before the 15 μm shift, but during vibrational conditions, the broadening starts approximately before 11 μm and achieves >0.7 ps higher broadening compared to the steady state. Pulse broadening was observed within fibers having a set length of 22 m. The situation is similar in the case of the shape of bandwidth statistics. The useful bandwidth continually (without considering peak values) decreases to zero. A connection offset causes a similarly useful bandwidth (~1000 MHz · km in the range of 0 to 10 μm and then it drops). The visible step determines where most of the optical power should be guided and limits the transmitted bandwidth. The bigger the radial shift of the launched beam, the more the modes

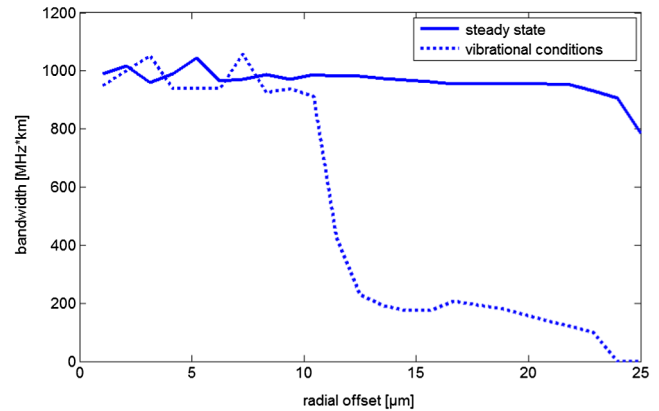


Fig. 14 Reduction of bandwidth due to radial shift.

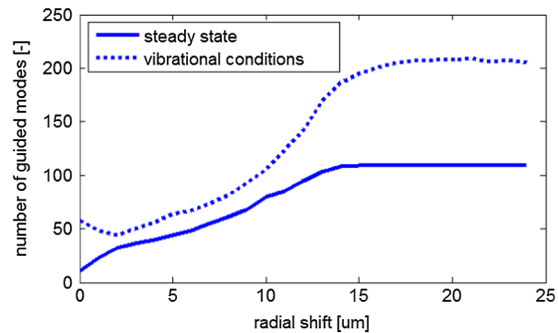


Fig. 15 Number of guided modes in fiber related to radial shift.

were guided in fibers and the higher the impact the DMD had on transmission characteristics. The dependence of guided modes on the radial shift is shown in Fig. 15 with the solid line representing a steady state and the discontinued line representing a situation with connection offsets due to vibrations.

Increasing the number of modes before the offset of $\sim 10 \mu\text{m}$ corresponds to an increase in DMD and a bandwidth reduction.

Simulation results imply that a harsh environment (from the point of view of temperature and vibrational changes) can easily modify the connection profile of fibers, especially for MM fibers with high tolerable recommendations and norms.

5 Conclusion

We have demonstrated the influences of MM class OM3 and OM4 optical links within a harsh environment, in particular in the field of avionics. Tests were designed to determine the impacts of thermal and vibrational changes on connectors and intersections. Simulation and experimental results show that although these effects could lead to slight changes of IL up to 1 dB for the whole optical link including various sections joined by connectors, the influence on bandwidth reduction has to be considered. Vibrational conditions, together with a low tolerance for fiber industry standards, lead to deformed mode-field characteristics and an increase of DMD. This substantially reduces the bandwidth to $<20\%$. Every additional connector joint (in aircraft, this is occasionally inevitable due to assembly) can randomly increase bandwidth reduction. Understanding mode distribution changes and substantial bandwidth reduction in a harsh environment is a key phenomenon that has to be considered to assure the consistently high reliability of aircraft optical networks.

Acknowledgments

This work was supported by the Czech Technical University Grant No. SGS14/190/OHK3/3T/13. The authors would like to thank SQS, Fiber Optics for providing access to the vibrational testing laboratory.

References

1. A. A. R. Lee and S. D. Rayner, "Avionic architectures incorporating optical fibre technology," in *IEEE Conf. on Avionics Fiber-Optics and Photonics*, pp. 10–11, IEEE, New York, NY(2006).
2. C. V. Oster, Jr., J. S. Strong, and C. K. Zorn, "Analyzing aviation safety: problems, challenges, opportunities," *Res. Transport. Econ.* **43**(1), 148–164 (2013).
3. R. Pirich and J. Mazurowski, "Engineering of fiber optics infrastructure," in *Systems, Applications and Technology Conf.*, pp. 1–4, IEEE, New York, NY(2012).
4. P. Jérôme, "Composite materials in the Airbus A380—from history to future," 2013, <http://www.iccm-central.org/Proceedings/ICCM13proceedings/SITE/PAPERS/paper-1695.pdf> (8 August 2014).
5. DAPHNE project, "Developing aircraft photonics networks," <http://www.fp7daphne.eu/> (August 2011).
6. K. Schulze et al., "Model-based design and evaluation of fault-tolerant fibre-optical networks for avionics," 2011, https://www.tu-ilmeneau.de/fileadmin/public/sse/Veroeffentlichungen/2012/PSAM_ESREL_2012_Final.pdf (8 August 2014).
7. J. Gomez et al., "Comparing polymer optical fiber, fiber Bragg grating, and traditional strain gauge for aircraft structural health monitoring," *Appl. Opt.* **48**(8), 1436–1443 (2009).
8. N. Takeda, "Embedded fiber optics shed light on aircraft damage," 2008, <http://spie.org/x20265.xml> (8 August 2014).
9. Q. Li et al., "Scaling star-coupler-based optical networks for avionics applications," *J. Opt. Commun. Netw.* **5**(9), 945–956 (2013).
10. H. J. White et al., "Developing aircraft photonic networks for airplane systems," *Proc. SPIE* **8720**, 87200V (2013).
11. J. C. Williams and E. A. Starke Jr., "Progress in structural materials for aerospace systems," *Acta Mater.* **51**(19), 5775–5799 (2003).
12. C.-L. Chen, *Elements of Optoelectronics & Fiber Optics*, Irwin Professional Publishing, Illinois (1996).
13. J. M. Anderson et al., "Report: lightwave splicing and connector technology," *AT&T Tech. J.* **66**(1), 45–64 (1987).
14. ITU-T Recommendation G.651.1, "Characteristics of a 50/125 μm multimode graded index optical fibre cable for the optical access network," 2007, <http://cds.cern.ch/record/1393442> (8 August 2014).
15. A. V. Bourdine, "Design of refractive index profile for multimode optical fibers with low differential mode delay," *J. Optoelectron. Eng.* **1**(1), 5–13 (2013).
16. D. H. Sim et al., "High-speed multimode fiber transmission by using mode-field matched center-launching technique," *J. Lightwave Technol.* **27**(8), 1018–1026 (2009).

Jan Bohata is a researcher at Czech Technical University (CTU) in Prague, Department of Electromagnetic Field. He received BS and MS degrees in electrical engineering from CTU in Prague in 2010 and 2012, respectively, where he is continuing his PhD studies. He has been involved in a few research projects focused on fiber optics problematics, including investigation of harsh environments for optical fibers. His current research interests include fiber optics, radio over optic systems, harsh environment for communications, and radio wave propagation.

Michael Písařík is a senior project manager at SQS. He received his MSc in 2002 from CTU in Prague. He leads the research department and R&D teams from SQS. His current research interest includes optical sensors, optics for harsh environment, fiber lasers, and modulators.

Stanislav Zvánovec is an associate professor and vice-head of the Department of Electromagnetic Field at the CTU in Prague. He received his MSc and PhD in 2002 and 2006, respectively, from CTU in Prague. He leads an optical team from Faculty of Electrical Engineering, CTU. His current research interests include fiber optical systems, sensors, and wireless optical communications.

Pavel Peterka received his MSc degree in physical engineering in 1993 and PhD degree in radioelectronics in 2000 from CTU in Prague. He is currently a senior research scientist in the Institute of Photonics and Electronics, Academy of Sciences of the Czech Republic. He has over 15 years of experience on design, characterizing, and development of specialty fibers and fiber lasers and amplifiers.

4.5 Testing of Optical Fiber Components for Harsh Environments

This chapter is a version of the published manuscript:

- [C1] J. Bohata, M. Pisarik and S. Zvanovec, "Testing of optical fiber components for harsh environments," in Avionics, Fiber-Optics and Photonics Conference (AVFOP), 2013, pp. 33-34.

Points pertaining to my PhD thesis:

This paper extends the previous chapter in the area of short-term influences and introduces special temperature environmental tests of optical connections which are needed for such a harsh environment. The MMF IL dependence on temperatures within the range of -60 °C to 85 °C was derived for different environmental scenarios.

TESTING OF OPTICAL FIBER COMPONENTS FOR HARSH ENVIRONMENTS

J. Bohata¹, M. Pisarik^{1,2}, S. Zvanovec¹

*¹Department of Electromagnetic Field, Czech Technical University in Prague
Prague, Czech Republic*

²SQS Vlaknova Optika a.s., Komenskeho 304, 509 01 Nova Paka, Czech Republic

Introduction

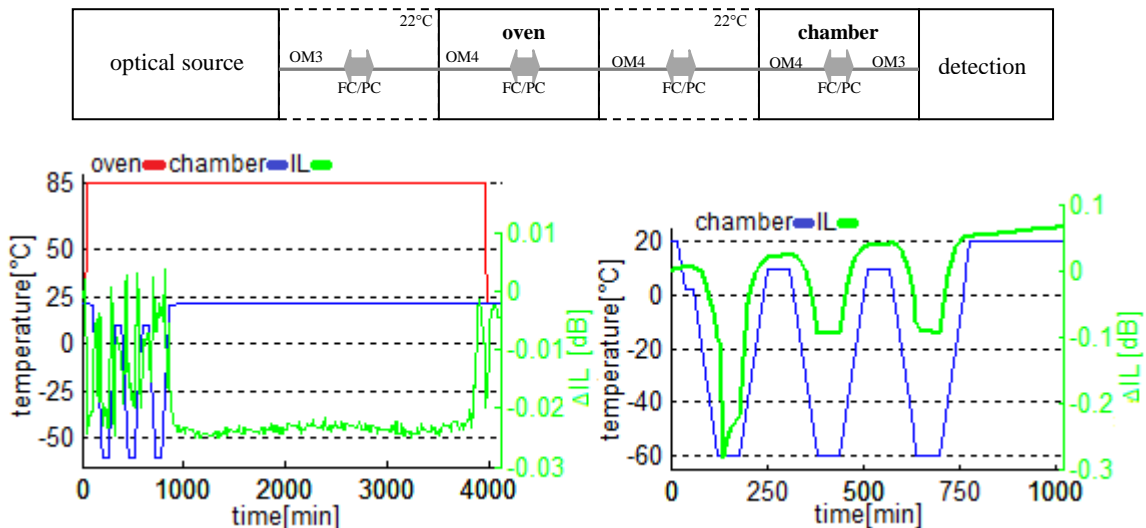
Optical fibers provide many benefits to the telecommunication systems and their usage has more and more current even in the avionics industry [1]. It offers an attractive solution for airplanes, such as replacing copper conductors to reduce weight of the plane, electro-magnetic interference, bring high-speed communications connection, implementation of optical sensors, etc. Nevertheless for extremely high requirements on safety it is also necessary to precede all inflight influences. For summary of potential threats see e.g. [2]. One can easily find a several conditions of a harsh environment or an unfriendly fiber surrounding which could have a fatal impact to the transmission characteristic as attenuation statistics leading to link drops, time jitters or pulse degradations in time domain. There are different temperature gradients on the deck through which the infrastructure can pass while experiencing differentiated degradation and thus changed conditions within a physical layer. This paper is focused on an analysis of temperature-dependend influences on insertion losses and other parameters of optical connectors, combining two types of multimode fibers, purposed for installation within an aircraft optical network.

Measurement and results

Optical multimode fibers 62.5/125(50/125) μm have been already integrated on A340 and A380 aircraft family as transport medium for digital cameras on the bottom side of aircraft (for landing camera). In order to assign behavior of such fibers, two types of multimode fibers - standard OM3 and OM4 respectively - were tested in measurement campaign taken by Czech Technical University and SQS, Fiber optics. To assign specific characteristic, two types of optical sources - monochromatic (DFB laser 1310) and polychromatic (halogen lamp Ocean optics HL-2000) – were utilized. The fibers were connected by four FC/PC connectors having each connection placed in differently temperature controlled areas with total length 6 m. Optical non-modulated signal traveled through four different environments which represented various conditions on the airplane (see deployment of measurement in Fig.1a). The first section introduced open-space area with temperature 22°C, followed by area with variable temperature expressed by the Mora oven having temperature range from 22°C to 85°C, connected to another open-space section and finally the fiber system was led through the second controlled chamber with temperatures varying from -60°C to 22°C.

Examples of measurement results expressed in terms of attenuation fluctuation measured at 1310 nm for both types of sources are shown in Fig. 1b) and Fig. 1c), respectively. Green line represents insertion loss of particular subsystems. It can be distinguished; the curve clearly follows temperature changes in the oven (red line) and in the chamber (blue line). The biggest difference was 0.03 dB, what implies about 12.5 % of total loss of whole optical system and what was also accurately correlated between both time-dependences. The second case (with halogen lamp) was measured with constant temperature in the oven set to 85°C and changing temperature in the chamber – see results in Fig. 1c. However the attenuation characteristic reached rapid fades up to almost 0.3 dB. It could be emphasized that fluctuation of temperature in optical connectors is followed by highly correlated change of attenuation - the attenuation increases with decrease of temperature in slight delay (mean delay value from numerous measurement approx. 13.3 min).

In order to get deep insight on long term transmission changes in optical fibers, connectors and splicing, a measuring polygon (cable-protected network exposed without some special shielding to both weather conditions and artificial influences) was installed on the roof of one building of Czech Technical University in Prague) - see Fig. 2.



To investigate influences of corrosive liquids, subparts of Prague subway optical network, flooded in 2002, was included within the monitoring campaign. The first results from this measuring network will be as well published at the conference. It has been experienced increased losses in the connectors (regardless this more than half of network was still available and particular segments have been used) and fibers, influence on polarization mode dispersion etc.

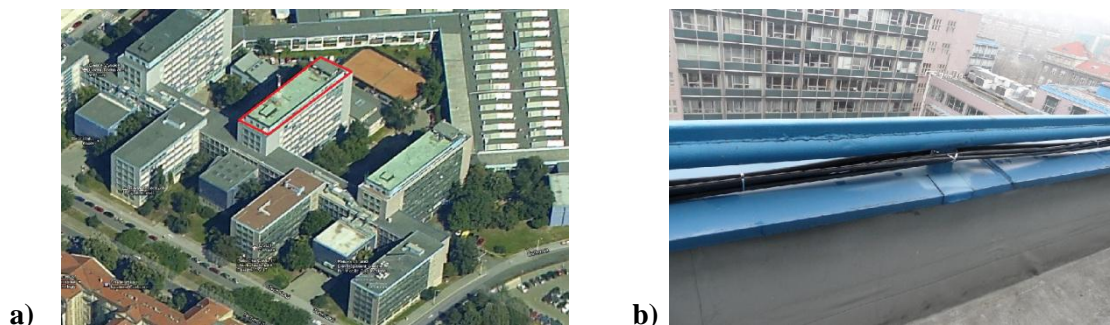


Figure 2. Testing polygon: a) CTU campus; b) cable-protected fibers

Conclusion

The influence of the harsh environment to optical connectors was evaluated. In order to keep similar conditions like on airplanes, various temperature areas along optical subsystem were investigated. High dependence of transmission parameters on temporal deviation was experienced. The biggest IL difference implies almost 0.03 dB and 0.3 dB for monochromatic and polychromatic source respectively with four fiber connections. This feature should be taken into account when planning and deployment aerial optical infrastructures especially based on multimodal fibers. Next research will be focused on analyzing of long-term based influences of optical components in harsh environment.

Acknowledgement

This work was supported by the CTU grant No. SGS12/142/OHK3/2T/13.

References

- [1] G.M.Proudley, N.Brownjohn and J.Baptista; "Developing aircraft photonic networks - an overview of the European DAPHNE project." *Avionics, Fiber- Optics and Photonics Technology Conference (AVFOP), 2011 IEEE.*
- [2] Ronald Pirich and Kristie D'Ambrosio, "Fiber Optics for Harsh Environments," *Systems, Applications and Technology Conference (LISAT), 2011 IEEE Long Island.*

4.6 Outdoor Atmospheric Influence on Polarization Mode Dispersion in Optical Cables

This chapter is a version of the published manuscript:

- [C2] J. Bohata, S. Zvanovec and M. Pisarik, “Outdoor atmospheric influence on polarization mode dispersion in optical cables,” in General Assembly and Scientific Symposium (URSI GASS), 2014, pp. 1-4.

Points pertaining to my PhD thesis:

The first unique results of temperature fluctuations and the corresponding PMD variations are presented from an uniquely developed optical testbed, purposed to form a novel methodology of long-term optical characteristic monitoring. Data were collected from four individually deployed routes. The results present the first insight on long-term PMD changes which strongly influence the quality of optical transmissions but which had been previously difficult to predict.

Outdoor atmospheric influence on polarization mode dispersion in optical cables

J. Bohata^{1,*}, S. Zvanovec¹, and M. Pisarik^{1,2}

¹*Department of Electromagnetic Field, Czech Technical University in Prague
Prague, Czech Republic*

²*SQS Vlaknova Optika a.s., Komenskeho 304, 509 01 Nova Paka, Czech Republic
bohataj2@fel.cvut.cz

Abstract

Oscillation of phenomena birefringence under atmospheric conditions is reported. Paper contains measured values of polarization mode dispersion from long term monitoring scenario and gives illustration about measuring of long time installed cables. Several commonly utilizing measuring techniques were used to determine birefringent properties of the fibers. Results are correlated with temperature changes during different terms to achieve proper comprehensive conception of progress.

1. Introduction

With new transmitted formats and modulations in optical communications and sensor networks, Polarization Mode Dispersion (PMD) has become very important parameter with significant impact to transmission capacity. For high bit rate transmissions with long reach ability, it is necessary to keep Differential Group Delay (DGD) low and thus it desires watching of PMD parameter and PMD coefficient which determine statistical distribution of DGD. The distribution is then presented for whole fiber length by PMD coefficient. In order to determine random behavior of birefringence there is requirement for long term PMD monitoring and the longer monitoring setup the more precise results are obtained. Long-term measurement of PMD was theoretically described in 2000 by M. Karlsson [1], who used the Jones matrices and statistical evaluation DGD. However during high PMD fibers measuring it is also required to define hazardous areas, containing high PMD sections, which can have fatal impact to accuracy and also to transmissions characteristic. For this purpose, the Polarization Optical Domain Reflectometer (POTDR) method was developed [2]. The method facilitates precise location of the mentioned sections which gives good tool for optical network infrastructure development and supervising.

According to recommendation ITU-T G.652[3] the longest distance for 40 Gbit/s system can be 80 km in case of PMD coefficient $0.2 \text{ ps/km}^{1/2}$ while it is decreased even up to 2 km for PMD around $0.5 \text{ ps/km}^{1/2}$. The random behavior of birefringence in installed cables comes most frequently with temperature and wavelength changes. In 2003, M. Brodsky presented papers on the optimal path length, measured to evaluate PMD[4], which concluded that some of the fibers can be characterized during the one week while a so called "live" fibers require characterization measurements over months or years. Poggiolini [5] performed 73-days' measurement metropolitan area networks in Turin, stating that the changes DGD are inherently limited due to the daily cycle and entire period. The impact of temperature to the cables was well discussed in [6]. Despite of recent made fibers and cables, old produced fibers have been still utilized within networks which have not had accurate PMD quality control. In the time of their installation, such parameters were not required. One have to take in consideration potential aging of photonics structures[7] which can be evoked by high optical powers and as well their possible damaging[8]. The paper presents comparison of commonly used PMD measuring methods and their validation during different terms in aged fiber structure. First results of atmospheric influence on PMD statistics measured in unique measuring polygon are published.

2. Measurement setup

In order to ensure real transmission characteristic for optical fibers and cables, a measuring polygon was designed and placed on the roof of Czech Technical University in Prague, Faculty of electrical engineering (see Fig. 1a). The scheme is involved for long term monitoring of transmission characteristics under environmental conditions such temperature, pressure, humidity or wind. For easy access to polygon its switch was placed to the optical laboratory. To achieve proper information about instant weather changes, two meteorological stations recording the temperature, humidity, atmospheric pressure, precipitation, rain intensity and the speed and direction of the wind were also placed on the roof of university campus. These stations' positions (A, B) with testing polygon (C) are shown in Fig.1.



Figure 1. Testing polygon: a) roof of CTU building b) Alcatel cable c) optical terminal

Cables, purposed for monitoring, were precisely selected especially because of containing of high PMD sections. The sections were at first characterized by P-OTDR measuring. Fibers within the cables originate from 1994 and they had been primary used for metropolitan optical network in Prague subway under different conditions. These fibers have not ever been investigated through PMD measuring or observing. Polygon setup consists of two same Alcatel cables containing 72 fibers within 6 tubes. Each cable is approx. 500 m long, welded together in the connection box placed also outside. Total length of links is then approx. 72 km, divided to four sections with lengths 12 and 24 km respectively. Sections are formed from separated tubes within cable to maintain consistent conditions. Measurement setup is shown in Fig. 2.

All 12 fibers in each tube were welded together so that each link passes 12-times through all circuit along the building wedge. In addition, the whole circuit is formed by 6 smaller circuits including different conditioned areas such as shadows, shielding and nearness electronic devices like an air condition, etc. Structure of cable and measurement scheme is described in Fig. 2.

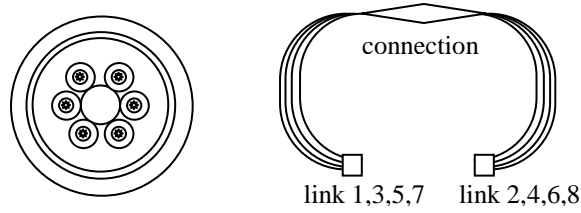


Figure 2. Measurement scheme: a) cable profile; b) optical links

We carried out initial measurements with different commonly used methods such interferometry (Traditional Analysis Interferometry – TINTY and General Analysis Interferometry – GINTY)[9], Scrambled State-of-Polarization Analysis (SSA)[10] and POTDR[11] on wavelengths 1520-1627 nm. Since the random behavior of birefringence and using different techniques then we have obtained relative high range of total PMD. In order to avoid mistakes with length mismatch of the cables, we investigated PMD coefficient applied to fiber length and contributions in each section were observed by POTDR. We assume the distances $L > 1$ km to ensure the PMD coefficient can be determined in terms of $\text{km}^{1/2}$ [12].

With assuming propagation constants in two orthogonal principle axes β_x and β_y at wavelength ω , these constants are different due to birefringence[13]:

$$\Delta\beta = (\beta_x - \beta_y) = \frac{\omega}{c} \Delta n_{eff}, \quad (1)$$

where Δn_{eff} refers to differential effective refractive index for the two modes. Relative group delay (referred as DGD) between two orthogonal polarization modes for fiber length L is expressed by:

$$\Delta\tau_g = \frac{L\Delta n_{eff}}{c}. \quad (2)$$

Differential Group Delay round trip in position z , used in PMD distributed measurement, is therefore computed as follows[14]:

$$DGD_{RT}^2(z) = \frac{1}{\delta\omega^2} \alpha_{dT} \Delta T_{ms}, \quad (3)$$

where $\delta\omega^2$ is relative wavelength spacing, α_{dT}^2 relative scrambling factor and ΔT_{ms} is mean-square value of number of wavelength differences.

3. Results

Measuring scheme contains older fibers which were historically (as can be case of majority of older laid infrastructures) tested mainly only over attenuation and Chromatic Dispersion (CD). To the authors best knowledge these parameters of the fibers to date have not experienced any detrimental changes. Despite of well-known random PMD oscillation influenced by stressed conditions, we characterized how these conditions, especially temperature, could influence long term PMD measurement with several measuring techniques.

This paper presents first demonstrations of PMD measurements at CTU polygon using different techniques described above. Fibers tests results are from April 2013 till January 2014. Root Mean Square (RMS) value was calculated to determine PMD coefficient. Then the variance of PMD coefficient, displayed in y- axes, was computed from RMS of the each measured value. The links were tested from both ends and they are designated as follows: four fibers with marked ends (link 1,2; link 3,4; link 5,6 and link 7,8). Table 1 contains PMD_{RMS} values for all links. Figure 3 represents RMS differences for two 12-km links and Figure 4 compares remaining two 24-km links.

Table 1. PMD values of the links

link:	1	2	3	4	5	6	7	8
$PMD_{RMS}[ps]$	0.758	1.028	4.968	5.131	3,44	3.194	7.074	6.820
$PMD_{coeff-RMS}[ps/km^{0.5}]$	0.232	0.243	1.419	1.460	0.742	0.661	1.462	1.419

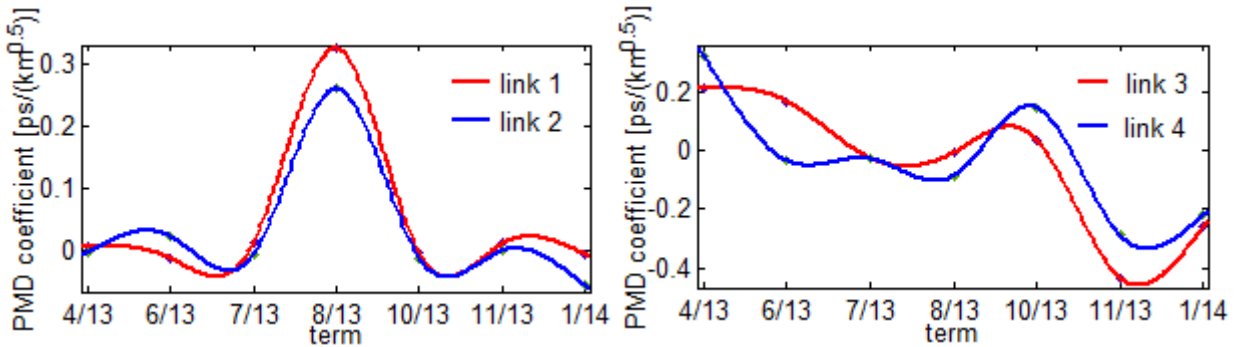


Figure 3. RMS difference: a) first 12 km links; b) second 12 km links

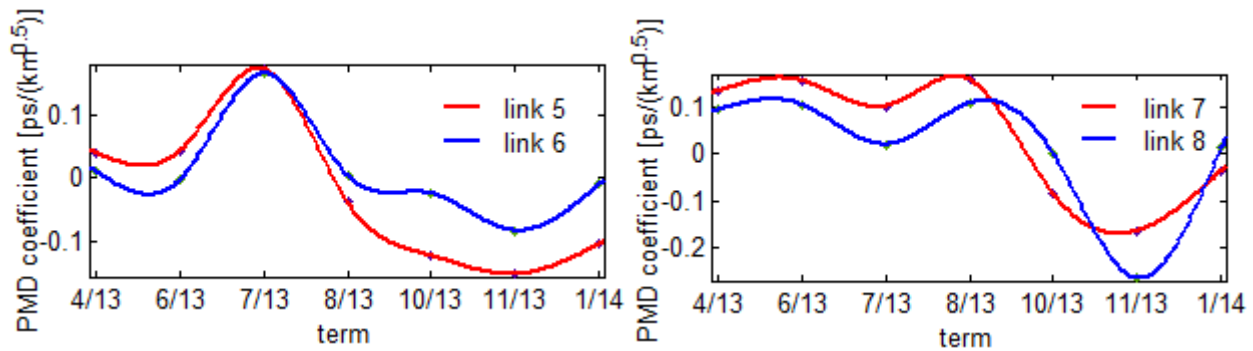


Figure 4. RMS difference: a) first 24 km links; b) second 24 km links

Results show fluctuations of PMD coefficient during measuring terms. We have observed fluctuations up to almost $\pm 0.3 ps/km^{1/2}$. It mostly comes from not-uniformed distribution of cumulative DGD along fibers. It seems that hazardous sections behave much different under the stressed conditions. The distribution of cumulated PMD was investigated by POTDR method. We have observed increased PMD in hazardous section (see peak in Fig.4a) which caused almost 20 % of all PMD in only 967 meters while some low PMD sections indicate invariable progress. After that, the oscillations of all links were correlated with temperature - see Fig. 5.

Measured temperature highly correlates with oscillation of PMD coefficient but the temperature has one but not the only impact to DGD results. Although the all fibers originate from one developer and they are clustered in one optical cable, the particular components evince very different behavior, especially in PMD point of view. A lot of splices also contribute to ambiguous results. More measured results will be available by term of the conference.

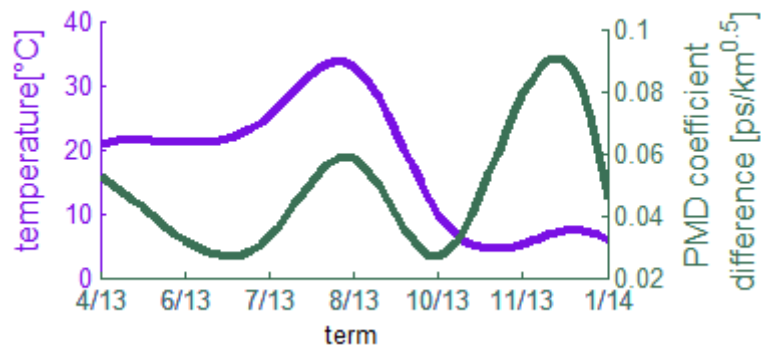


Figure 5. Thermal changes vs. PMD difference

5. Conclusion

The paper discussed various measuring accuracy of birefringence phenomena with aiming to long time statistics observed on installed fibers. PMD features were monitored in harsh environment. First results from measuring polygon indicate fluctuations of PMD with thermal changes along optical fibers up to 1 ps for 12 km link and 1.8 ps for 24km link respectively and fluctuating of PMD coefficient up to $0.3 \text{ ps/km}^{1/2}$. When considering PMD recommended limits for 40 Gbit/s systems or higher, such numbers exceeded the limits more than three times in particular links. This could be together with continuing oscillations of birefringence due to aging of the structure crucial for optical infrastructures. From several tested PMD measuring methods, the best way for next PMD monitoring of aged infrastructure revealed to a combination of accurate and distributed measuring. To further validate results over seasonal weather influences a long term measuring campaign has been set at Czech Technical University in Prague.

6. Acknowledgments

This work was supported by the CTU grant no. OHK3-037/14 and TACR project TA3020439. Authors would like to thank T-Systems and Sitel for cooperation with development of measuring polygon.

7. References

- [1] M. Karlsson, *et al.*, "Long-term measurement of PMD and polarization drift in installed fibers," *Lightwave Technology, Journal of*, vol. 18, pp. 941-951, 2000.
- [2] S. V. Shatalin and A. J. Rogers, "Location of High PMD Sections of Installed System Fiber," *Lightwave Technology, Journal of*, vol. 24, pp. 3875-3881, 2006.
- [3] "ITU-T Recommendation G.652: Characteristics of a single-mode optical fibre cable [online]. <http://www.itu.int/rec/T-REC-G.652-200911-I/en>," ed.
- [4] M. Brodsky, *et al.*, "'Long-term' PMD characterization of installed fibers-how much time is adequate?," in *Optical Fiber Communication Conference, 2004. OFC 2004*, 2004, p. 3 pp. vol.2.
- [5] A. Nespola and S. Abrate, "Long term PMD characterization of installed G.652 fibers in a metropolitan network," in *Optical Fiber Communication Conference, 2005. Technical Digest. OFC/NFOEC*, 2005, p. 3 pp. Vol. 3.
- [6] K. Borzycki, "Temperature dependence of PMD in optical fibres and cables," in *Transparent Optical Networks, 2005. Proceedings of 2005 7th International Conference*, 2005, pp. 441-444 Vol. 1.
- [7] V. M. Pestrikov, "The long-term strength of optical fibers under conditions of ageing of the material," *Glass Physics and Chemistry* 26, vol. 26, pp. 169-178, 2000.
- [8] W. Moore and T. Kiktyeva, "Optical damage in fiber optic components," in *Optical Fiber Communications Conference, 2003. OFC 2003*, 2003, pp. 525-527 vol.2.
- [9] N. Cyr, "Polarization-mode dispersion measurement: generalization of the interferometric method to any coupling regime," *Lightwave Technology, Journal of*, vol. 22, pp. 794-805, 2004.
- [10] R. Roberge, "Case Study: PMD Measurement on Aerial Fiber under Wind-Induced Oscillations and Vibrations," in *EXFO technical note* vol. Technical note 039, ed, 2009.
- [11] A. Galtarossa and L. Palmieri, "POTDR techniques for measurement of fiber birefringence properties," in *Optical Fiber Communication Conference and Exhibit, 2002. OFC 2002*, 2002, pp. 174-175.
- [12] G. P. Agrawal, *Fiber-optic communication systems*: Wiley, 1997.
- [13] R. Hui and M. S. O'Sullivan, *Fiber Optic Measurement Techniques*: Elsevier/Academic Press, 2009.
- [14] N. Cyr, *et al.*, "Random-Scrambling Tunable POTDR for Distributed Measurement of Cumulative PMD," *Lightwave Technology, Journal of*, vol. 27, pp. 4164-4174, 2009.

4.7 Long-Term Polarization Mode Dispersion Evolution and Accelerated Aging in Old Optical Cables

This chapter is a version of the published manuscript:

- [J4] J. Bohata, J. Jaros, S. Pisarik, S. Zvanovec and M. Komanec, “Long-Term Polarization Mode Dispersion Evolution and Accelerated Aging in Old Optical Cables,” *Photonics Technology Letters*, vol. 29(6), 2017, pp. 519-522.

Points pertaining to my PhD thesis:

This article publishes, in detail, the entire methodology for long-term fiber characteristics monitoring and demonstrates the longest PMD and optical aging measurement campaign in a special testbed as has so far been published. This unique testbed contains a testing and a reference route, with the testing route permanently loaded by optical power of 27 dBm at 1550 nm. Since the long-term aging process had not been investigated in the past, and given the ever-increasing demands for the utilization of optical fiber infrastructures, the article delivers insightful and original results. The analyzed testing loaded route shows an increase of about 0.15 dB/year in IL when compared to the reference route. Moreover, a new statistical model of significant seasonal PMD drift was derived which affords a better view of exposed optical cable behavior. Last, but not least, the methodology for aging process monitoring is presented for first time.

Long-Term Polarization Mode Dispersion Evolution and Accelerated Aging in Old Optical Cables

J. Bohata, J. Jaros, S. Pisarik, S. Zvanovec, and M. Komanec

Abstract—Today’s optical networks are composed of thousands of kilometers of aging optical cables. Many of these cables are located in harsh environments, which contribute to induced birefringence of the fibers and a corresponding increase of polarization mode dispersion (PMD). This letter introduces derived statistics from the longest-known running evaluation of a PMD measuring campaign and an investigation into how higher optical power affects these aging systems. Results indicate strong seasonal dependence of PMD on temperature for an optical cable test bed exposed to atmospheric changes, leading to a 16% increase of a mean PMD value in summer. This fluctuation causes bit error rate limits to be exceeded for 10 and 40 Gbps non-return-to-zero signals, which is a critical issue for applications where high reliability is required. Moreover, due to the high optical power load within old optical infrastructures, a more than 0.15 dB increase of relative loss per year in tested routes, compared with reference routes, has been observed.

Index Terms—Optical fiber, harsh environment, polarization mode dispersion, aging.

I. INTRODUCTION

OPTICAL fibers offer numerous benefits that allow them to be widely deployed in hazardous areas or harsh conditions such as nuclear power plants and undersea links, or in power lines operating at up to 400 kV within a specified temperature range from $-40\text{ }^{\circ}\text{C}$ to $+85\text{ }^{\circ}\text{C}$ [1]. Novel active optical networks demand significantly greater transmission characteristics, but the costs of replacing old optical infrastructures are high and challenging (222 million kilometers of optical fibers were installed between 1998 and 2000 though older fibers and cables still coexist [2]).

The reliability of an optical communication system in a hazardous area may be adversely affected by temperature variation, pressure, humidity, high voltage transmission, and radiation. In such circumstances, optical fibers undergo structural changes that may result in their transmission characteristics being temporarily or permanently degraded [3]. The temperature-induced attenuation of optical fibers for an avionics application was investigated in [4], where a single-mode optical fiber (SMF) with acrylate, or silicone coating,

was exposed to temperatures from $-196\text{ }^{\circ}\text{C}$ to $122\text{ }^{\circ}\text{C}$ resulting in increased attenuation of up to 1 dB/km depending on the materials in question. Temperature has a significant influence on optical losses, even for shorter optical fiber links connected by optical connectors as was experimentally demonstrated in [5] for an aircraft multimode (MM) optical network.

In addition to attenuation, polarization mode dispersion (PMD) has a profound influence upon the optical system as PMD is induced by birefringence in optical fibers and defined by differential group delay (DGD); the mean DGD value is then referred as a PMD value [6]. Due to its strong structural dependence, random behavior and high sensitivity to strain or temperature, PMD has become a useful indicator of the aging process of optical fiber-based infrastructures [7]. Special cables proposed for leading power lines were investigated in environmental tests, in a temperature range of $-40\text{ }^{\circ}\text{C}$ to $+85\text{ }^{\circ}\text{C}$, while observing PMD changes for variable cable buffer materials [1], [8]. Results indicated PMD increases of up to 500 % at temperatures below $-20\text{ }^{\circ}\text{C}$ within primary coated fibers. Several long-term PMD monitoring campaigns have been performed to determine the state of polarization (SOP) and corresponding DGD changes in optical fibers. The Müller matrix method (MMM) was adopted for a two-day measurement of 150 km long optical route with semiconductor optical amplifier (SOA) in the bandwidth of 100 nm, showing a slowly varying long-term structure to DGD spectra [9]. Detailed characterization of installed long-haul buried optical cables with MMM and summarized experimental data in an empirical model was shown in [10]. Based on these results, authors published a new model of temporal dependence of PMD for long fiber links in [11]. The Jones matrix method (JME) approach was also used in a detailed 35-day-long PMD-measurement of two 127 km-long dispersion shifted fibers (DSF), resulting in an average daily DGD drift of around 10% which was mainly attributed to temperature changes in exposed sections of the cable [12]. Another measurement campaign using the JME method was performed in a long-term five-month PMD continuous measurement [13]. Two cables, 79.5 km and 24.5 km long, experienced a daily variation of up to 10% of the DGD in synchronicity with temperature changes. The results imply- the bigger the PMD value, the higher the PMD variation. The most detailed long-term PMD measurement to date was an 18-month field observation of SOP and corresponding PMD on three fiber links employing 40 Gbps transmissions [14]. It revealed that DGD changes in the order of days can be described by the Maxwell distribution. However, the above-mentioned papers have not investigated the detailed connection between the aging of optical fibers and long-term PMD drift, so extended tests are needed.

Manuscript received October 11, 2016; revised January 11, 2017; accepted January 30, 2017. Date of publication February 2, 2017; date of current version March 1, 2017. This work was supported in part by TACR under Project TA3020439 and in part by SGS under Grant SGS14/190/OHK3/3T/13.

J. Bohata, S. Zvanovec, and M. Komanec are with the Faculty of Electrical Engineering, Czech Technical University in Prague, 16627 Prague, Czech Republic (e-mail: bohataj2@fel.cvut.cz).

J. Jaros is with the Technical University of Ostrava, 70800 Ostrava, Czech Republic (e-mail: jakub.jaros@vsb.cz).

S. Pisarik is with T-Mobile Czech Republic, 14800 Prague, Czech Republic (e-mail: svatoslav.pisarik@t-mobile.cz).

Color versions of one or more of the figures in this letter are available online at <http://ieeexplore.ieee.org>.

Digital Object Identifier 10.1109/LPT.2017.2662739

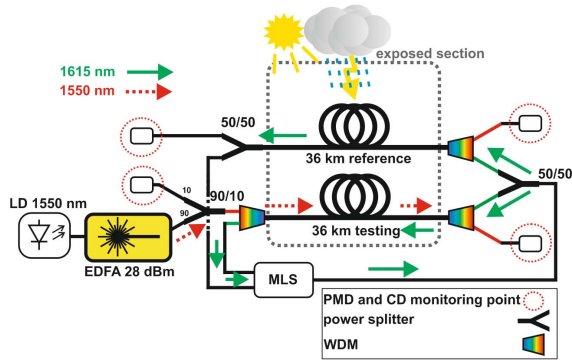


Fig. 1. Monitoring scheme: of laser diode (LD), erbium-doped fiber amplifier (EDFA), a monitoring link system (MLS), polarization mode dispersion (PMD) and chromatic dispersion (CD) monitoring points

To the best of our knowledge, this letter represents the longest experimental investigation of aging of optical cables.

II. LONG-TERM MONITORING SETUP

A special testing testbed was assembled on the roof of the Czech Technical University (CTU) in Prague as the location suitably simulates a harsh environment exposed to seasonal and spatial temperature variations. Alcatel optical cable, dating from 1997 and fulfilling ITU-T G.652 [15], was selected to monitor optical cable aging. The cable was formerly used in the optical network of the Prague metro system prior to this measurement. The 1 km-long cable contains six tubes each of which has twelve fibers spliced together to create a 72 km-long optical route. The optical cable was installed on the edge of the building roof in six approx. 130-meter-long circles next to the banister to ensure high exposure to atmospheric effects. To compare the accelerated aging process in the fibers better, the link was further divided into two 36 km-long routes – the reference and the testing routes. The initial PMD coefficient of the testing route was $1.45 \text{ ps}/\sqrt{\text{km}}$. The reference route carried only a weak monitoring signal ($< 0 \text{ dBm}$), in contrast an optical power load of 27 dBm was launched into the testing route using a seed signal from a laser diode (LD) (type KTI KC-300D-W5315) amplified by an erbium-doped fiber amplifier (EDFA) via a power splitter (PS) and a wavelength-division multiplexer (WDM) at the wavelength of 1550 nm (see scheme in Fig. 1). Note that the power load along the testing route has been distributed corresponding to a conventional optical link, where the power gradually decreases from maximum fed at the beginning of the testing route. Prior to the measurement, the testing route was characterized by an optical time domain reflectometer (OTDR), proving the fiber attenuation of 0.33 dB/km and additional insertion losses by several splices and components in the route resulting in received route output power of 12.9 dBm. Furthermore, 4.2% of the launched power load was rejected due to stimulated Brillouin scattering (SBS). However, we kept the measurement below the Brillouin threshold, due to the wide spectral bandwidth (on the order of GHz) of the seed laser and also owing to higher fiber attenuation. Continuous power monitoring was performed in the opposite direction at a wavelength of 1615 nm by a monitoring link system (MLS) device. The testbed was designed to monitor optical attenuation,

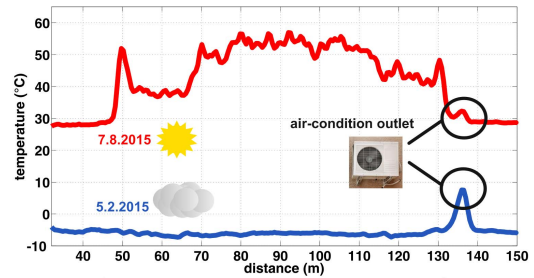


Fig. 2. Distributed temperature measurements in the first 150 meters of the reference route for hot (upper line) and cold (lower line) days in 2015.

chromatic dispersion (CD) and PMD (see PMD monitoring points in Fig. 1). Since PMD was captured at 1550 nm, the aging load from the EDFA had to be turned off when PMD was measured. Along with the PMD measurement, the temperature within the testbed was continuously monitored by a weather station and, in particular periods, by a distributed temperature sensing (DTS) device (Ditest STA-R) exploiting Brillouin scattering at wavelengths from 1528 nm to 1595 nm. The fully equipped testbed was completed in September, 2014, and the reference and testing routes, since then, have been periodically monitored.

III. LONG-TERM MONITORING RESULTS

The optical cable has been exposed to thermal changes over year-long cycles and intense thermal variations can be experienced throughout one measurement moment due to the heating of the black surface of the cable and diverse orientation/shadowing on the roof. Figure 2 shows a comparison of distributed temperature measurements via DTS in the first 150 meters of the cable from February (blue) and June (red), 2015. The greatest observed temperature difference along the fiber between a cloudy day in February and a sunny day in June, was $65 \text{ }^\circ\text{C}$, clearly illustrating the variety of operating conditions experienced during the year. In contrast to a set measured one day in February, which evinced flat characteristics, with the exception of one spike due to an air-conditioning unit outlet, the thermal distribution from the sunny June day varied considerably. The shadowed areas can be easily identified in Fig. 2 by drops in the temperature profile, whereas the sections exposed to the sun are, more or less, heated over an ambient temperature of up to approx. $60 \text{ }^\circ\text{C}$. Note that the surface temperature of the cable, measured by an IR camera, climbed up to $80 \text{ }^\circ\text{C}$. Further, a comparison between the average temperature inside the cable (dashed orange line) and the ambient temperature outside (solid green line) is provided courtesy of an 800-day-long cycle in Fig. 3. Note that the temperature from the fiber represents the average temperature for the first kilometer of the cable, even though the maximal difference between inner and outer temperatures is more than $10 \text{ }^\circ\text{C}$, especially on hot summer days. Periodic PMD monitoring has been running for more than two years. Several PMD monitoring methods – a general interferometry technique (GINTY – EXFO FTB5500), a scrambled state-of-polarization analysis (SSA – EXFO FTB5700) and a polarization optical time domain reflectometer (POTDR – EXFO FTB 5600)] have been adopted to test the standard PMD measurement tools in practice. Fig. 4 shows a three-day PMD measurement

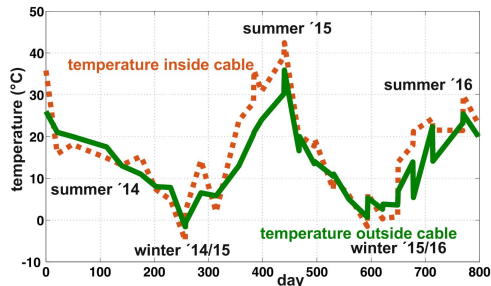


Fig. 3. Comparison of outside ambient temperature (green solid curve) vs. average temperature inside optical cable (orange dashed curve).

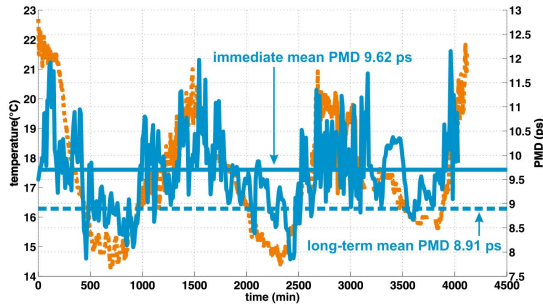


Fig. 4. Three-day polarization mode dispersion (PMD) measurement (blue) in testing route displayed showing ambient temperature (orange).

TABLE I
COMPARISON OF THE PMD METHODS ACCURACY

PMD method	PMD UNCERTAINTY (PS)
GINTY – EXFO FTB5500	$\pm (0.02 + 2 \% \text{ of PMD})$
POTDR – EXFO FTB5600	$\pm (0.10 + 5 \% \text{ of PMD})$
SSA - EXFO FTB5700	$\pm (0.20 + 5 \% \text{ of PMD})$

from June 2016, using the GINTY method at the testing route together with the capture of an ambient temperature profile. The horizontal lines, having a difference of 0.71 ps, show the long-term and immediate (measured over three days) mean PMDs. The long-term mean value is being reached only at night when temperatures drop. The measured PMD then correlates with an immediate temperature at the value of the Pearson correlation coefficient of 0.57. The maximal difference of the instant PMD and long-term mean PMD is 38 % and this was observed under an enormous increase of the temperature between 3700 and 4200 min. To validate the long-term measurement results, three methods were used. The results are influenced by the accuracy of the particular methods, which is shown in Tab. I, or, when compared to GINTY, SSA and POTDR were measured from only the end of the fiber that resulted in reduced accuracy. The mean long-term value with GINTY is 8.91 ps, 9.49 ps for SSA and 8.08 ps for POTDR. The total differences of SSA and POTDR against the GINTY method in testing are, thus, 6.5 % and 9.4 %, respectively. However, not all POTDR and SSA results were obtained at the same time, so both methods have an identical trend as a GINTY curve.

Figure 5 depicts PMD results from the long-term measurement campaign in the testing route from September 2014, as compared to the average monthly changes of ambi-

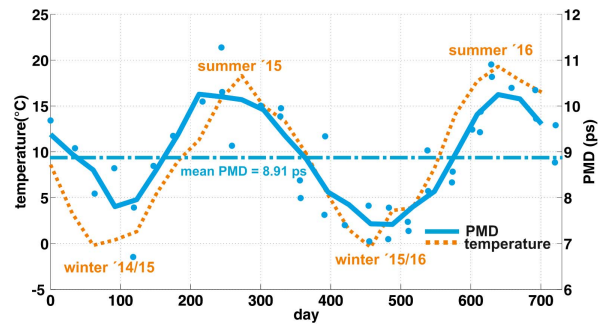


Fig. 5. Average temperature in Prague (dashed orange line) vs. average polarization mode dispersion (PMD) (solid blue line) within the testing fiber.

TABLE II
MAXIMAL DGD LIMITS ACCORDING TO [17]

Optical tributary signal	MAXIMUM DGD
2.5 Gbps NRZ	120.0 ps
10 Gbps NRZ	30.0 ps
40 Gbps NRZ	7.5 ps

ent temperature. All PMD results were obtained using the GINTY method as the reference [16] in a bandwidth between 1526 - 1595 nm. Periodic measurements have subsequently been conducted at least once a month (most of the measurements taking place once in the evening and again the following morning). Each measurement point represents the average value taken from five consecutive measurements from both ends of the fiber. The solid line represents the average PMD values over a two-month period, while the horizontal line determines the long-term mean PMD. Figure 5 also reveals the seasonal behavior of PMD changes due to temperature differences. We can observe a 16 % fluctuation of moving averaged PMD characteristic from the long-term mean PMD for both summer and winter periods. The maximum recorded PMD variation, in an almost two-year cycle, achieved 30% difference from mean PMD value in the testing route. It must be taken into consideration that PMD is a mean value of a number of DGDs, given by the Maxwell's distribution, so the maximal observed DGD values are a few times higher. The PMD in the testing route reaches a correlation coefficient of 0.71 with the immediate temperature in cables, whereas the moving averaged PMD has a higher correlation coefficient (0.85) with the temperature of a particular month. The standard deviation of PMD from the 6-, 12- and 24- month periods reached values of 0.876 ps, 1.120 ps and 1.190 ps respectively. It also derived a 0.120 ps increase in standard deviation per year. To fully describe the distribution of measured PMD values, a histogram from measured data, as shown in Fig. 5, is provided in Fig. 6. The derived bimodal distribution of measured values is bound by normalized probability density functions (PDF) for a normal distribution for lower and upper PMD values with standard deviations of 0.58 ps and 0.64 ps, respectively. The mean values of particular modes then approx. correspond to mean winter (7.85 ps) and summer (10.25 ps) PMD values.

Therefore, it is crucial to determine the correct seasonal behavior of such an optical cable as it may lead to a higher

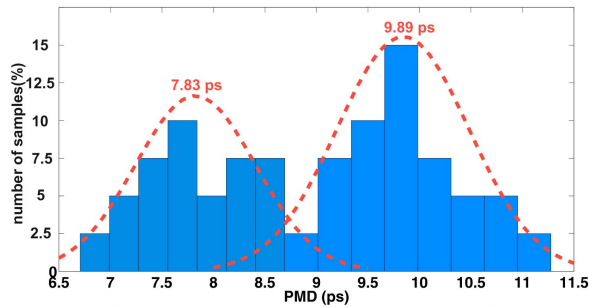


Fig. 6. Bimodal distribution of measured polarization mode dispersion (PMD) values with a PDF for the normal distribution of a particular mode.

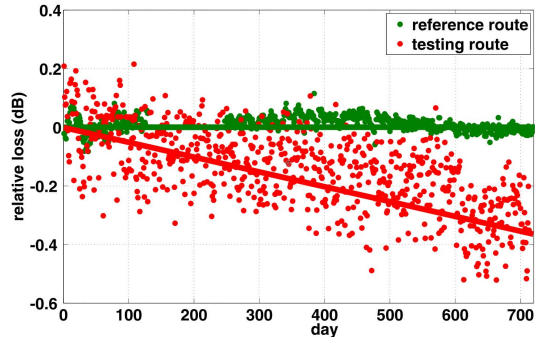


Fig. 7. Relative loss for reference (green) and testing (red) routes during the monitoring campaign.

probability of an optical network outage. The maximal values of DGD for particular optical signals without PMD compensation and at a bit error rate (BER) target of 10^{-12} , provided by ITU-T G.959.1 [15], are displayed in Tab. II. To ensure high network reliability, the maximum tolerable PMD is determined to be around three to four times smaller than the maximum tolerable DGD. That is, the PMD of optical fiber, employing a 10 Gbps non-return-to-zero (NRZ) signal, has to be at least three times smaller than 30 ps to guarantee a 4.2×10^{-5} probability [15] (22 minutes per year) of the exceeding limit. When assuming the average winter PMD (7.85 ps) or the long-term average PMD (8.91 ps) in the testing route, the limit of the maximal tolerable DGD is fulfilled. However, the average PMD value in summer reached 10.25 ps resulting in a maximal DGD of 30.75 ps which is beyond the limit of 30 ps [15]. To fulfill the probability of the limit exceeding 7.4×10^{-9} (less than one second per year), the PMD value has to be multiplied by four for the 10 Gbps NRZ. Subsequently, this leads to the recommendation that such an exposed and aged network must be extremely well characterized in at least a one-year period.

Figure 7 shows the results of the influence of a permanent high-power signal in optical fibers and components on the accelerated aging process. The testing route is permanently loaded by an optical power of 27 dBm (as described in Chapter II) and compared to a reference route to describe degradation in time. Each point in Fig. 7 represents the average value of normalized received power from any particular day containing more than 10,000 measurements done by MLS. The presence of EDFA has resulted in a higher variation of measured values (with a standard deviation of 0.13 dB) compared to unloaded fiber (0.025 dB). We can observe the significant increase of

relative loss in the power-based accelerated aging process, and a neutral trend in the reference trace. The testing route experienced a drop of more than 0.3 dB during the two-year monitoring campaign with the slope of the linear trend of 0.0125 dB/month attributed to the higher load.

IV. CONCLUSION

A long-term monitoring scheme in a unique testbed has been evaluated and discussed. Hazardous effects on old exposed optical cable were characterized, as well as the PMD variations and long-term attenuation changes. Derived statistics imply that significant seasonal PMD average dependence on temperatures reaches up to 16 % of the mean value. Based on these results, the behavior of old, or high-PMD, cables can be predicted better while being designed for high data rate transmissions, especially in places where the deployment of advanced optical system is costly or difficult. Please note, the results shown pertain to exposed cables, so for buried cables, less PMD variations are expected.

In addition, we have observed attenuation changes in the testing route under a load of a 27 dBm optical signal at 1550 nm, resulting in 0.15 dB/year increase of testing route attenuation compared to the reference route.

REFERENCES

- [1] K. Borzycki, "Temperature dependence of PMD in optical fibres and cables," in *Proc. ICTON*, Barcelona, Spain, Jul. 2005, pp. 441–444.
- [2] A. A. Huurdeman, *The Worldwide History of Telecommunications*. Hoboken, NJ, USA: Wiley, 2003, pp. 455–456.
- [3] J. C. Schlesinger, *Optical Fibers Research Advances*. New York, NY, USA: Nova Science Publishers, 2007, pp. 355–368.
- [4] A. A. Stolov *et al.*, "Effects of low temperature and hot steam on reliability of specialty optical fibers designed for avionics applications," in *Proc. AVFOP*, San Diego, CA, USA, Oct. 2013, pp. 29–30.
- [5] J. J. Bohata, M. Písařík, S. Zvánovec, and P. Peterka, "Reliability of aircraft multimode optical networks," *Opt. Eng.*, vol. 53, no. 9, p. 096102, Sep. 2014.
- [6] R. Hui and M. O'Sullivan, *Fiber Optic Measurement Techniques*. Amsterdam, The Netherlands: Elsevier, 2009, pp. 409–438.
- [7] J. Bohata, S. Zvanovec, and M. Písařík, "Outdoor atmospheric influence on polarization mode dispersion in optical cables," presented at the URSL, Beijing, China, Aug. 2014, pp. 1–4.
- [8] K. Borzycki, "Influence of temperature and aging on polarization mode dispersion of tight-buffered optical fibers and cables," *J. Telecommun. Inf. Technol.*, vol. 3, pp. 96–104, Mar. 2005.
- [9] M. Brodsky, P. Magill, and N. J. Frigo, "Polarization-mode dispersion of installed recent vintage fiber as a parametric function of temperature," *IEEE Photon. Technol. Lett.*, vol. 16, no. 1, pp. 209–211, Jan. 2004.
- [10] M. Brodsky, N. J. Frigo, M. Boroditsky, and M. Tur, "Polarization mode dispersion of installed fibers," *J. Lightw. Technol.*, vol. 24, no. 12, pp. 4584–4599, Dec. 2006.
- [11] A. Mecozzi, C. Antonelli, M. Boroditsky, and M. Brodsky, "Characterization of the time dependence of polarization mode dispersion," *Opt. Lett.*, vol. 29, no. 22, pp. 2599–2601, 2004.
- [12] O. Karlsson, J. Brentel, and P. A. Andrekson, "Long-term measurement of PMD and polarization drift in installed fibers," *J. Lightw. Technol.*, vol. 18, no. 7, pp. 941–951, Jul. 2000.
- [13] T. Kawasaki, W. Ichihara, T. Kataok, and S. Matsuoka, "Over 5-months long-term PMD continuous measurement in installed fiber cables with an exposed fiber section," in *Proc. OFC/NFOEC*, Anaheim, CA, USA, 2007, pp. 1–3.
- [14] S. L. Woodward *et al.*, "Long-term observation of PMD and SOP on installed fiber routes," *IEEE Photon. Technol. Lett.*, vol. 26, no. 3, pp. 213–216, Feb. 1, 2014.
- [15] *Transmission Systems and Media, Digital Systems and Networks, G Series*, document Rec. ITU G.652 and G.959, ITU-T, 2016.
- [16] *Measurement Methods and Test Procedures—Polarization Mode Dispersion*, document IEC 60793-1-48:2007, 2007, p. 100.

4.8 Adaptation of Transmitting Signals over Joint Aged Optical Fiber and Free Space Optical Network under Harsh Environments

This chapter is a version of the published manuscript:

- [J5] J. Bohata, S. Zvanovec, M. Komanec, J. Jaros and Z. Ghassemlooy, “Adaptation of Transmitting Signals over Joint Aged Optical Fiber and Free Space Optical Network Under Harsh Environments,” *Optik - International Journal for Light and Electron Optics*, 2017 (accepted).

Points pertaining to my PhD thesis:

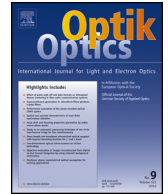
The paper provides a thorough summarization of the more than 2-year-long continuous measurement with uniquely derived statistics from the long-term evaluation. Based on the new statistical model, the mean PMD value can be predicted for a long-term measurement in such meteorologically exposed cables. Moreover, this paper combines previous short-term system experiments, now applied over the long-term aged infrastructure - the application of various transmission signals, including common 10 Gbps NRZ OOK and recently proposed DP RoF and RoFSO systems within the aged optical infrastructure, is experimentally investigated more in detail. Furthermore, the additional simulations of higher modulation formats were carried out to verify the impacts of such an aged infrastructure on high bit rate transmission systems. Finally, the reduction of PMD in systems using DP multiplexing was experimentally verified for the first time.



Contents lists available at ScienceDirect

Optik

journal homepage: www.elsevier.de/ijleo



Original research article

Adaptation of transmitting signals over joint aged optical fiber and free space optical network under harsh environments

Jan Bohata^{a,*}, Stanislav Zvanovec^a, Matej Komanec^a, Jakub Jaros^b, Zabih Ghassemlooy^c

^a Department of Electromagnetic Field, Czech Technical University in Prague, 2 Technicka, 16627 Prague, Czech Republic

^b Technical University of Ostrava, 17, Listopadu 15/2172, Ostrava 70833, Czech Republic

^c Optical Communications Research Group, NCRLab, Faculty of Engineering and Environment, Northumbria University, Newcastle-upon-Tyne NE1 8ST, UK

ARTICLE INFO

Article history:

Received 23 March 2017

Received in revised form 12 July 2017

Accepted 1 August 2017

Keywords:

Free space optics

Optical fiber

Polarization mode dispersion

Harsh environment

Aging

Turbulence

ABSTRACT

Over the last two decades, a large amount of optical fiber (OF) cables has been deployed as part of the global communication networks. Both the aging of OFs as well as the need to increase transmission data rates, particularly in the backbone, have become hot topics. We present the study of the aged OF deployment in various optical networks including free space optics (FSO) link as a part of modern optical communication networks. Here, we show extended results obtained using a dedicated OF testbed focusing on the long-term monitoring of polarization mode dispersion (PMD) because of its time-varying nature. The adaptation of polarization multiplexed radio over fiber (RoF) and radio over FSO (RoFSO) systems as well as 10 Gbps on-off-keying (OOK) non-return-to-zero (NRZ) intensity modulation with the direct detection system, which is common cost-effective transmission system in passive networks, are demonstrated. Moreover, simulation of 100 and 200 Gbps return-to-zero (RZ) differential quadrature phase shift keying (DQPSK) with direct detection is outlined to verify the impact of aged OF network connected with FSO under turbulence conditions. Results reveal more than 6 dB of power penalty with the aged OF route for 100 Gbps systems. In addition, there is a 0.8 dB power penalty due to the strong seasonal induced PMD fluctuations. The influence of scintillations in terms of Rytov variance for the FSO link is also investigated for weak to moderate turbulence. Finally, we derive an expression for the long-term mean PMD value determined over one-month measured frequency response.

© 2017 Elsevier GmbH. All rights reserved.

1. Introduction

The optical technologies are finding still new areas of applications and challenges due to the increasing demands on the capacity, cost reduction or safety [1]. In [2] the utilization of both optical fiber (OF) and optical wireless infrastructures as part of the next generation networks was discussed. The optical infrastructures are frequently utilized for mobile networks

* Corresponding author.

E-mail address: bohataja2@fel.cvut.cz (J. Bohata).

fronthauls, where the radio over fiber (RoF) technology [3] can be adopted to benefit from the combined features of OF fronthaul and the simplification of base stations. The long-term evolution (LTE), known as the 4th generation of mobile network, has been widely deployed worldwide and furthermore, the technology provides challenges for RoF applications leading to cost reduction [4,5]. One of the key benefits of the RoF technology is its utilization as a solution for the cloud radio access network (C-RAN) architecture where baseband units (BBUs) are centralized in a central office or BBU hotel [6]. The converged optical/wireless systems can support the distribution of broadband signals in future wireless systems such as 5 G and 60 GHz networks. The capacity of RoF-based links can be significantly increased by using the polarization division multiplexing (PDM) technique as proposed in [7]. A dual polarization (DP) scheme was utilized for transmission of LTE-A 2×2 multiple-input multiple-output (MIMO) over up to a 100 km of single mode fiber link.

Large sections of the OF based telecommunication networks, which are still in-service, are many years old. For example, more than 222 million kilometers (corresponding to the distance between the Mars and the Sun) of OFs were installed between 1998 and 2000 [8] and many of them have been still in use with some even under harsh environments. Such infrastructures were initially designed to support on-off keying (OOK) non-return-to-zero (NRZ) signal formats with a speed of 2.5 Gbps or 10 Gbps. However, the subsequent higher bit rate systems (>40 Gbps) are mostly operating with higher optical transmit power and minimum system requirements of 50 GHz spacing, optical signal-to-noise-ratio (OSNR) tolerance not greater than 16 dB and a maximum mean polarization mode dispersion (PMD) tolerance of 30 ps with an outage probability of 10^{-5} [9]. Therefore with the coexistence of old and new OF based telecommunication infrastructures, it is essential to ensure that OF properties are fully characterized to ensure the quality of services. One of the cost-effective and energy-efficient solutions for 100 Gbps systems is the deployment of differential quadrature phase shift keying (DQPSK) modulation format enabling dense wavelength division multiplexing (DWDM) with a spacing of 100 GHz [10,11].

However, replacing of the existing OFs and installing new ones is highly time-consuming and costly especially in dense urban areas. Alternatively, the free space optics (FSO) technology, which offers OF features (i.e., high data rates and longer transmission span), could be one option that can be deployed rapidly over a transmission spans up to a few km [12,13]. In [14,15], a combination of radio over FSO (RoFSO) and the RoF technology with PDM was reported to transmit two independent radio signals at the same radio frequency within the optical channel. The authors investigated the performance and reliability of the system under the atmospheric turbulence. Note that OFs, used as part of the system, were kept inside the laboratory environment. However, there is the need for assessing the system performance under a real environmental condition, where OFs are also exposed to the harsh outdoor conditions.

In this paper, we present original results on the utilization of the real aged OF infrastructure affected by thermal changes and interconnected with the FSO subsystem under a harsh environment. The paper provides analyses of the various types of optical transmission systems and discusses a methodology to achieve improved statistics and reliability of the network. The unique extended results are and based on, to our best knowledge, the longest studies and monitoring of PMD, capturing long-term drift. The paper is organized as follows. Section 2 describes OF testbed and its characterization obtained from long-term PMD monitoring. Section 3 provides the comparison of experimental campaigns for (i) DP RoF and RoFSO, and (ii) 10 Gbps NRZ system, which is still very commonly used in practice, over the tested infrastructure. We compare statistics for three cases – an optical power load aged OF, aged OF without load, and new OF infrastructure – all interconnected with FSO subpart. Moreover, to extend the influence of atmospheric conditions on the proposed link, additional simulation results at higher data rates are provided under specific conditions. Finally, the summary concludes the paper.

2. Accelerated aging process in old optical infrastructure

One of the key parameters in OF communications, which limits the higher bit rate transmissions, is PMD (the mean value of differential group delays (DGD)) [16]. Due to its strong structural dependence, random behavior and high sensitivity to strain or temperature, PMD has become a useful indicator of the OF's aging process [17]. Moreover, to fully characterize an OF link in terms of PMD, a longer period of measuring is required. A long-term PMD measurement based on Jones matrix method using installed G.653 optical cables with exposed sections was carried out over a 5 months period [18]. The optical path with the exposed sections displayed a significantly higher variance of the mean of DGD. In [19] longer-term PMD measurement (~10,000 h) using an installed OF link span from 30 to 273 km was carried out by means of observing the state of polarization on the Poincaré sphere. Although these research findings have demonstrated a strong daily temperature based PMD fluctuations, they do not show longer-term seasonal PMD drift, especially for systems with exposed installed OFs.

In [20] one of the most extensive investigations on monitoring PDM of old and exposed OF over a long period (>2.5 years) was reported. In this paper, we extend the results from [20] to fully characterize experimental testbed over a long-term monitoring campaign in order to further analyse data transmission over a combined OF and FSO link span. The measurement campaign is mostly focused on monitoring of the key OF parameters and its characteristics under a harsh test environment as well as investigating the long-term system reliability.

Fig. 1(a) shows an aerial view of the building at Czech Technical University in Prague where the proposed testbed is located on the edge of the roof. The fiber routes are consisting of a 1 km long optical cable containing 72 fibers (type G.652) [21] from 1997, which are spliced together with a total length of 72 km and are laid on the roof next to the banister (green dashed line). The link is divided into two 36 km long sections – the reference and testing paths. An optical signal with a power of 27 dBm at 1550 nm is launched into the testing route for emulating accelerated aging process and high power load

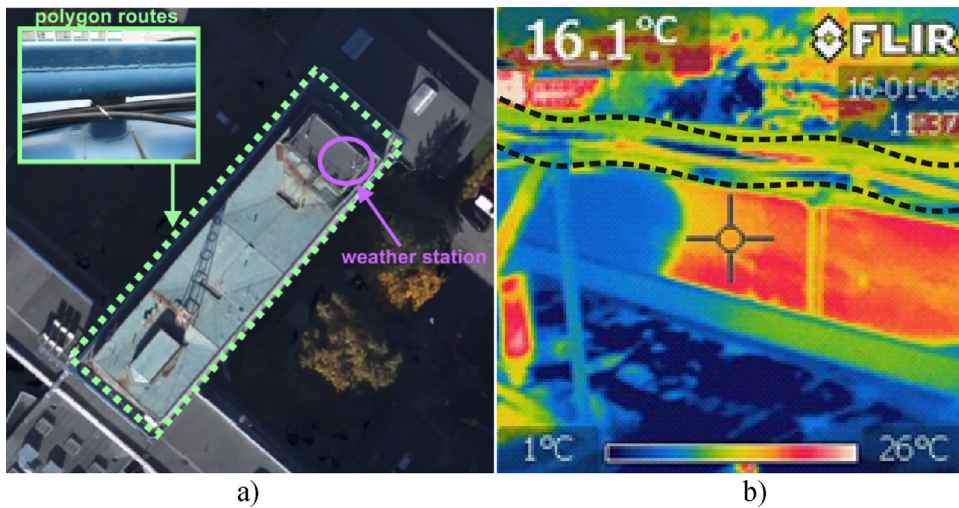


Fig. 1. (a) Aerial view of the testbed placed on the roof of the CTU in Prague, and (b) an IR image obtained in January 2016 with optical fiber located within the black dashed lines.

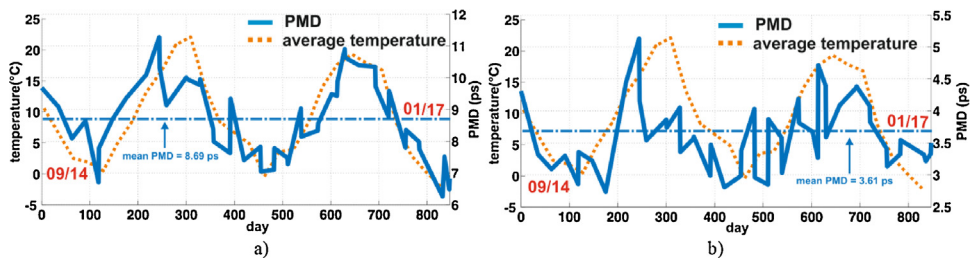


Fig. 2. Measured PMD (blue) and the average temperature (orange) against the days for: (a) testing route, and (b) reference route. (For interpretation of the references to colour in this figure legend, the reader is referred to the web version of this article.)

in OF, whereas for the reference route we used an optical power level of 0 dBm from the monitoring link system in order to measure received power. To fully monitor weather conditions, we placed a weather station next to the testbed as depicted in Fig. 1(a). Since the outside jacket of the OF cable is a dark color, therefore on exposure to the sunlight the temperature on the black cable surface can reach 80 °C or more during the peak times. Fig. 1(b) shows an infrared (IR) image taken in January 2016 outlining the temperature distribution of the testbed. Note that, the shadowed areas are shown as cold with the air temperature around 1 °C, whereas the area with sun has a temperature >20 °C. These differences along the route then influence the transmission characteristics and in particular PMD.

We measured both PMD and chromatic dispersion (CD) of the reference and testing routes periodically once every month since September 2014. PMD is measured based on the general interferometry technique (GINTY – EXFO FTB5500) as in [22] mostly in the morning and in the evening to capture daily fluctuations. The measurements were repeated five times from both ends, and then we used the average value of PMD per route. Fig. 2 depicts the average monthly temperature profiles and the PMD for the reference and testing routes paths for wavelength span between 1526 and 1595 nm.

We can observe the seasonal behavior of PMD, which is strongly dependent on the weather. The reference route correlates with the actual temperature at the value of the Pearson correlation coefficient [23] of 0.64 and testing route correlates with the actual temperature at the value of 0.81. The mean values of PMD, μ_{PMD} , represented by the horizontal blue lines, are 8.69 ps and 3.61 ps for testing and reference route, respectively, with the standard deviation values of 1.24 ps and 0.53, respectively. For testing of the real data transmission over the aged infrastructure, we carried out a more detailed assessment of PMD on a daily basis based on short-term measurements. Fig. 3 illustrates both the temperature and PMD plots performed over three days in June 2016 (red) and January 2017 (blue). As shown in Fig. 3, the immediate values of PMD reflect the daily temperature changes (i.e., orange curves). Dashed colored (red and blue) and black horizontal lines represent the two short-term and the overall long-term μ_{PMD} of 9.62 ps, 6.26 ps and 8.69 ps, respectively. Note that, the difference in mean values between June and January is 3.36 ps, which corresponds to μ_{PMD} change of 38%.

PMD influences mostly systems with higher data rates with no compensation and complex detection. The maximal values of DGD (DGD_{max}) for OOK based optical transmission with no PMD compensation and with a bit error rate (BER) target of 10^{-12} defined by ITU-T G.959.1 [21] are provided in Table 1. To ensure high network reliability, the maximum tolerable PMD is determined to be around three to four times smaller than tolerable DGD_{max} . For example, for 10 Gbps return-to-zero (NRZ) OF transmission at a BER of 4.2×10^{-5} (i.e., 22 min per year), PMD must be at least three times smaller than 30 ps [21].

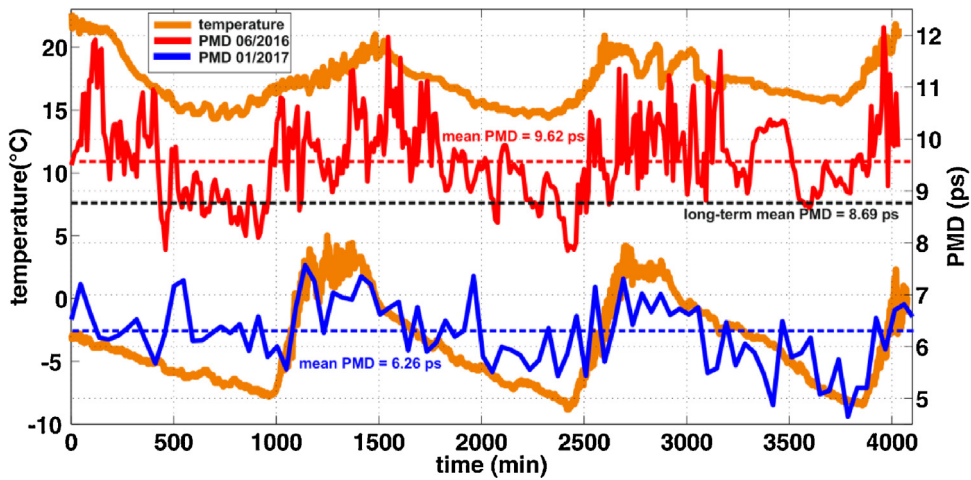


Fig. 3. The comparison of three-day PMD measurements in the testing route from June 2016 and January 2017. Orange lines represent actual temperatures, and horizontal lines illustrate short and long-term μ_{PMD} . (For interpretation of the references to colour in this figure legend, the reader is referred to the web version of this article.)

Table 1

Maximal DGD limits according to recommendation ITU-T G.959.1.

Optical tributary signal	DGD _{max}
2.5 Gbps NRZ	120.0 ps
10 Gbps NRZ	30.0 ps
40 Gbps NRZ	7.5 ps

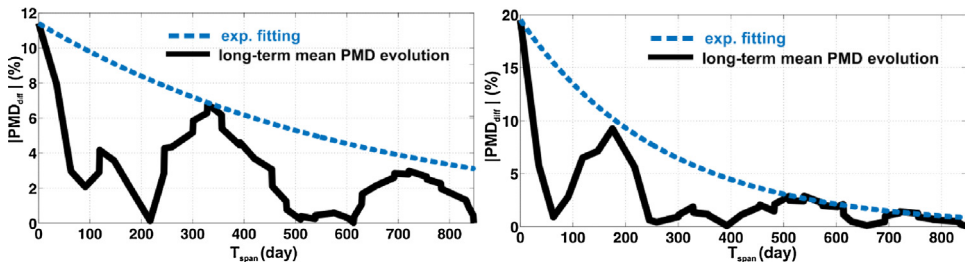


Fig. 4. The convergence of PMD_{diff} to the long-term μ_{PMD} for (a) testing route, and (b) reference route.

DGD_{max} is satisfied for PMD values of 7.41 ps and 8.69 ps for the winter and long-term cases, respectively. However, PMD of 10.25 ps (summer time) results in a DGD_{max} of 30.75 ps, which exceeds the limit of 30 ps [21]. To fulfill the probability of the limit exceeding 7.4×10^{-9} (less than one second per year), the PMD value should be four times lower for a 10 Gbps NRZ optical link. Note that, for 100 Gbps OOK NRZ with direct detection the tolerated magnitude of DGD is reported to be ~ 3 ps [24].

To fully access the performance of the route, which is aged by long term loading of high optical power, it is necessary to distinguish for how long the fluctuations of μ_{PMD} starts to converge to a stable value. Fig. 4 shows the evolution of μ_{PMD} differences (PMD_{diff}) determined for a particular period as it converges to the long-term μ_{PMD} value corresponding to 8.69 ps and 3.61 ps for the testing route as in Fig. 4(a) and the reference route in Fig. 4(b), respectively. Note that, PMD_{diff} is expressed in terms of the absolute value. Results indicate that to achieve an accurate long term μ_{PMD} within $\pm 5\%$ – fully covering the seasonal fluctuation of the exposed part of the transmission paths – links need to be monitored for more than 12 months at given time intervals. Also shown in the figure is the expected curve fitting, which provides the upper limit and is given by:

$$|PMD_{diff}(T_{span})| = |PMD_{diff,0}| \times e^{-\left(\frac{T_{span}}{S_{PMD} \times 75}\right)}, \quad (1)$$

where T_{span} is the monitoring period in days, S_{PMD} is the long term mean value of PMD for a particular route in ps and $PMD_{diff,0}$ stands for the biggest difference from μ_{PMD} in percent. Note that, for shorter monitoring period the recommended minimal $PMD_{diff,0}$ value is 20%. Using (1) and assuming the same monitoring period, we can obtain μ_{PMD} for the testing route with accuracy better than 5% within the period of 450 days.

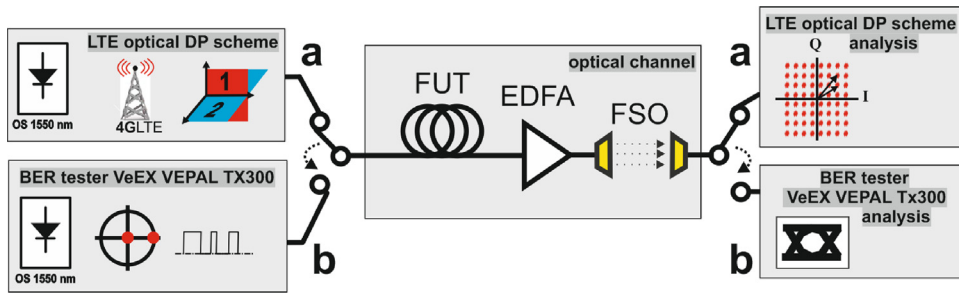


Fig. 5. The simplified measurement schemes for: (a) dual-polarization RoF & RoFSO system transmitting LTE signal with EVM evaluation, and (b) OOK NRZ 10 Gbps transmissions with BER and eye-diagram evaluation.

3. Optical transmissions over aged optical infrastructure

In this section, we assess the performance of the combined link of the aged optical infrastructure and FSO for two cases, see Fig. 5.

Case 1 – Dual-polarization radio over fiber and FSO (DP RoF & RoFSO), see Fig. 5(a): At the transmitter (Tx), the optical signal (OS) was split into two arms via a polarization beam-splitter (PBS) prior to modulating by radio signals using the LTE evolved universal terrestrial radio access (E-UTRA) test model-2 (TM2) with 64-QAM [25]. Both modulated light beams were then converted into a PDM scheme (for details about Tx see [15]) prior to transmission over the optical channel (i.e., OF and FSO). At the receiver (Rx), following optical to electrical conversion and the link performance evaluation in terms of the error vector magnitude (EVM). We have adopted the LTE setup parameters that were reported in our previous work [15].

Case 2 – 10 Gbps OOK NRZ, see Fig. 5(b): A bit error rate tester (BERT) was used to generate an optical signal with a transmit power of 1.7 dBm. At the Rx, we assessed the directly detected link performance in terms of the BER performance.

The hybrid optical channel was composed of a 36 km long OF (hereinafter denotes as a fiber under test (FUT)), an Erbium doped fiber amplifier (EDFA) (Keopsys – KPS-BT2-C-10-LN-SA) and a 2 m long FSO link. Three types of FUT were considered: (i) FUT1–for the testing route; (ii) FUT2 – the reference route (both described in the previous chapter); and (iii) FUT3 – a new OF link (G.652) [21].

All key system parameters are given in Table 2.

Table 2
 Measuring setup parameters.

Parameter	Value
General	
Wavelength	1550 nm
FSO channel length	2 m
FSO channel loss	15 dB
FUT1 loss	26.0 dB
FUT2 loss	21.0 dB
FUT3 loss	8.4 dB
EDFA	
-output power	0 dBm
-noise figure	<5 dB
-return loss	>40 dB
RoF & RoFSO	
Optical power	8.0 dBm
RF power	–5 dBm
RF carrier frequency	2.6 GHz
RF System bandwidth	1.4–20.0 MHz
OFDM subcarriers	667
Modulation scheme	64-QAM
LTE test model	E-TM2 [25]
PIN responsivity	0.75 A/W
TIA bandwidth	10 kHz–12 GHz
OOK NRZ 10 Gbps BERT	
Output power	1.7 dBm

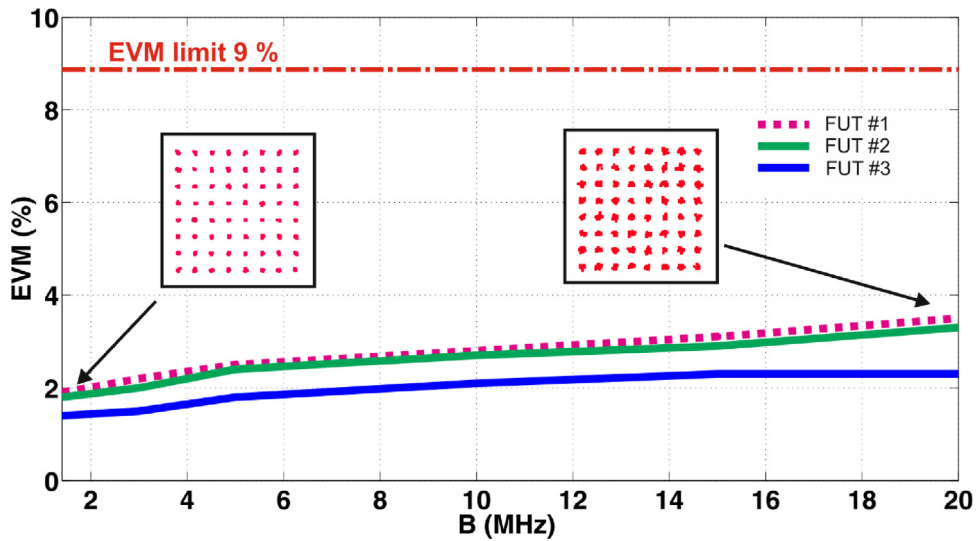


Fig. 6. Experimentally measured EVM vs. bandwidth for FUT1-3.

3.1. Dual-polarization RoF and RoFSO

Here, we investigate the LTE signal transmission for E-UTRA TM2 at a bandwidth of 1.4–20.0 MHz and a carrier frequency of 2.6 GHz. Note that, the power budgets of both reference and test routes were normalized to compensate for different insertion losses (IL). Fig. 6 shows the EVM as a function of bandwidth for FUTs 1–3. Insets represent the constellation diagrams of 64-QAM for a particular EVM. There is also shown the EVM limit of 9% as a reference. As shown, the EVM values increase with the bandwidth for all three FUTs and are considerably lower than 9%. FUT3 followed by FUT2 display the lowest EVM compared with FUT1.

Fig. 7 depicts the EVM performances for FUT1-3 against the variation in OSNR, which is caused due to IL changes. Note that, FUT3 offers the best EVM (i.e., 2% lower than the 9% limit for OSNR of 6 dB) compared to FUT1&2, which are higher than the 9% limit. FUT1&2 display almost the same EVM profile (with a difference of 0.5%), even though $\mu_{\text{PDM-FUT1}} > 2 \mu_{\text{PDM-FUT2}}$. The maximum OSNR values for FUT1, FUT2 and FUT3 were 25.5 dB, 26.5 dB and 30.5 dB, respectively. Note that, the bandwidth of LTE TM2 signal in this case was 20 MHz.

The impact of atmospheric turbulence within FSO link results in worse EVM and higher fluctuating received power magnitude of the whole system. With connected 2 m long laboratory FSO link, we observed 5.5% increase in EVM when we

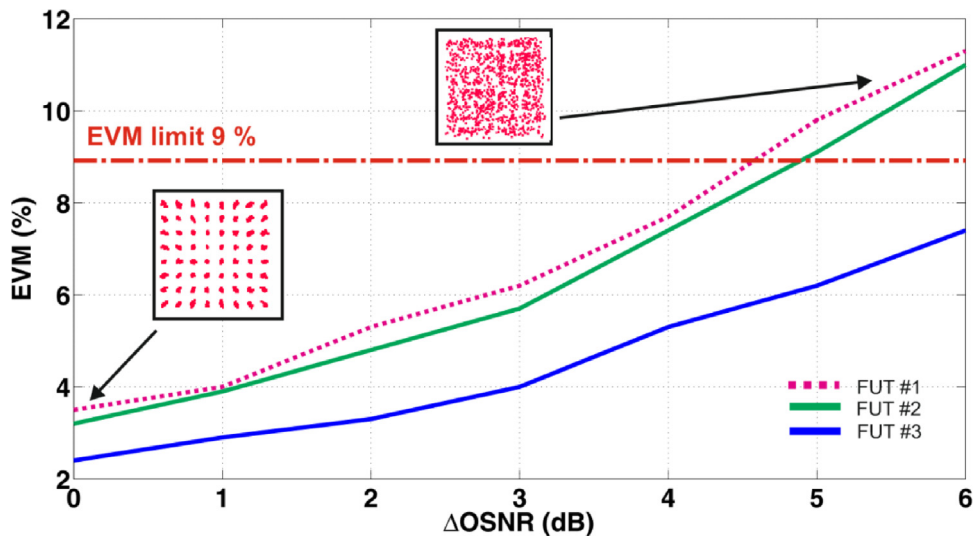


Fig. 7. Experimentally measured EVM vs. changes in OSNR for FUT1-3.

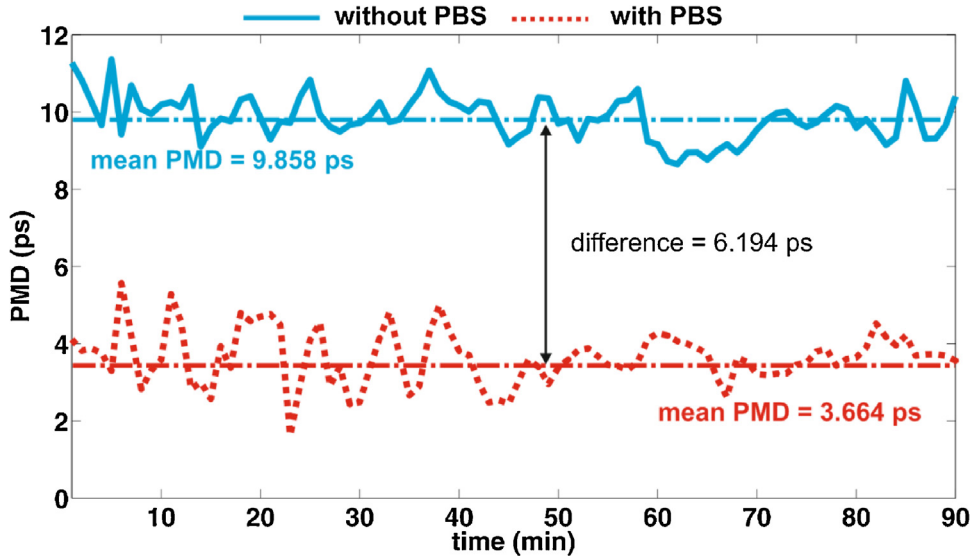


Fig. 8. Comparison of measured PMD of the testing route with and without PBS applied.

ten times increased Rytov variance σ_R^2 from 0.002 to 0.02 (more details on σ_R^2 describing turbulence effects of optical link performance are given in [26]).

At the Rx, a PBS was used to split the polarization multiplexed signal into two orthogonal polarization states. Note that, PBS also reduces the impact of PMD. Fig. 8 illustrates the measured PMD as a function of time for the testing route with and with no PBS (in June 2016). As can be seen, with PBS PMD is reduced by 63% from 9.86 ps to 3.66 ps, thus, demonstrating the resistance of such a system to PMD.

3.2. OOK NRZ signal

Next, we transmitted a 10 Gbps OOK NRZ signal over the proposed link as in Fig. 5(b). Fig. 9 shows the BER performance against the OSNR for FUT1-3. The insets show the measured eye diagrams corresponding to the BER values of 10^{-2} (upper) and 10^{-7} (lower). Note that, all plots show almost the same profile up to OSNR of 25 dB. Beyond the OSNR of 25 dB FUT1 displays higher BER. This can be attributed to higher PMD compared to the reference OF. Generally, a μ_{PD} of 8.69 ps for FUT1 is not that significant in 10 Gbps NRZ transmissions. On the other hand, for higher bit rates PMD should be taken into consideration, especially in hazardous areas with high temperature variations. Please note, we only illustrated PMD

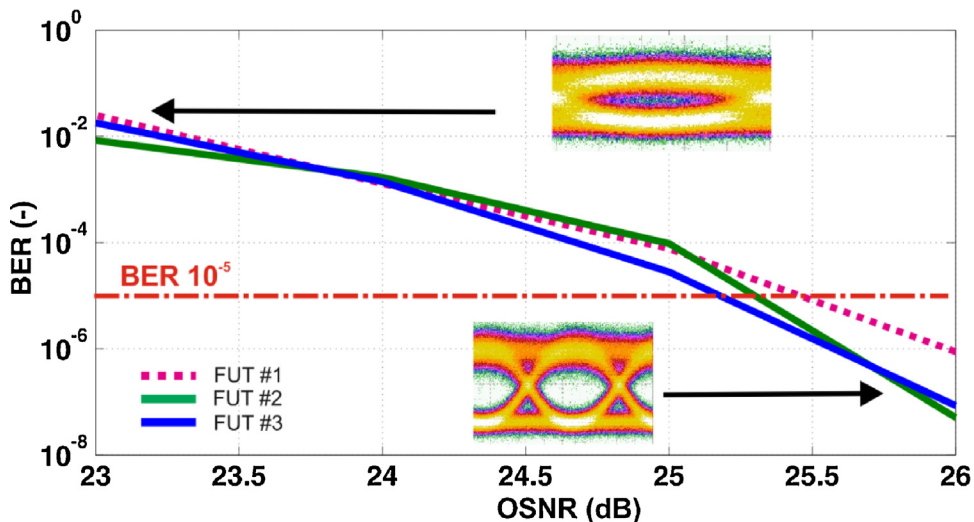


Fig. 9. Experimentally measured BER as a function of OSNR for 10 Gbps OOK NRZ in the case of implemented FUT1-3.

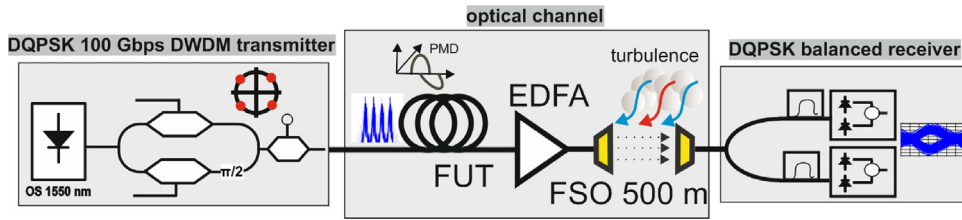


Fig. 10. 100 Gbps RZ DQPSK transmission system.

Table 3
 Simulation parameters.

Parameter	Value
General	
Modulation type	DQPSK
Coding	RZ
Wavelength	1550 nm
Tx power	3 dBm
Channel spacing	100 MHz
Symbol rate	50/100 Gbaud
FSO channel length	500 m
FSO channel loss	16.5 dB
FUT length	36 km
FUT loss	12.6 dB
EDFA gain	32 dB
PIN responsivity	0.6 A/W

influence, however, to reach higher BER values (i.e., 10^{-6}) there will be additional requirements on the Tx and Rx (higher power or smaller noise level) and the bandwidth of transimpedance amplifier used at the Rx.

3.3. Higher data rates

Here, we have simulated transmission of return-to-zero (RZ) DQPSK over the old infrastructure combined with a longer FSO length (i.e., 500 m), see a simplified scheme in Fig. 10. We have considered data rates of 100 Gbps (4×25 Gbps) and 200 Gbps (4×50 Gbps) in a 100 MHz DWDM grid at the wavelength of 1550 nm. At the Rx, a direct detection based balanced detector was used. Further information from modulation setup is provided in Table 3.

Fig. 11 depicts the OSNR performance against OSNR for 100 Gbps RZ DQPSK for a range of PMD covering 0.3 ps (FUT3), 6.3 ps (FUT1 minimal winter values) and 11.1 ps (FUT1 maximal summer values). The green and red plots show the difference between PMD_{min} and PMD_{max} during the year. Insets provide example of the eye diagrams for OSNR of 28 dB. As can be

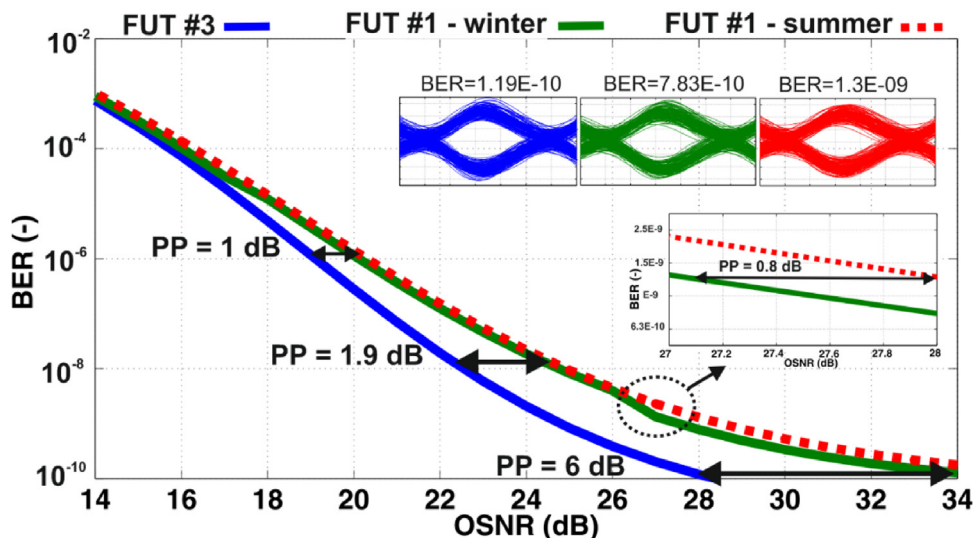


Fig. 11. Simulated BER vs. OSNR for a range of PMD of 0.3 ps (FUT3), 6.3 ps (FUT1 winter) and 11.1 ps (FUT1 summer) for 100 Gbps RZ DQPSK.

seen, the BER plots for FUT1 are almost the same but higher than FUT3. The utilization of such an old infrastructure can be translated to induced power penalty (PP) for a fixed BER. E.g., considering FUT3 and a BER of 1×10^{-6} the PP is 1 dB, which is increased to 1.9 dB at a BER of 1×10^{-8} compared to FUT1. Note that, at lower OSNR (i.e., <16 dB) the BER plots converge reaching at BER of 10^{-3} at OSNR of -14 dB, thus implying negligible impact of the higher PMD in comparison with lower OSNR levels. Despite the small difference between curves for FUT1 influenced by summer and winter conditions (i.e., red and green curves), the difference in BER performance should be still taken into account. Insets illustrate 1.7 times higher BER experienced in summer compared to the winter for OSNR and PP of 28 dB and 0.8 dB, respectively at a BER of 1×10^{-9} . Note that, the BER results will depend on the adopted modulation formats as well as on the electrical SNR (except OSNR).

Finally, we investigated the impact of atmospheric turbulence on the entire system performance for 100 Gbps and 200 Gbps RZ DQPSK. Note that, the scintillation is characterized by Rytov variance as given by [26]:

$$\sigma_R^2 = 1.23k^{\frac{7}{6}}C_n^2L^{\frac{11}{6}}, \tag{2}$$

where k is the wave number, L is the length of the channel and C_n^2 is the refractive index structure parameter, which depends on the strength of the turbulence and is defined as:

$$C_n^2 = \left(79 \times 10^{-6} \frac{P_a}{T^2}\right)^2 C_T^2, \tag{3}$$

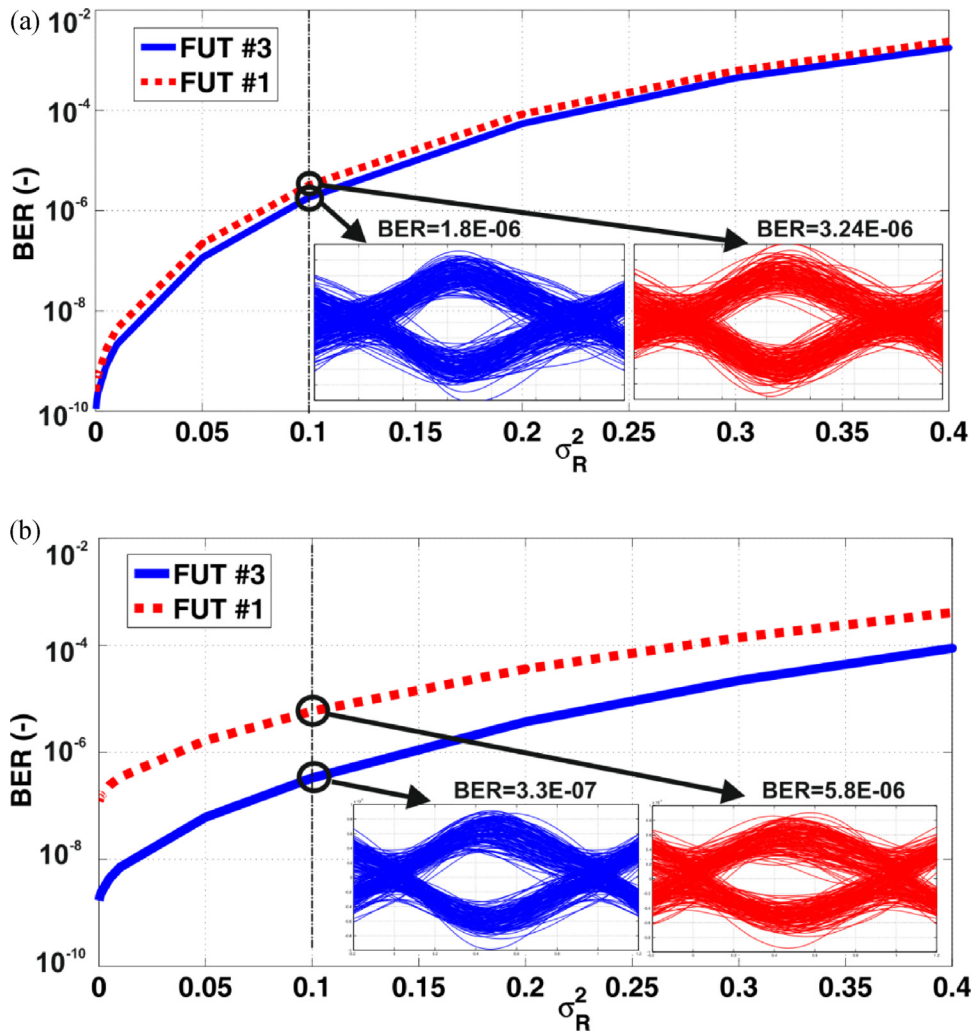


Fig. 12. Simulated BER vs. Rytov variance for FUT #1 (red) and FUT #3 (blue) in: (a) 100 Gbps RZ DQPSK, and (b) 200 Gbps RZ DQPSK transmission scheme; insets show eye diagrams for $\sigma_R^2 = 0.1$.. (For interpretation of the references to colour in this figure legend, the reader is referred to the web version of this article.)

where P_a is the atmospheric pressure in millibars. C_T^2 is the temperature structure constant, which is defined as:

$$C_T^2 = (T_1 - T_2)^2 / L_p^{2/3}, \tag{4}$$

where T_1 and T_2 are temperatures at two points separated by the distance L_p . Knowing the thermal distribution along the FSO propagation path, it is possible to determine C_T^2 and then C_n^2 . The impact of atmospheric turbulence on the propagating optical beam is given in detailed in [27].

Fig. 12 displays the BER performance against the scintillation for FUT1 and FUT3 for 100 Gbps and 200 Gbps RZ DQPSK. For the 100 Gbps link we observe almost the same BER profile regardless of the turbulence regime, see Fig. 12(a). The insets show the eye diagrams for σ_R^2 of 0.1, illustrating a very small difference in BER for the 100 Gbps system. For the 200 Gbps link FUT3 displays considerably lower BER profile compared to FUT1, see Fig. 12(b).

4. Summary

We have presented a study on the aged OF infrastructure combined with the FSO channel for various transmission systems. Extended and updated results based on a long-term PMD monitoring and measurements were evaluated and presented. We described strong daily and seasonal PMD drift with long-term μ_{PMD} difference estimation on the daily and seasonal basis. Based on the results, to achieve a variation in μ_{PMD} lower than 5%, at least 450 days of measurement campaign on a monthly basis would be required. The measuring period should be increased to 1642 days to achieve μ_{PMD} better than 1% for the aged and exposed network. The seasonal differences were further discussed together with the simulation of 100 Gbps RZ DQPSK transmissions, with a power penalty of 0.8 dB at a BER of 10^{-9} . We showed that at a BER of 10^{-10} there was a 6 dB of PP between the aged and normal OF based networks with the FSO link. Based on the experimental results for 10 Gbps OOK NRZ, the difference between FUT1 ($\mu_{\text{PMD}} = 8.69$ ps) and FUT2 ($\mu_{\text{PMD}} = 3.61$ ps) were negligible. For RoF and RoFSO with 64-QAM, for a range of OSNR and RF bandwidth at the carrier frequency of 2.6 GHz, the average difference in PDM was <0.5% of EVM. Moreover, we demonstrated an average of 64% reduction in PMD while using a polarization beam splitter, which led to improved robustness against the changes in PMD.

Finally, the impact of scintillation on the FSO part of the link was evaluated for 100 Gbps and 200 Gbps RZ DQPSK transmissions. We recorded almost two and five times higher BER for FUT1 and FUT3 at 100 Gbps and 200 Gbps, respectively. Furthermore, we showed that the normal and aged OF paths offered converging performance profiles for a Rytov variance value of up to 0.5, behind which considerably higher PMD impact (i.e., higher BER) was observed for the aged route case. The results indicated that adaptation of higher data rates with lower BER is possible, provided the aged routes are precisely characterized and the potential FSO effects are considered.

Acknowledgments

This work was supported by CTU grant SGS17/182/OHK3/3T/13. Authors would like to thank T-Mobile, Sitel and SQS, fiber optics for support with establishment of the measuring site.

References

- [1] P. Petropoulos, *Optical fibre technologies for future communication networks*, 42nd European Conference on Optical Communication (ECOC) 2016 (2016) 1–3.
- [2] T.V. Nguyen, H.T. Nguyen, H. Ch. Le, N.D. Nguyen, T. Dang, Performance analysis of gigabit-capable mobile backhaul networks exploiting TWDM-PON and FSO technologies, *Advanced Technologies for Communications (ATC)* (2016) 180–185, <http://dx.doi.org/10.1109/ATC.2016.7764770>.
- [3] C.H. Lee, *Microwave Photonics*, second edition, Taylor & Francis, 2013.
- [4] A. Saadani, M.E. Tabach, A. Pizzinat, M. Nahas, P. Pagnoux, S. Purge, Y. Bao, Digital radio over fiber for LTE-advanced: opportunities and challenges, *17th International Conference on Optical Network Design and Modeling (ONDM)* (2013) 194–199.
- [5] T. Kanesan, R. Mohamad, S.M. Mitani, H.M. Hizan, W.P. Ng, Z. Ghassemlooy, P.A. Haigh, et al., Solution to reduce nonlinearity in LTE RoF system for an efficient DAS topology: a brief review (invited), *10th International Symposium on Communication Systems Networks and Digital Signal Processing (CSNDSP)* (2016) 1–4, <http://dx.doi.org/10.1109/CSNDSP.2016.7573933>.
- [6] D. Novak, R.B. Waterhouse, A. Nirmalathas, Ch. Lim, P.A. Gamage, et al., Radio-over-fiber technologies for emerging wireless systems, *IEEE J. Quantum Electron.* 52 (2016) 1, <http://dx.doi.org/10.1109/jqe.2015.2504107>.
- [7] M. Morant, J. Prat, R. Liorente, Radio-over-fiber optical polarization-multiplexed networks for 3GPP wireless carrier-aggregated MIMO provision, *J. Lightwave Technol.* 32 (20) (2014) 3721–3727, <http://dx.doi.org/10.1109/jlt.2014.2317591>.
- [8] A.A. Huurdeman, *The WorldWide History of Telecommunications*, Wiley, 2003.
- [9] M. Camera, 100GbE optical transport, appropriate modulation formats, and impact on deployed transport networks, *Optical Fiber Communication, Collocated National Fiber Optic Engineers Conference (OFC/NFOEC)* (2010) 1–3, <http://dx.doi.org/10.1364/NFOEC.2010.NME3>.
- [10] E. Lach, W. Idler, Modulation formats for 100G and beyond, *Opt. Fiber Technol.* 17 (5) (2011) 377–386, <http://dx.doi.org/10.1016/j.yofte.2011.07.012>.
- [11] A. Chowdhury, M. Huang, Z. Jia, J. Yu, R. Younce, G. Chang, 10x 100-Gb/s transmissions using optical carrier suppression and separation technique and RZ-DQPSK modulation for metro-ethernet transport system, *LEOS 2008-21 st Annual Meeting of the IEEE Lasers and Electro-Optics Society (LEOS)* (2008) 479–480, <http://dx.doi.org/10.1109/LEOS.2008.4688699>.
- [12] C.B. Naila, K. Wakamori, M. Matsumoto, A. Bekkali, K. Tsukamoto, Transmission analysis of digital TV signals over a Radio-on-FSO channel, *IEEE Commun. Mag.* 50 (8) (2012) 137–144, <http://dx.doi.org/10.1109/MCOM.2012.6257540>.
- [13] W.S. Tsai, H. Lu, Ch. Li, T. Lu, H. Lin, B. Chen, Ch. Wz, A 50 m/320 Gbps DWDM FSO communication, *IEEE Photonics Conference (IPC)* (2016) 43–44, <http://dx.doi.org/10.1109/IPC.2016.7830972>.
- [14] J. Bohata, S. Zvanovec, M.M. Abadi, Z. Ghassemlooy, Characterization of dual-polarization LTE radio over a free-space optical turbulence channel, *Appl. Opt.* 54 (23) (2015) 7082–7087, <http://dx.doi.org/10.1364/ao.54.007082>.

Please cite this article in press as: J. Bohata, et al., Adaptation of transmitting signals over joint aged optical fiber and free space optical network under harsh environments, *Optik - Int. J. Light Electron Opt.* (2017), <http://dx.doi.org/10.1016/j.ijleo.2017.08.004>

- [15] J. Bohata, S. Zvanovec, P. Pesek, T. Korinek, M.M. Abadi, Z. Ghassemlooy, Experimental verification of long-term evolution radio transmissions over dual-polarization combined fiber and free-space optics optical infrastructures, *Appl. Opt.* 55 (8) (2016) 2109–2116, <http://dx.doi.org/10.1364/ao.55.002109>.
- [16] R. Hui, M. O'Sullivan, *Fiber Optic Measurement Techniques*, Elsevier Science, 2009.
- [17] J. Bohata, S. Zvanovec, M. Pisarik, Outdoor atmospheric influence on polarization mode dispersion in optical cables, General Assembly and Scientific Symposium (URSI GASS) (2014) 1–4, <http://dx.doi.org/10.1109/URSIGASS.2014.6929421>.
- [18] T. Kawasaki, W. Ichihara, T. Kataoka, S. Matsuoka, Over 5-months long-term PMD continuous measurement in installed fiber cables with an exposed fiber section, *Optical Fiber Communication and the National Fiber Optic Engineers Conference (OFC/NFOEC)* (2007) 1–3, <http://dx.doi.org/10.1109/OFC.2007.4348365>.
- [19] S.L. Woodward, S.L. Woodward, L.E. Nelson, Ch. R. Schneider, L.A. Knox, Long-term observation of PMD and SOP on installed fiber routes, *Photonics Technol. Lett.* 26 (3) (2014) 213–216, <http://dx.doi.org/10.1109/lpt.2013.2290473>.
- [20] J. Bohata, J. Jaros, S. Pisarik, S. Zvanovec, M. Komanec, Long-term polarization mode dispersion evolution and accelerated aging in old optical cables, *Photonics Technol. Lett.* 29 (6) (2017) 519–522, <http://dx.doi.org/10.1109/lpt.2017.2662739>.
- [21] Transmission systems and media, digital systems and networks, G Series, document Rec. ITU G.652 and G.959, ITU-T, 2016.
- [22] N. Cyr, Polarization-mode dispersion measurement: generalization of the interferometric method to any coupling regime, *J. Lightwave Technol.* 22 (3) (2004) 794–805, <http://dx.doi.org/10.1109/jlt.2004.824564>.
- [23] D.R. Cox, D.V. Hinkley, *Theoretical Statistics*, Chapman and Hall, 1974.
- [24] E. Pincemin, H. Poignant, Paradigms of 40/100 Gbps deployments on France Telecom long-haul transport network: overcoming transmission impairments while adapting network architecture and analyzing economical impact, 36th European Conference and Exhibition on Optical Communication (ECOC) (2010) 1–15, <http://dx.doi.org/10.1109/ECOC.2010.5621091>.
- [25] LTE; Evolved Universal Terrestrial Radio Access (E-UTRA); Base Station (BS) conformance testing, 3GPP TS 36.141 version 10.1.0 Release 10, Technical specification (2011) Available online: (http://www.etsi.org/deliver/etsi_ts/136100_136199/136141/10.01.00_60/ts_136141v100100p.pdf).
- [26] Z. Ghassemlooy, W. Popoola, S. Rajbhandari, *Optical Wireless Communications: System and Channel Modelling with MATLAB®*, Taylor & Francis, 2012.
- [27] L.C. Andrews, R.L. Phillips, *Laser Beam Propagation Through Random Media* (SPIE, 2005).

5 Conclusions

5.1 Contribution of the thesis

This thesis provides new insights on the reliability of optical structures in harsh environments. A methodology for the evaluation of the influence of aging processes on optical fiber infrastructures has been derived. Moreover the combined DP RoF and RoFSO system has been proposed. In addition, the short-term influences of the optical network operation have been validated in a specific case relating to a very peculiar area of avionics [J3], [C1]. The comprehensive methodology for the characterization of the aging process of optical infrastructures has been published, including significant amounts of data and novel, derived statistics [J4], [C1], [C2]. The results determine the specific service limitations for optical network design and a long-term outlook of structural changes. The proposed measurement methodology reveals strong seasonal dependence of PMD on temperature. This methodology has been statistically described. The utilization of older aged optical infrastructures with various transmission formats have been experimentally verified in terms of outage probability [J5]. Within this testing, a DP RoF and RoFSO systems performance was verified on the aged infrastructure, doubling the capacity of the optical channel and allowing for the simpler architecture of xG mobile networks [J1], [J2]. The work has already been cited by other international teams in international journals.

The presented results offer greater insight to optical communications which have become an inseparable part of a variety of applications, some of which involve hazardous areas. Such areas are primarily characterized by significant temperature variations and the presented results, thus, enable more accurate predictions of optical fiber network behavior. Moreover, the great benefit of this thesis lays in the longest overall monitoring of crucial transmission characteristics which has ever been published.

5.2 Future research opportunities

Due to the long-term testing and monitoring which is still ongoing, we expect to receive more detailed results in the near future and, as was revealed in this thesis, to capture significant material structural changes of the aging process, though this will require a notably extended period of research. I would like to continue to evaluate testbed route behavior and further adapt this test to real applications as indicated in [J5]. Moreover, more environmental tests would have great value to better describe short-term changes whose concepts were described in the thesis.

I would also like to continue to investigate changes in modal behavior of MMF under special conditions as introduced in [J3]. Due to the enormous number of data centers being built with MMF connections, modal influence is certain to play a significant role.

Last but not least, during the writing of this thesis, many new challenges have emerged in RoF and RoFSO applications, in particular those related to the launch of 5G networks and new (higher) frequencies usage. We have already started several new measurement campaigns with foreign research institutions in this field.

6 List of author's publications

List of author's publications related to the doctoral thesis

Papers in Peer-Reviewed Journals with Impact Factor

- [J1] J. Bohata, S. Zvanovec, M. M. Abadi and Z. Ghassemlooy, "Characterization of dual-polarization LTE radio over a free-space optical turbulence channel," *Applied Optics*, vol. 54(23), 2015, pp. 7082-7087.
- [J2] J. Bohata, S. Zvanovec, P. Pesek, T. Korinek, M. M. Abadi and Z. Ghassemlooy, "Experimental verification of long-term evolution radio transmissions over dual-polarization combined fiber and free-space optics optical infrastructures," *Applied Optics*, vol. 55(8), 2016, pp. 2109-2116..
- [J3] J. Bohata J., S. Zvanovec and S. and Peterka P., "Reliability of aircraft multimode network," *Optical engineering*, vol. 53(9), 2014.
- [J4] J. Bohata, J. Jaros, S. Pisarik, S. Zvanovec and M. Komanec, "Long-Term Polarization Mode Dispersion Evolution and Accelerated Aging in Old Optical Cables," *Photonics Technology Letters*, vol. 29(6), 2017, pp. 519-522.
- [J5] J. Bohata, S. Zvanovec, M. Komanec, J. Jaros and Z. Ghassemlooy, "Adaptation of Transmitting Signals over Joint Aged Optical Fiber and Free Space Optical Network Under Harsh Environments," *Optik - International Journal for Light and Electron Optics*, 2017 (accepted).

Papers and Abstracts in Conference Proceedings Listed in the Web of Knowledge

- [C1] J. Bohata, M. Pisarik and S. Zvanovec, "Testing of optical fiber components for harsh environments," in *Avionics, Fiber-Optics and Photonics Conference (AVFOP)*, 2013, pp. 33-34.
- [C2] J. Bohata, S. Zvanovec and M. Pisarik, "Outdoor atmospheric influence on polarization mode dispersion in optical cables," in *General Assembly and Scientific Symposium (URSI GASS)*, 2014, pp. 1-4.

Citations in Web of Knowledge and SCOPUS (except self-citations):

- [Ci1] M. T. Dabiri, M. J. Saber and S. M. S. Sadough, "BER Performance of OFDM-Based Wireless Services Over Radio-on-FSO Links in the Presence of Turbulence and Pointing Errors," in *8 th International symposium on telecommunications (IST)*, 2016. – citing [J1]
- [Ci2] M. T. A. Khan, M. A. Shemis, A. M. Ragheb, H. Fathallah, S. Alshebeili and M. Z. M. Khan, "64 Gb/s Quantum-dash Laser based Indoor Free Space Optical Communication," in *Wireless and Optical Communication Conference (WOCC)*, 2017, pp. 1-4. – citing [J2]

- [Ci3] M. T. A. Khan, M. A. Shemis, A. M. Ragheb, M. A. Esmail, H. A. Fathallah, S. Alshebeili and M. Zahed, "4 m/100 Gb/s Optical Wireless Communication Based on Far L-band Injection Locked Quantum-Dash Laser," IEEE photonics journal, vol. 9(2), 2017. – citing [J2]

List of author's publications non-related to the doctoral thesis

Papers in Peer-Reviewed Journals with Impact Factor

- [J6] N. A. M. Nor, Z. Ghasemlooy, J. Bohata, P. S. Saxena, M. Komanec, S. Zvanovec, M. R. Bhatnagar and M. A. Khalighi, "Experimental Investigation of All-Optical Relay-Assisted 10 Gbps FSO Link over the Atmospheric Turbulence Channel," Journal of Lightwave Technology, vol. 35(1), 2017, pp. 45-53.
- [J7] P. Koška, Y. Baravets, P. Peterka, J. Bohata and M. Pisarik, "Mode-field adapter for tapered-fiber bundle signal and pump combiners," Applied optics 54(4), 2015, pp. 751-756.
- [J8] H. K. Al-Musawi; T. Cseh; J. Bohata; W. P. Ng; Z. Ghassemlooy; S. Zvanovec; E. Udvary and P. Pesek, "Adaptation of Mode Filtering Technique in 4G-LTE Hybrid RoMMF-FSO for Last-Mile Access Network," Journal of Lightwave Technology, vol. 29(17), 2017, pp. 3758-3764.

Papers and Abstracts in Conference Proceedings Listed in the Web of Knowledge

- [C3] J. Bohata, S. Zvanovec, T. Nemecek and M. Komanec, "Detailed Analysis of Multi-Mode Optical Components for Utilization in Data Centers," in Global Information Infrastructure and Networking Symposium (GIIS'2017), 2017.
- [C4] J. Bohata, P. Pesek, S. Zvanovec and Z. Ghassemlooy, "Extended Measurement Tests of Dual Polarization Radio over Fiber and Radio over FSO Fronthaul in LTE C-RAN architecture," in 12th International Conference on Wireless and Mobile Computing, Networking and Communications (WiMob), 2016, pp. 1-3.
- [C5] J. Bohata, S. Zvanovec, M M. Abadi and Z. Ghasemlooy, "Channel Characterization of a Last-mile Access Radio Over Combined Fibre and Free-Space Optics System," in International Conference on Automation, Cognitive Science, Optics, Micro Electro-Mechanical System, and Information Technology (ICACOMIT), 2015, pp 27 – 30.
- [C6] J. Bohata, S. Zvanovec, T. Korinek, M. M. Abadi and Z. Ghasemlooy, "Investigation LTE Radio over a Free-Space Optical link in turbulence regime," in Proceedings of Optical Communications 2015, pp 8-11. ISBN: 978-80-86742-41-0.
- [C7] P. Pesek, J. Bohata, S. Zvanovec and J. Perez, "Characterization of Dual-Polarization analogue Radio over Fiber Fronthaul for LTE C-RAN Architecture," in 10th International Symposium on Communication Systems, Networks and Digital Signal Processing (CSNDSP), 2016.

- [C8] P. Pesek, J. Bohata, S. Zvanovec and J. Perez, “Analyses of dual polarization WDM and SCM Radio over Fiber and Radio over FSO for C-RAN architecture,” in 25th Wireless and Optical Communication Conference (WOCC), 2016, pp 1-4.
- [C9] N. A. M. Nor, J. Bohata, Z. Ghassemlooy, S. Zvanovec, P. Pesek, M. Komanec, J. Libich and M. A. Khalighi, “10 Gbps all-optical relay-assisted FSO system over a turbulence channel,” in 4th International Workshop on Optical Wireless Communications (IWOW), 2015, pp 69 – 72.
- [C10] H. K. Al-Musawi, T. Cseh, J. Bohata, P. Pesek, W. P. Ng, Z. Ghassemlooy, E. Udvary, S. Zvanovec and M. Ijaz, “Fundamental investigation of extending 4G-LTE signal over MMF/SMF-FSO under controlled turbulence conditions,” in 10th International Symposium on Communication Systems, Networks and Digital Signal Processing (CSNDSP), 2016, pp. 1-6.
- [C11] H. K. Al-Musawi, T. Cseh, J. Bohata, P. Pesek, W. P. Ng, Z. Ghassemlooy, E. Udvary, T. Berceci and S. Zvanovec “Experimental Optimization of the Hybrid RoMMF-FSO system using Mode Filtering Techniques,” in International Conference on Communications Workshops (ICC), 2016, pp 405 – 410.
- [C12] P. Koška, Y. Baravets, P. Peterka, J. Bohata and M. Pisarik, "Optimized mode-field adapter for low loss fused fiber bundle signal and pump combiners," In Conference Proceeding - Fiber Lasers XII: Technology, Systems, and Applications, 2015, pp. 93442I-93442I-7.
- [C13] E. Giacomidis, J. Wei, M. A. Jarajreh, S. T. Le1, P. A. Haigh, J. Bohata, et al, “Numerical Analysis of Artificial Neural Network and Volterra-based Nonlinear Equalizers for Coherent Optical OFDM,” in 36th Progress In Electromagnetics Research Symposium (PIERS), 2015, pp 2473 – 2477.
- [C14] P. Chvojka, J. Bohata, J. Libich, S. Zvanovec and J. Perez, “Laboratory and outdoor availability and spatial coherence tests of wireless optical links,” in 2nd International Workshop on Optical Wireless Communications (IWOW), 2013, pp. 109 – 1128.

Citations in Web of Knowledge and SCOPUS (except self-citations):

- [Ci4] S.K. Liaw, K.Y. Hsu, J.G. Yeh, Y.M. Lin and Y.L. Yu, “ Impacts of environmental factors to bi-directional 2×40 Gb/s WDM free-space optical communication, optics communication,” Optics communications, 2017, pp. 127-133. – citing [J6]
- [Ci5] K. Liu, C. Zhao, Y.g Yang, X. Chen, J. Wang, B. He, et al., “Low beam quality degradation, high-efficiency pump and signal combiner by built- in mode field adapter,” Applied optics, vol. 56(10), 2017, pp. 2804 - 2809. – citing [J7]
- [Ci6] D. Stachowiak, P. Kaczmarek and K.M. Abramski, “High-power pump combiners for Tm-doped fibre lasers,” Opto-electronics review, vol. 23(4), 2015. – citing [J7]

- [Ci7] D. Stachowiak, P. Kaczmarek and K.M. Abramski , “ $(5 + 1) \times 1$ pump and signal power combiner with $9/80 \mu\text{m}$ feed-through signal fiber,” *Optics & Laser Technology*, vol. 93, 2017, pp. 33-40. – citing [J7]
- [Ci8] D. H. Ai, H. D. Trung and D. T. Tuan, “AF relay-assisted MIMO/FSO/QAM systems in Gamma-Gamma fading channels,” in *Information and Computer Science (NICS)*, 2016. – citing [C9]

7 References

- [1] B. Bangerter, Shilpa Talwar, Reza Arefi and Ken Stewart, "Networks and devices for the 5G era," *IEE Communications Magazine*, vol. 52(2), 2014, pp. 90-96.
- [2] A. Gupta and R. K. Jha, "A Survey of 5G Network: Architecture and Emerging Technologies," *IEEE Access*, vol. 3, 2015, pp. 1206-1232.
- [3] S. Ahmed, "Performance analysis of Mobile WiMAX Technology," in *Computing for Sustainable Global Development (INDIACom)*, 2014, pp. 959-961.
- [4] P. Petropoulos, "Optical Fibre Technologies for Future Communication Networks," in *European Conference on Optical Communication (ECOC)*, 2016, pp. 1-3.
- [5] Y. K. Huang, M. -F. Huang; E. Ip; E. Mateo; A. Tanaka; D. Qian, et al., "16.2-Tb/s field trial over 2,531-km of installed SSMF with DP-QPSK optical superchannels," in *Opto-Electronics and Communications Conference (OECC)*, 2012, pp. 33-34.
- [6] Z. Ghassemlooy, L. N. Alves, S. Zvanovec and M. A. Khalighi, „Visible Light Communications: Theory and Applications“, CRC Press, 2017.
- [7] M. A. Khalighi and M. Uysal, "Survey on Free Space Optical Communication: A Communication Theory Perspective," *IEEE Communications Surveys & Tutorials*, vol. 16 (4), 2014, pp. 2231-2258.
- [8] A. A. Huurdeman, „The Worldwide History of Telecommunications“, Wiley, 2003.
- [9] C. Ranaweera, E. Wong, A. Nirmalathas, C. Jayasundara, C. Lim, "5G C-RAN architecture: A comparison of multiple optical fronthaul networks," in *International Conference on Optical Network Design and Modeling (ONDM)*, 2017, pp. 1-6.
- [10] R. Pirich, "Fiber optics for use in air and space harsh environments," in *Avionics, Fiber- Optics and Photonics Technology Conference (AVFOP)*, 2011, pp. 3-4.
- [11] M. Camera, "100GbE optical transport, appropriate modulation formats, and impact on deployed transport networks," in *Optical Fiber Communication, collocated National Fiber Optic Engineers Conference (OFC/NFOEC)*, 2010, pp. 1-3.
- [12] E. Lach and W. Idler, "Modulation formats for 100G and beyond," *Optical Fiber Technology*, vol. 17,(5), 2011, pp. 377-386.
- [13] A. Chowdhury, M. F. Huang, Z. Jia, J. Yu, R. Younce and G. K. Chang , "10x100-Gb/s transmissions using optical carrier suppression and separation technique and RZ-DQPSK modulation for metro-ethernet transport system," in *21st Annual Meeting of the IEEE Lasers and Electro-Optics Society (LEOS)*, 2008, pp. 479-480.
- [14] T. J. Xia, G. A. Wellbrock, Y. K. Huang, M. F. Huang, E. Ip, P. N. Ji, et al., "21.7 Tb/s field trial with 22 DP-8QAM/QPSK optical superchannels over 1,503-km of installed SSMF," in *Optical Fiber Communication, collocated National Fiber Optic Engineers Conference (OFC/NFOEC)*, 2012, pp. 1-3.
- [15] J. G. Andrews, S. Buzzi, W. Choi, S. V. Hanly, A. Lozano, A. C. K. Soong. et al., "What Will 5G Be?," *IEEE Journal on Selected Areas in Communications*, vol. 32(6), 2014, pp. 1065-1082.
- [16] S. Kanchi, S. Sandilya, D. Bhosale, A. Pitkar and M. Gondhalekar, "Overview of LTE-A technology," in *Global High Tech Congress on Electronics (GHTCE)*, 2013, pp. 195-200.
- [17] A. Checko, H. L. Christiansen, Y. Yan, L. Scolari, G. Kardaras, M. S. Berger, L. Dittmann, et al., "Cloud RAN for Mobile Networks - A Technology Overview," *Communications Surveys & Tutorials*, vol. 17 (1), 2015, pp. 405-426.
- [18] L. Cheng, L. Zhang, M. Zhu, J. Wang, L. Cheng, G. K. Chang, "A Novel Multi-Service Small-Cell Cloud Radio Access Network for Mobile Backhaul and Computing Based on Radio-Over-Fiber Technologies," *Journal of Lightwave Technology*, vol. 31(17), 2013, pp. 2869-2875..

- [19] B. Lannoo, A. Dixit, D. Colle, J. Bauwelinck, B. Dhoedt, B. Jooris, et al., "Radio-over-fibre for ultra-small 5G cells," in International Conference Transparent Optical Networks (ICTON), 2015, pp. 1-4.
- [20] H. Al-Raweshidy and S. Komaki, „Radio Over Fiber Technologies for Mobile Communications Networks,“ Artech House, 2002.
- [21] D. Pham Tien, A. Kanno and T. Kawanishi, "Radio-on-radio-over-fiber: efficient fronthauling for small cells and moving cells," *Wireless Communications*, vol. 22 (5), 2015, pp. 67-75.
- [22] M. Morant, J. Perez and R. Llorente, "Polarization Division Multiplexing of OFDM Radio-over-Fiber Signals in Passive Optical Networks," *Advances in Optical Technologies*, vol. 2014, 2014.
- [23] M. Morant, J. Prat and R. Llorente, "Radio-over-Fiber Optical Polarization-Multiplexed Networks for 3GPP Wireless Carrier-Aggregated MIMO Provision," *Journal of Lightwave Technology*, vol. 32(20), 2014, pp. 3721-3727.
- [24] C. H. Lee, „Microwave Photonics, Second Edition,“ Taylor & Francis, 2013.
- [25] W. S. Tsai, H. H. Lu, C. Y. Li, T. C. Lu, H. H. Lin, B. R. Chen, et al., "A 50 m/320 Gbps DWDM FSO communication," in *IEEE Photonics Conference (IPC)*, 2016, pp. 43-44.
- [26] L. C. Andrews and R. L. Phillips, „Laser beam propagation through random media,“ SPIE Press, 2005.
- [27] M. Uysal, C. Capsoni, Z. Ghassemlooy, A. Boucouvalas and E. Udvary, (2016). *Optical wireless communications: an emerging technology*,“ Springer, 2016.
- [28] E. Ciaramella, Y. Arimoto, G. Contestabile, M. Presi, A. D'Errico, V. Guarino and M. Matsumoto, "1.28-Tb/s (32 times 40 Gb/s) Free-Space Optical WDM Transmission System," *Photonics Technology Letters*, vol. 21 (16), 2009, pp. 1121-1123.
- [29] C. B. Naila, K. Wakamori, M. Matsumoto, A. Bekkali and K. Tsukamoto., "Transmission analysis of digital TV signals over a Radio-on-FSO channel," *Communications Magazine*, vol. 50 (8), 2012, pp. 137-144.
- [30] A. Arockia Bazil Raj, J. A. V. Selvi and S. Durairaj, "Comparison of different models for ground-level atmospheric turbulence strength (Cn²) prediction with a new model according to local weather data for FSO applications," *Applied Optics*, vol. 54 (4), 2015, pp. 802-815.
- [31] Z. Ghassemlooy, W. Popoola and S. Rajbhandari, „Optical Wireless Communications: System and Channel Modelling with MATLAB®,“ Taylor & Francis, 2012.
- [32] D. Pham Tien, A. Mohammad, S. K. Kazaura, K. Wakamori, T. Suzuki, K. Takahashi, et al., "A study on transmission of RF signals over a turbulent free space optical link," in *International Topical Meeting on Microwave Photonics jointly held with the Asia-Pacific Microwave Photonics Conference*, 2008, pp. 173-176.
- [33] Y. Peng, X. Yi and Z. Liu, "Research on Radio Frequency Assignment Mechanism of the Distributed Antenna System Based on Radio over Free Space Optics Technology," in *Services Asia-Pacific Computing Conference (APSCC)*, 2010, pp. 526-530.
- [34] A. Bekkali, C. B. Naila, K. Kazaura, K. Wakamori and M. Matsumoto, "Transmission Analysis of OFDM-Based Wireless Services Over Turbulent Radio-on-FSO Links Modeled by Gamma-Gamma Distribution," *Photonics Journal*, vol. 2 (3), 2010, pp. 510-520.
- [35] Corning SMF28 Ultra optical Fiber, product information, Available: www.corning.com
- [36] A. A. Stolov, A. S. Hokansson, R. S. Dyer, K. L. Marceau, B. E. Slyman, D. J. Cote, et al., "Effects of low temperature and hot steam on reliability of specialty optical

- fibers designed for avionics applications," in Avionics, Fiber-Optics and Photonics (AVFOP), 2013, pp. 29-30.
- [37] H. J. Reinsch T., "Temperature dependent characterization of optical fibres for distributed temperature sensing in hot geothermal wells," *Geophysics*, vol. 21(9), 2012.
- [38] A. Walter and G. S. Schaefer, "Chromatic dispersion variations in ultra-long-haul transmission systems arising from seasonal soil temperature variations," in *Optical Fiber Communication Conference and Exhibit (OFC)*, 2002, pp. 332-333.
- [39] H. C. Ji, J.H. Lee and Y. C. Chung, "Evaluation on system outage probability due to temperature variation and statistically distributed chromatic dispersion of optical fiber," *Journal of Lightwave Technology*, vol. 22(8), 2004, pp. 1893-1898.
- [40] P. S. Andre, A. N. Pinto and J. L. Pinto, "Effect of temperature on the single mode fibers chromatic dispersion," in *International Microwave and Optoelectronics Conference (IMOC)*, vol. 1, 2003, pp. 231-234
- [41] S. Vorbeck and R. Leppla, "Dispersion and dispersion slope tolerance of 160-Gb/s systems, considering the temperature dependence of chromatic dispersion," *Photonics Technology Letters*, vol. 15(10), 2003, pp. 1470-1472.
- [42] W. Hatton and M. Nishimura, "Temperature dependence of chromatic dispersion in single mode fibers," *Journal of Lightwave Technology*, vol. 4(10), 1986, pp. 1552-1555.
- [43] M. J. Hamp, J. Wright, M. Hubbard, B. Brimacombe, "Investigation into the temperature dependence of chromatic dispersion in optical fiber," *Photonics Technology Letters*, vol. 14 (11), 2002, pp. 1524-1526.
- [44] T. Kato, Y. Koyano and M. Nishimura, "Temperature dependence of chromatic dispersion in various types of optical fibers," in *Optical Fiber Communication Conference*, vol. 1, 2000, pp. 104-106.
- [45] R. Hui and M. O'Sullivan, „*Fiber Optic Measurement Techniques*,“ Elsevier, 2009.
- [46] V. Musara, W. T. Ireta, L. Wu and A. W. R. Leitch, "The General interferometry technique: Interferogram analysis in the presence of a high polarization mode dispersion segment," in *AFRICON*, 2011, pp. 1-4.
- [47] N. Cyr, "Generalized interferometric method for accurate match with DGD measurements and comparison against standard references," in *Optical Fiber Measurements*, 2004, pp. 85-90.
- [48] N. Cyr, "Polarization-mode dispersion measurement: generalization of the interferometric method to any coupling regime," *Journal of Lightwave Technology*, , vol. 22(3), 2004, pp. 794-805.
- [49] IEC, "IEC 60793-1-48:2007," *Measurement methods and test procedures - Polarization mode dispersion*, 2007, p. 100.
- [50] "PMD Measurement on Aerial Fiber under Wind-Induced Oscillations and Vibrations," EXFO technical note, 2009.
- [51] A. Galtarossa and L. Palmieri, "POTDR techniques for measurement of fiber birefringence properties," in *Optical Fiber Communication Conference and Exhibit (OFC)*, 2002, pp. 174-175.
- [52] N. Cyr, H. Chen and G. W. Schin, "Random-Scrambling Tunable POTDR for Distributed Measurement of Cumulative PMD," *Journal of Lightwave Technology*, , vol. 27(18), 2009, pp. 4164-4174.
- [53] D. Fritzsche, M. Paul, L. Schuerer, A. Ehrhardt, D. Breuer, W. Weiershausen, et al., "Measuring the cumulative PMD of buried fibers in the network of Deutsche Telekom in a field trial using an RS-POTDR prototype," in *Photonic Networks Symposium*, 2008, pp. 1-4.

- [54] D. Fritzsche, M. Paul, L. Schuerer, A. Ehrhardt, D. Breuer, W. Weiershausen, et al., "Measuring the Link Distribution of PMD: Field Trial Using an RS-POTDR," in Optical Fiber communication/National Fiber Optic Engineers Conference (OFC/NFOEC), 2008, pp. 1-3.
- [55] A. Ehrhardt, et al., "Field trial to improve the fibre infrastructure towards 40Gbit/s transmission and beyond and decrease economically efficient the link PMD by exploitation of a POTDR," in Transparent Optical Networks, 2009. ICTON '09. 11th International Conference on, 2009, pp. 1-4.
- [56] A. Ehrhardt, M. Paul, L. Schurer, C. Gerlach, W. Kronert, D. Fritzsche et al., "Characterisation of the PMD distribution along optical fibres by a POTDR," in International Conference on Transparent Optical Networks (ICTON), 2008, pp. 173-177.
- [57] M. Brodsky, P. Magill and N. J. Frigo, "Polarization-mode dispersion of installed recent vintage fiber as a parametric function of temperature," Photonics Technology Letters, vol. 16(1), 2004, pp. 209-211.
- [58] M. Brodsky, N. J. Frigo, M. Boroditsky, M. Tur, "Polarization Mode Dispersion of Installed Fibers," Journal of Lightwave Technology, vol. 24(12), 2006, pp. 4584-4599.
- [59] A. Mecozzi, C. Antonelli, M. Boroditsky and M. Brodsky, "Characterization of the time dependence of polarization mode dispersion," Optics Letters, vol. 29(22), 2004, pp. 2599-2601.
- [60] M. Brodsky, P. Magill and N. J. Frigo, "Long-term" PMD characterization of installed fibers-how much time is adequate?," in Optical Fiber Communication (OFC), vol. 2, 2004, p. 3.
- [61] ITU-T, "ITU-T Recommendation G.652: Characteristics of a single-mode optical fibre," 2009. Online: <https://www.itu.int/rec/T-REC-G.652/en>.
- [62] A. Nespola and S. Abrate, "Long term PMD characterization of installed G.652 fibers in a metropolitan network," in Optical Fiber Communication Conference (OFC/NFOEC), vol. 3, 2005, p. 3 pp..
- [63] M. Karlsson, J. Brentel and P. A. Anderkson, "Long-term measurement of PMD and polarization drift in installed fibers," Journal of Lightwave Technology, vol. 18(7), 2000, pp. 941-951.
- [64] T. Kawasaki, W. Ichihara, T. Kataoka and S. Matsuoka, "Over 5-months Long-Term PMD Continuous Measurement in Installed Fiber Cables with an Exposed Fiber Section," in Optical Fiber Communication and the National Fiber Optic Engineers Conference (OFC/NFOEC), 2007, pp. 1-3.
- [65] S. L. Woodward, L. E. Nelson, C. R. Schneider, L. A. Knox, M. O'Sullivan and C. Laperle, et al., "Long-Term Observation of PMD and SOP on Installed Fiber Routes," Photonics Technology Letters, vol. 26(3), 2014, pp. 213-216.
- [66] K. Borzycki, "Temperature dependence of PMD in optical fibres and cables," in Transparent Optical Networks, vol. 1, 2005, pp. 441-444.
- [67] ITU, "Recommendation G.655 Characteristics of a non-zero dispersion-shifted single-mode optical fiber and cable," 2009. Online: <https://www.itu.int/rec/T-REC-G.655/en>.
- [68] K. Borzycki and M. Jaworski, "Temperature Dependence of PMD in Optical Fibres and Cables: Part II," in Transparent Optical Networks, 2006, pp. 209-212.
- [69] K. Borzycki, "Influence of temperature and aging on Polarization Mode Dispersion of tight-buffered optical fibers and cables," Journal Telecommunications and Information Technology, vol. 14(3), 2005, pp. 96-104.
- [70] C. Laperle, B. Villeneuve, Z. Zhang, D. McGhan, H. Sun, M. O'Sullivan, "WDM Performance and PMD Tolerance of a Coherent 40-Gbit/s Dual-Polarization QPSK Transceiver," Journal of Lightwave Technology, vol. 26(1), 2008, pp. 168-175.

- [71] S. Oda, T. Tanimura, T. Hoshida, C. Ohshima, H. Nakashima, Y. Aoki, et al., "Interplay between PMD and nonlinearity in 112 Gb/s DP-QPSK transmission with co-propagating 10.7 Gb/s NRZ channels," in Optical Fiber Communication Conference and National Fiber Optic Engineers Conference (OFC/NFOEC), 2011, pp. 1-3.
- [72] L. E. Nelson, S. L. Woodward, S. Foo, X. Zhou, M. D. Feuer, D. Hanson, et al., "Performance of a 46-Gbps Dual-Polarization QPSK Transceiver With Real-Time Coherent Equalization Over High PMD Fiber," *Journal of Lightwave Technology*, vol. 27(3), 2009, pp. 158-167.
- [73] T. J. Xia, G. Wellbrock, M. Pollock, W. Leem D. Peterson, D. Doucet, et al., "92-Gb/s field trial with ultra-high PMD tolerance of 107-ps DGD," in Optical Fiber Communication (OFC), 2009, pp. 1-3.
- [74] X. Chongjin, "Impact of nonlinear and polarization effects on coherent systems," in European Conference on Optical Communication (ECOC), 2011, pp. 1-3.
- [75] V. M. Pestrikov, "The long-term strength of optical fibers under conditions of ageing of the material," *Glass Physics and Chemistry*, vol. 26, 2000, pp. 169-178.
- [76] W. Moore and T. Kiktyeva, "Optical damage in fiber optic components," in Optical Fiber Communications (OFC), vol. 2, 2003, pp. 525-527.
- [77] G. G. Karady, B. Shi, Q. Huang, D. Srinivasan and M. W. Tuominen, "Experimental investigation of the aging process on ADSS optical fiber cables," in Power Engineering Society General Meeting, vol. 1, 2003, p. 228.
- [78] P. Jongwoo and D. S. Shin, "Degradation of fiber optical communication devices under damp-heat aging," *Photonics Technology Letters*, vol. 15(8), 2003, pp. 1106-1108.
- [79] R. El Abdi, M. Poulain, A. D. Rujinski and I. Severin, "Damage analysis for optical fibers aged in aggressive reagents," in Photonics Society Summer Topical Meeting Series, 2011, pp. 95-96.
- [80] P. S. Andre, F. Domingues, M. Granada and Marta, "Impact of the maritime environment on the aging of optical fibers," in Conference on Lasers and Electro-Optics (CLEO), 2011, pp. 1-2.
- [81] B. Bakshi, L. Rahman, G. Mobs, M. Van, W. W. Patterson, J. X. Cai et al., "Impact of fiber aging and cable repair in an installed 28-nm transatlantic 96 x 10 Gb/s DWDM system," in Optical Fiber Communication Conference (OFC/NFOEC), 2005, pp. 169-171.
- [82] T. J. Xia, G. A. Wellbrock, M. F. Huang, S. Zhang, Y. K. Huang, D. Chang, et al., "Transmission of 400G PM-16QAM channels over long-haul distance with commercial all-distributed Raman amplification system and aged standard SMF in field," in Optical Fiber Communications (OFC), 2014, pp. 1-3.

8 Curriculum Vitae

Personal information

Name: **Ing. Jan Bohata**
E-mail: **bohatja2@fel.cvut.cz**
Nationality: Czech
Birth: 3.1. 1988, Prague



Work experience:

2012 – Researcher and PhD student in Department of electromagnetic field, Faculty of Electrical Engineering .

Education

2010 - 2012

Master's degree in Faculty of Electrical Engineering, Czech Technical University in Prague, Technicka 2, Prague 6, Czech Republic.

2007 - 2010

Bachelor's degree in Faculty of Electrical Engineering, Czech Technical University in Prague, Technicka 2, Prague 6, Czech Republic.

2003 – 2007

High school SPSST Panska 3, Prague 1, Czech Republic.

Research activities:

Research filed is focused on optical fiber and wireless technology, microwave photonics and optical sensors.

Projects:

Running:

- Analysis of mode structure in optical components, MPO TRIO, FV10519.

Finished:

- Fiber optic detection of liquids (Technology Agency of the Czech Republic), 2012-2016, project members SQS and Czech Technical University in Prague, TACR grant TA03010060.
- Optical packet switch (Technology Agency of the Czech Republic), 2013-2017, principal investigator, project partners SQS, Institute of Photonics and Electronics, Czech Technical University in Prague, TACR grant TA01011105.

- Safety of optical critical infrastructure (Technology Agency of the Czech Republic), 2013-2017 project partners SQS, T-Mobile, Sitel, Kabex, Technical University of Ostrava, TACR grant TA03020439.
- COST project IC1101 Optical wireless communications, OPTICWISE, http://www.cost.eu/domains_actions/ict/Actions/IC1101.
- Research on the impact of ambient conditions to modern broadband optical wireless networks, RAINBOWS, MSMT COST CZ project LD12058.
- Advanced components techniques for fiber sensors. CTU project SGS, SGS12/142/OHK3/2T/13.

Professional activities:

2016 - IEEE student member.